The effect of activated coagulation factor X (FXa) inhibition on platelets in the context of acute myocardial infarction and stroke

Inaugural-Dissertation

zur Erlangung des Doktorgrades
der Mathematisch-Naturwissenschaftlichen Fakultät
der Heinrich-Heine-Universität Düsseldorf

vorgelegt von

Maike Barcik
aus Witten

Düsseldorf, September 2023

aus der Klinik für Kardiologie, Pneumologie und Angiologie

der Heinrich-Heine-Universität Düsseldorf

Klinikdirektor: Prof. Dr. Malte Kelm

Gedruckt mit der Genehmigung der

Mathematisch-Naturwissenschaftlichen Fakultät der

Heinrich-Heine-Universität Düsseldorf

Berichterstatter:

1. PD Dr. Amin Polzin

2. Prof. Dr. Axel Gödecke

Tag der mündlichen Prüfung:

Table of Contents

List of tables

List of figures

List of abbreviations

A. ..... *Arteria*
ADP ..... *adenosine diphosphate*
AF ..... *atrial fibrillation*
AIS ..... *acute ischemic stroke*
AMI ..... *acute myocardial infarction*
aPC ..... *activated Protein C*
APC-Cy ..... *allophycocyanin-cyanin*
ATP ..... *adenosine triphosphate*
BSA ..... *bovine serum albumin*
Bw ..... *bodyweight*
Ca^{2+} ..... *calcium*
CAD ..... *coronary artery disease*
CNS ..... *central nervous system*
CO ..... *cardiac output*
CON ..... *control*
DAPI ..... *4',6-diamidino-2-phenylindol*
DMEM ..... *Dulbecco's Modified Eagle's Medium*
ECG ..... *electrocardiogram*
EDV ..... *enddiastolic volume*
EF ..... *ejection fraction*
ESV ..... *endsystolic volume*
FCS ..... *fetal calf serum*
FII ..... *factor II, prothrombin*
FIIa ..... *activated factor II, thrombin*
FIII ..... *factor III , tissue factor*
FITC ..... *fluoresceinisothiocyanate*
FIX ..... *factor IX*
FMD ..... *flow mediated dilatation*
FS ..... *fractional shortening*
FVII ..... *factor VII*
FVIII ..... *activated factor VIII*
FX ..... *factor X*
FXa ..... activated coagulation factor X
FXI ..... *factor XI*
FXII ..... *factor XII*
GAPDH *glycerinaldehyde-3-phosphate-dehydrogenase*
gDNA ..... *genomic deoxyribonucleic acid*
GM-CSF ..... *granulocyte-macrophage colony-stimulating factor*
GPCR ..... *G-protein coupled receptor*
GPIIb/IIIa ..... *glycoprotein IIb/IIIa*
HF ..... *heart failure*
HFrEF ..... *heart failure with reduced ejection fraction*
HIER ..... *heat-induced epitope retrieval*
HMWK ..... *high molecular weight kininogen*
HR ..... *heart rate*
HRP ..... *horse radish peroxidase*
I/R ..... *ischemia/reperfusion*
Iba1 ..... *ionized calcium binding adaptor molecule 1*
IFN-ɣ ..... *interferon gamma*
IFN-β ..... *interferon beta*
IL-12p70 ..... *interleukin-12p70*
IL-17A *interleukin-17A*
IL-18 ..... *interleukin-18*

IL-1α ..... *interleukin-1 alpha*
IL-1β ..... *interleukin-1 beta*
IL-23 ..... *interleukin-23*
IL-27 ..... *interleukin-27*
IL-6 ..... *interleukin-6*
K^+ ..... *potassium*
LAD ..... *left anterior descending coronary artery*
LTA ..... *light transmission aggregometry*
MACS ..... *magnet activated cell sorting*
MAP ..... *mean arterial pressure*
MCA ..... *middle cerebral artery*
MCP1 ..... *monocyte chemotactic protein 1*
Mo/Mp ..... *monocytes/macrophages*
MPO ..... *myeloperoxidase*
Na^+ ..... *sodium*
NaCl ..... *sodium chloride*
NET ..... *neutrophile extracellular trap*
NO ..... *nitric oxide*
NOACs ..... *non vitamin K antagonist oral anticoagulants*
PAR1 ..... *protease-activated receptor 1*
PAR4 ..... *protease-activated receptor 4*
PCI ..... *percutaneous coronary intervention*
P_{dias} ..... *diastolic pressure*
PE ..... *phycoerythrin*
PFA ..... *paraformaldehyd*
PGI2 ..... *prostacyclin*
PK ..... *prekallikrein*
pKr-2 ..... *prothrombin kringle-2*
PRP ..... *platelet rich plasma*
PSLA ..... *parasternal long axis*
P_{sys} ..... *systolic pressure*
qPCR ..... *real-time polymerase chain reaction*
RIVA ..... *rivaroxaban*
RNA ..... *ribonucleic acid*
RT ..... *room temperature*
s.c. ..... *subcutaneous*
SAX ..... *short axis*
SNAP ..... *synaptosomal-associated proteins*
SNARE ..... *solube N-ethylmaleimide-sensitive-factor attachment receptor*
SV ..... *stroke volume*
TGF-β1 ..... *transforming growth factor-beta 1*
tMCAO ..... *transient middle cerebral artery occlusion*
TNFα ..... *tumor necrosis factor alpha*
TTC *2,3,5-triphenyltetrazolium-chloride*
TxA_2 ..... *thromboxane A_2*
VAMP ..... *vesicle-associated membrane proteins*
VAMP-8 ..... *vesicle associated membrane protein-8*
VKA ..... *vitamin K antagonist*
vWF ..... *von-Willebrand-factor*
WBC ..... *white blood cells*
β-ME ..... *β-Mercaptoethanol*
δ-granules ..... *dense granules*

1. Introduction

1.1 Ischemia

Ischemia is defined as a lack of oxygen in an organ, in a part of an organ or in tissue, because of reduced, but also interrupted blood flow. The result of ischemia is hypoxia, which leads to necrosis of tissue or an infarction, if it is prolonged (Nikol, 2023).

1.1.1 Acute myocardial infarction

Acute myocardial infarction (AMI), also known as heart attack, is one of the leading causes of death worldwide (Cheng et al., 2023). According to the federal statistical office, more than 45,000 people died from an AMI in Germany in 2021 (Statistisches Bundesamt, 2022). The greatest risk of an AMI is the irreversible damage of the myocardium because the tissue is no longer supplied with oxygen. This phase, where oxygen is lacking, is called ischemia. The infarcted myocardial tissue becomes necrotic and dysfunctional. AMI can lead to either restoration of cardiac function, or scar tissue formation with decreased diastolic and systolic function. This adverse effect is called heart failure (HF). Malignant arrhythmias can occur from the scar tissue. Therefore, the main focus is the reperfusion of the myocardium and the restoration of blood flow (Mechanic et al., 2023). The two most common types of AMI are 1) non-ST-segment elevation MI (NSTEMI) and 2) ST-segment elevation MI (STEMI) and can be divided by an analysis via electrocardiogram (ECG). The two types differ in the severity of the infarction. Usually, STEMI refers to a transmural myocardial ischemia, whereas NSTEMI affects smaller areas of the myocardium. Therefore, percutaneous coronary intervention (PCI) within 120 minutes after STEMI diagnosis is the best reperfusion strategy for patients. In NSTEMI - depending on the individual patient risk - PCI must be conducted within 2-72 h after diagnosis (Ibanez et al., 2018).

The main reason for the development of an AMI is an occlusion of a coronary artery by the formation of a thrombus, which leads to ischemia (Bui et al., 2009). Most thrombi leading to AMI occur after an atherosclerotic plaque rupture (Badimon et al., 2014; Golforoush et al., 2020). In atherosclerosis, a pathological deposition of cholesterol, calcium and other substances results in the formation of a calcified plaque, which can be found in the tunica intima, the inner wall of blood vessels (Kalampogias et al., 2016). If such a plaque ruptures, thrombus formation is initiated, where platelets play a crucial role (Asada et al., 2020).

Thrombus formation is a highly complex process in which platelets interact with the endothelial and subendothelial matrix of the blood vessel (Burke et al., 2007). Platelet activation occurs

through the release of various mediators from the vessel wall (including von-Willebrand-factor (vWF) and collagen) and the subsequent adhesion to the subendothelial matrix via integrins (e.g., glycoprotein Ib-receptor) (Mustard et al., 1990; Asada et al., 2018). Various intracellular signaling pathways are activated. Activation of glycoprotein IIb/IIIa (GPIIb/IIIa, CD41/CD61) leads to the binding of fibrinogen (Lefkovits et al., 1995), which is the beginning of crosslinking of platelets and arterial thrombus formation.

The main focus of medical treatment peri-AMI is revascularization of the affected tissue, so that the blood flow through the coronary vessels is restored (NVL chronische KHK, 2022). A comparison between the prevalence of AMI in the German population (Gößwald et al., 2013) and the mortality rate shows that a large proportion of patients survive the acute cardiovascular event. Immediately after AMI, the remodeling process in the heart begins. This is characterized by the death of cardiomyocytes, the start of inflammatory processes and the scar formation of the infarcted tissue (Jung et al., 2017). The quality and quantity of these processes determine the long-term outcome after AMI with respect to cardiac function (Frangogiannis, 2008). The better and earlier the remodeling, the better the outcome after AMI. Pathological remodeling can lead to cardiac dysfunction, HF and even cardiovascular death (Vieira et al., 2018; Berezin et al., 2020).

1.1.2 Stroke

Another leading cause of death worldwide are cerebral ischemias. According to the federal statistical office, more than 10,600 people died from a stroke in Germany in 2021 (Statistisches Bundesamt, 2022). It is a disease with often severe and subsequent impairments (Norrving et al., 2018). The genesis of 87 % of acute ischemic strokes (AIS) are cerebral ischemias.

The main cause of AIS are atherosclerotic or atherothrombotic stenosis of the extra- or intracranial brain-supplying vessels (approx. 85 %). Further causes are systemic embolisms, which are mostly of cardiac origin, as well as microangiopathies (Ay et al., 2005). Basically, the extent of brain damage depends on the duration of ischemia and the size and localization of the affected area. Affected areas of the brain stop working within seconds and suffer from necrosis in around five minutes after hypoxia and the stop of glucose supply (DeSai et al., 2023). Neurons switch from functional to maintenance metabolism until the reserves of adenosine triphosphate (ATP), which were provided by glycolysis, are emptied (Wahlgren et al., 2004). Due to the loss of energy, the sodium (Na^+)/ potassium (K^+) -ion exchange stands still or is strongly reduced, causing the cells to depolarize and calcium-ions (Ca^{2+}) to flow in. This leads to membrane damage by activation of proteases, which results in cell death.

Another cause for the massive Ca^{2+}-influx is an increased release of the neurotransmitter glutamate, which additionally contributes to necrotic cell death (Dirnagl et al., 1999; Wahlgren et al., 2004). In addition, the increased Ca^{2+} concentration activates phospholipases, which lead to DNA fragmentation with necrotic cell death due to free oxygen radicals or to apoptotic cell death due to mitochondrial damage (Wahlgren et al., 2004).

1.2 Hemostasis

Andrew LaPelusa and Heeransh D. Dave define hemostasis as a mechanism with different linked steps, that lead to prevention and to the end of bleeding from a blood vessel. This happens via a cascade, which ends with a blood clot to close the injured part of a blood vessel (LaPelusa et al., 2023). Four different steps are defined by the authors for the mechanism of hemostasis:

I. Constriction of the blood vessel
II. Formation of a temporary “platelet plug"
III. Activation of the coagulation cascade
IV. Formation of “fibrin plug” or the final clot.

Hemostasis is also defined as the first stage of wound healing and divided in two parts, primary and secondary hemostasis (Schultz et al., 2011).

1.2.1 Primary hemostasis

Primary hemostasis is known to be the first step in the repairing process of vascular damage in mammalian organisms. A crucial role plays the interaction between platelets, proteins (like vWF and collagen) which are located in the subendothelial matrix and circulating fibrinogen. In the end, a fibrin network can then be formed around a stable platelet clot, which is the result of primary hemostasis (McRae, 2011).

1.2.1.1 Platelets

Platelets, also known as thrombocytes, are small, circulating blood cells without a nucleus and with a diameter of 2 - 4 µm (Josefsson et al., 2020). They show a discoid shape and contain a cytoskeleton consist of actin, tubulin, spectrin and filamin (Shin et al., 2017). This cell type is formed by its constriction from megakaryocytes in the bone marrow and after that, they are released in the blood stream (Kuter, 1996). The lifespan of platelets is about one to two weeks before they are degraded mainly in the spleen (Josefsson et al., 2020). Their concentration in

the blood is about 150,000 – 450,000/ µl (Giannakeas et al., 2022). Even though they are anucleate, they interact with their environment and are metabolically active (McRae, 2011). The main function of platelets is adhesion followed by aggregation to seal injuries to a blood vessel and thus minimize potential blood loss. To maintain blood flow, these processes do not take place constitutively, but only upon activation. Activated and thus aggregating platelets play a central role in the formation of a thrombus and thus also in the development of ischemic events, such as AMI or stroke (Gawaz et al., 1996; Gidlof et al., 2013). Moreover, they contribute to tissue regeneration in these settings (Y. Liu et al., 2011; Ziegler et al., 2016). In addition to their central role in primary hemostasis and pathogenesis of acute atherothrombosis, platelets contribute to the maintenance of vascular integrity (Menter et al., 2017) as well as defense mechanisms of the innate and acquired immune system. Thus, platelets have a major issue in protective immunothrombosis, the interaction of the innate immune system with the coagulation system, but also in pathological thromboinflammation (Engelmann et al., 2013).

1.2.1.2 Platelet activation and adhesion

Normally, prostacyclin (PGI2) and nitric oxide (NO) are released by the endothelium, inhibiting the adhesion of platelets and prevent platelet activation (Thomas et al., 2015). When the endothelium shows a defect or is injured, e.g. after atherosclerotic plaque rupture or vascular injury, collagen is emerged to the surface and platelets are activated. After the membrane of platelets starts to dismantle, the GPIb/IX/V complex is released onto platelets membrane. The complex contains four transmembrane sub units GPIba, GPIbb, GPIX and GPV, with the N-terminal globular domain of GPIba, which interacts with the A1-domain of vWF (McRae, 2011). GPIb/IX/V complex is linked to the exposed collagen fibers via vWF, which is produced by endothelial cells (Shin et al., 2017). The vWF molecule is formed by disulphide-linked multimers with up to 20,000 kDa (Ware et al., 1993). The vWF multimers, with their high molecular weight, are broken down into smaller pieces by metalloprotease ADAMTS13 (a disintegrin and metalloprotease with a thrombospondin type 1 motif, member 13), when it is released into the plasma. The chance of unforced platelet aggregation is reduced by the smaller forms of vWF, because they do not bind fast to platelet receptors (McRae, 2011). The exposed fibers can also bind directly to platelets via GPIa/IIa (Thomas et al., 2015; Yun et al., 2016) as well as to GPVI (Kamiguti et al., 2000). It is known that collagen has a triple helical structure which is recognized by GPIa/IIa and GPVI (Monnet et al., 2000; Moroi, 2000). These receptors are expressed when they recognize the collagen structure. Intracellular metabolic pathways lead to the activation of GPIIb/IIIa which is involved in platelets crosslinking via binding to fibrinogen (**Fig.1**).

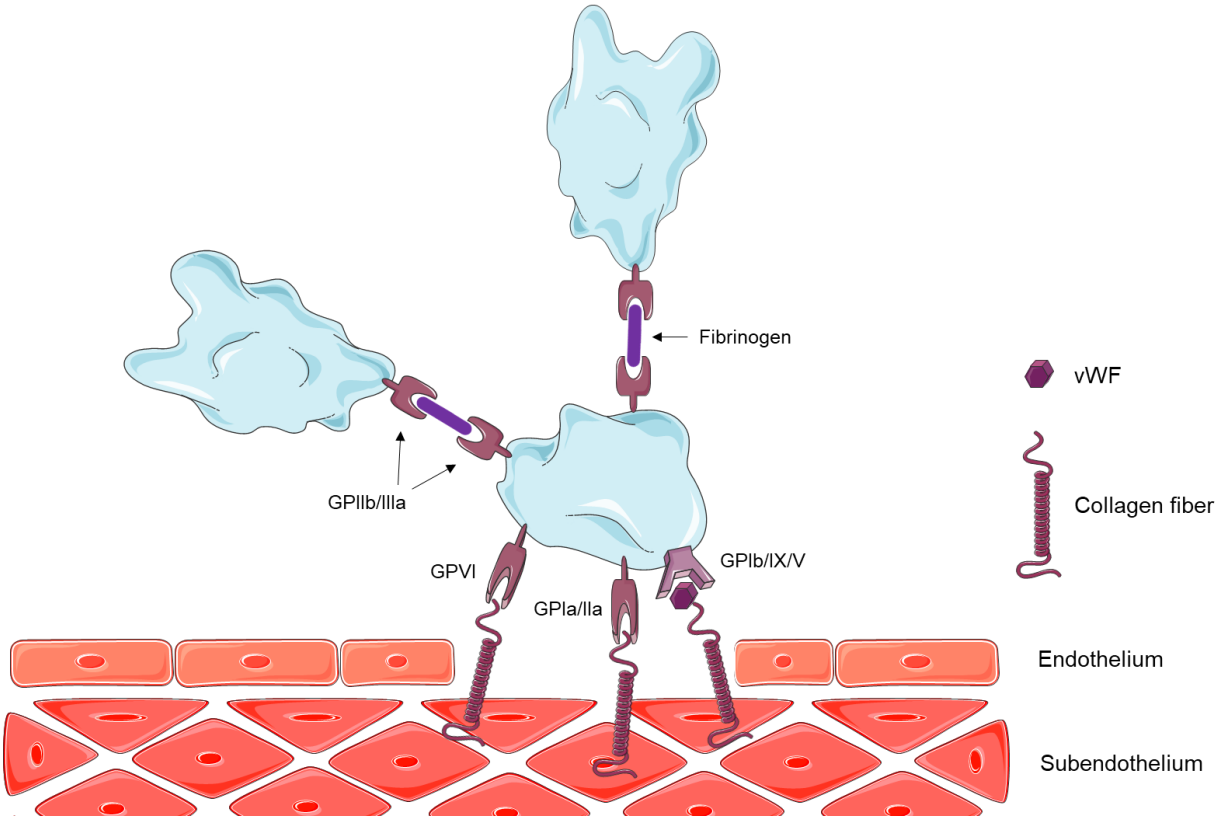

Figure 1: Schematic diagram of platelet adhesion on defect endothelium.

Subendothelial collagen fibers are exposed on the endothelial surface after an endothelial defect. Collagen fibers carry the von Willebrand factor (vWF) and platelets can bind to the collagen fibers and to the vWF via glycoprotein Ia/IIa (GPIa/IIa) and glycoprotein Ib/IX/V (GPIb/IX/V). The resulting platelet activation leads to the activation of glycoprotein IIb/IIIa (GPIIb/IIIa). Fibrinogen fibers can bind to this receptor and this is the initial step of platelet activation and aggregation (modified from doctoral thesis of Dr. Marcel Benkhoff (Benkhoff, 2022)).

Next to the exposition of collagen, a variety of different activators, which are released during activation of other cells, can mediate the activation of platelets following their adhesion (Yun et al., 2016) (**Fig. 2**). Activators like adenosine diphosphate (ADP), thrombin and thromboxane activate the G-protein coupled receptors (GPCRs). After receptor activation, calcium levels are increased, and specific intracellular pathways are activated. Damaged endothelial cells release ADP and activate platelets via $P2Y_1$ and $P2Y_{12}$ GPCRs, which results in the activation of other platelets and the further strengthened release of ADP, stored in dense granules. Activated platelets release thromboxane A_2 (TxA_2) and activate further platelets which promote the formation of a plug (Yun et al., 2016). The strongest agonist in the context of platelet activation is thrombin, which promotes the conversion from fibrinogen to fibrin and stabilizes the plug (Thomas et al., 2015). Protease-activated receptor 1 (PAR1) and 4 (PAR4) on the platelets' surface are the responsible GPCRs for platelet activation with thrombin. Both receptors are present on human and rodent platelets, whereas PAR1 does not activate murine platelets (Kahn et al., 1999). The process of activation leads to platelet shape change via reconstruction

and reorganization of the cytoskeleton (Aslan et al., 2012; Shin et al., 2017) and promotion of adhesion via integrin activation. During activation platelets are forced to release their different types of granules. Via the release of soluble mediators from granules, platelet aggregation is enhanced (Golebiewska et al., 2015). Mechanistically, processes are largely regulated by the secretion of the platelet granule compartment (Mezger et al., 2019). The secretome of thrombocytes consists of a variety of bioactive substances and is mainly stored in three intracellular granule types (Sharda et al., 2018).

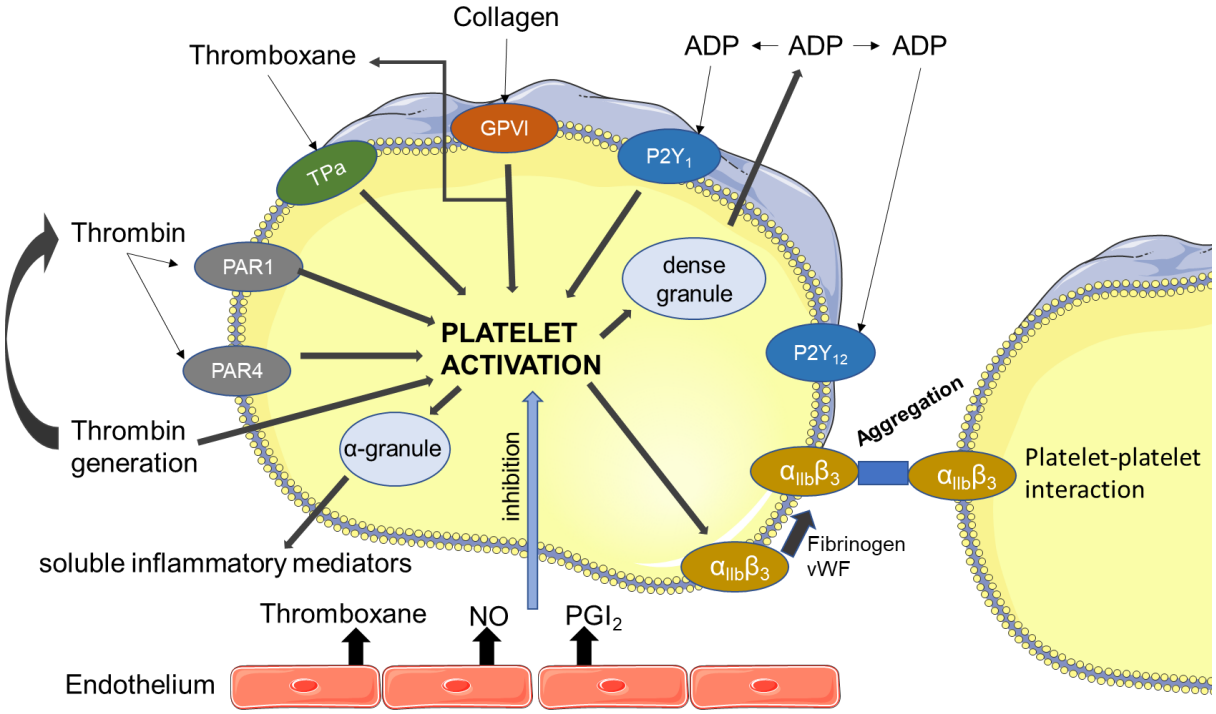

Figure 2: Schematic diagram of the mechanism of platelet activation.

Platelet activation is forced via various mediators and metabolic pathways. Normally, prostacyclin (PGI2) and nitric oxide (NO) are released by the endothelium, which inhibits the adhesion of platelets and prevent platelet activation. The release of soluble mediators from granules enhances platelet aggregation. Modified from (Thomas et al., 2015).

1.2.1.3 Alpha granules

Platelets contain a variety of different granules that fuse with the outer cell membrane after platelet activation and release mediators afterwards. The α-granules represent the most abundant and largest population, containing over 300 proteins (Gawaz et al., 2005). One platelet contains around 50-80 α-granules (Thomas et al., 2015). More than half of all granules present in platelets are α-granules (Heijnen et al., 2015). Recent secretome analyses show that the 200-500 nm diameter α-granules (Frojmovic et al., 1982) can release over 300 soluble proteins and mediators (Maynard et al., 2007; Piersma et al., 2009). If platelet activation and the associated increase of Ca^{2+}-ions in the cytosol occurs, SNARE proteins (soluble N-ethylmaleimide-sensitive-factor attachment receptor) ensure the fusion of granule membrane

and platelet membrane. Important representatives of these proteins are the vesicle-associated membrane proteins (VAMP) (Polgár et al., 2002), and the synaptosomal-associated proteins (SNAP), whose role in α-granule release is well described (Lemons et al., 2000; Lai et al., 2003). Three of the most important mediators released from α-granules are vWF (Ruggeri, 1999), fibrinogen (Kaplan et al., 1979), and P-selectin (Orkin et al., 2009). While vWF and fibrinogen are released into the environment, what leads to an increased formation of a thrombus, P-selectin (also CD62P) reaches the cell surface of the activated platelet through the fusion of the granule and platelet membrane. There, together with other glycoproteins, P-selectin plays an important role in ongoing platelet aggregation through platelet-fibrin and platelet-platelet binding (Jurk et al., 2005). Once secreted, these influence various physiological and pathophysiological processes in the context of hemostasis, inflammation, as well as tumor diseases (Gawaz et al., 2005; Walsh et al., 2018).

1.2.1.4 Dense granules

The second type of granules are the electron microscopically “dense” granules (δ-granules). Each platelet contains around 3-8 granules with a diameter of 150 nm each (White, 1998; Sharda et al., 2018). They contain bioactive messengers such as ATP, ADP, serotonin, histamine and larger amounts of cations (including calcium (Ca^{2+})) and thus contribute decisively to the para- and autocrine secondary activation of additional platelets and immune cells.

1.2.1.5 Lysosomes

The third and smallest subpopulation, with 1 to 3 per platelet, are lysosomes (White, 1998), which contain antibacterial proteins, proteases and glycosidases and contribute to the innate immune response. Lysosomes contain also proteolytic enzymes, which contribute to the remodeling of a thrombus (Meng et al., 2015). Their release needs strong stimuli like high doses of collagen or thrombin (Ciferri et al., 2000).

1.2.2 Secondary hemostasis

The secondary hemostasis contains two different pathways which work as a coagulation cascade. The intrinsic and the extrinsic pathway are triggered from different sites but come together at the stage of factor X (FX) and follow a common final pathway. The result is a platelet plug, stabilized by fibrin mesh (Chaudhry et al., 2023).

The intrinsic pathway starts with different factors after contact activation of damaged endothelium. The first activated factors are factor XII (FXII), which switches in its activated form FXIIa after exposure to collagen, the high-molecular-weight kininogen (HMWK) and the

prekallikrein (PK). FXIIa catalyzes the activation of factor XI (FXI) to FXIa. Afterwards, FXIa activates factor IX (FIX) to FIXa. Activated factor VIII (FVIIIa) acts as a cofactor for the FIXa-mediated activation of FX (Davie et al., 1964; van Herrewegen et al., 2012). Every activated factor can activate many other factors in following steps (**Fig. 3**).

The extrinsic pathway is the shorter one of the secondary hemostasis. When a vessel is damaged, cells of the endothelium release tissue factor, which activates factor VII (FVII) to FVIIa. This activates FX to FXa and both pathways follow the common one.

The common pathway starts with FX which is activated to FXa and this is a complicated reaction. The complex that divide FX into FXa, is called tenase. This complex has two forms and is present on the surface of activated platelets, because the needed phospholipids exist in their cell membrane. The first form is the extrinsic one, consisting of FVII, tissue factor (FIII) and Ca^{2+}. The second one is the intrinsic form, which is made of FVIIIa, FIXa, which is a phospholipid and Ca^{2+}. When FX is activated to FXa, it then activates prothrombin (FII) into thrombin (FIIa). To split prothrombin into thrombin, FXa needs FV as a cofactor. Then thrombin activates the reaction from fibrinogen into fibrin, and also factors in the intrinsic pathway like FXI, FV, FVIII and FXIII. When fibrin is formed from fibrinogen, its subunits form fibrin strands. Fibrin strands are formed like a mesh with the impact of FXIII. The formed fibrin mesh stabilizes the existing plug of platelets (Chaudhry et al., 2023).

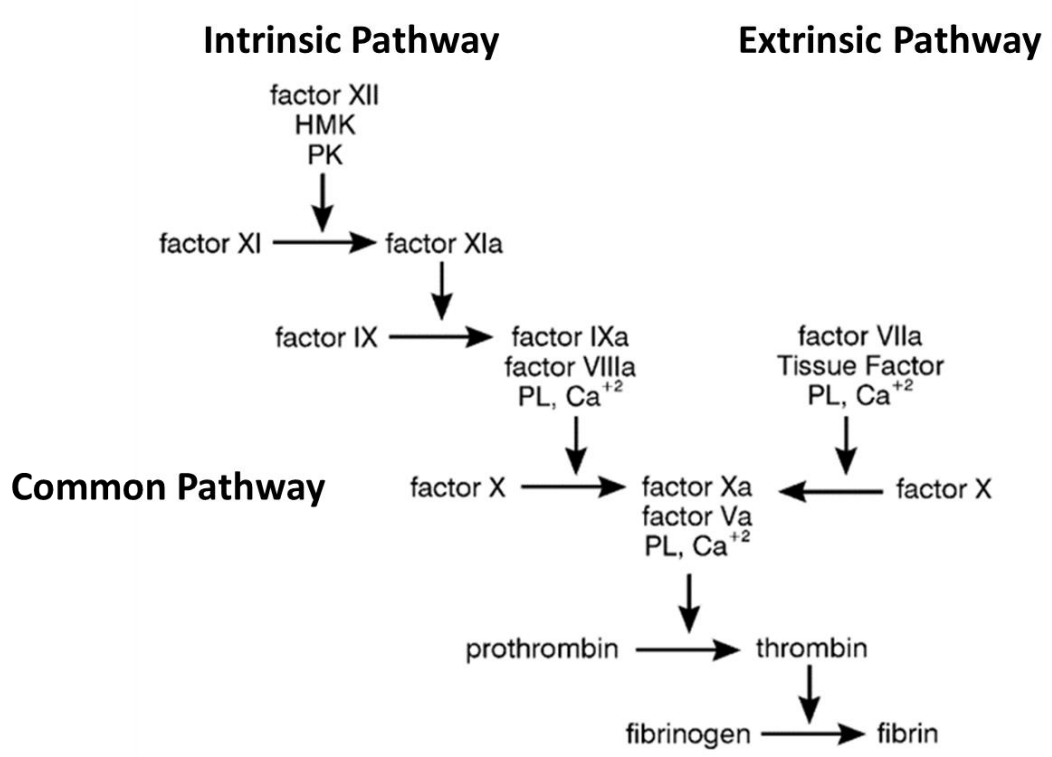

Figure 3: The coagulation cascade.

The secondary hemostasis starts on two different points, but the intrinsic and the extrinsic pathway come together at the stage of factor X and follow a common pathway (modified from Hoffmann et al., 2001).

1.2.3 Activated factor X

FXa, the activated form of FX, shows up in the coagulation cascade at the junction between the intrinsic and the extrinsic pathway, as described above. When one molecule of FXa is inhibited, the following production of more than hundred molecules of thrombin is inhibited as well (Cade et al., 1984). Because FXa has an upstream impact on the production of thrombin, it became an interesting target for inhibition (Alexander et al., 2005).

1.3 Anticoagulation

Anticoagulants are drugs inhibiting the coagulation of blood and used to protect the blood from clotting and subsequently vessels from occlusion. The use of those drugs is called anticoagulation therapy and is necessary in different clinical situations. Anticoagulation is mostly used to prevent clotting in thrombogenic conditions, like atrial fibrillation (AF), pulmonary embolism or deep vein thrombosis. It is used therapeutically and prophylactically (Morisch, 2017).

1.3.1 Non vitamin K antagonist oral anticoagulants

Non vitamin K antagonist oral anticoagulants (NOACs) are the first choice for preventing ischemic complications in patients with AF (Kirchhof et al., 2016). Currently, inhibitors of FXa (apixaban, edoxaban, rivaroxaban (RIVA) (**Fig. 4**)) and thrombin (FIIa) (dabigatran) are approved. All available NOACs show superiority to vitamin K antagonists (VKA) in reducing bleeding complications. Thereby, they show equivalent efficacy in preventing stroke (Connolly et al., 2009; Granger et al., 2011; Patel et al., 2011; Giugliano et al., 2013). Nevertheless, differences exist between the different NOACs in terms of their effect in acute atherothrombosis. Patients under FXa inhibition showed a numerical reduction in AMI, whereas patients with FIIa inhibition had more AMI (Connolly et al., 2009; Granger et al., 2011; Patel et al., 2011; Gibson et al., 2016; Cannon et al., 2017; Lopes et al., 2019). In previous studies, the acute effects of NOACs on platelet function were examined and an increased reactivity with dabigatran was demonstrated (Petzold et al., 2016; Achilles et al., 2017). In contrast, it was shown that RIVA, apixaban and edoxaban reduce platelet reactivity, resulting in decreased thrombus formation and platelet adhesion (Petzold et al., 2019). This is due to a previously unknown direct, thrombin-independent effect of FXa on platelets: mediated via activation of PAR1, stimulation with FXa leads to platelet activation. By inhibiting de novo generated FXa at a vascular injury, FXa inhibitors mediate an antiplatelet effect with reduced platelet reactivity (Petzold et al., 2019).

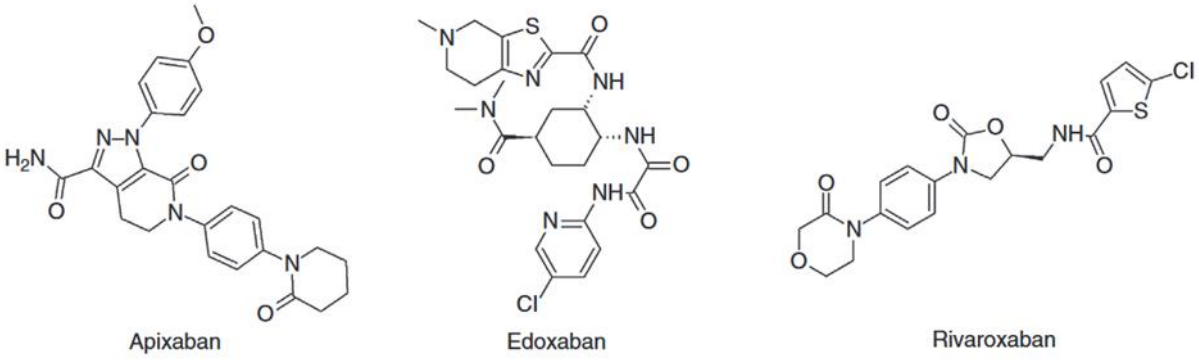

Figure 4: Chemical structure of direct FXa inhibitors.

Three different non vitamin K antagonist oral anticoagulants (NOACs) are used as a drug in the clinic. Apixaban, edoxaban and rivaroxaban (RIVA) are direct factor Xa inhibitors (Dobesh et al., 2019).

1.3.2 Rivaroxaban

RIVA is a reversible FXa-inhibitor, which is oxazolidinone-based and selective (**Fig. 4**). It has a molecular weight of 435.88 g/mol and a 10,000 times higher selectivity for FXa than the factors of the coagulation cascade (**Fig. 3**). The function of RIVA is the inhibition of free FXa, prothrombinase-bound FXa and FXa which is associated with a platelet plug (Perzborn et al., 2010). RIVA is authorized since 2008 for clinical use and is administered orally. Bioavailability of RIVA is around 80-100 %. It is approved for the prophylaxis of venous thrombosis and embolism in patients with hip or knee replacement, to prevent patients with AF of an ischemic stroke and for the acute and chronic treatment of patients suffering from deep vein thrombosis and pulmonary embolism (Perzborn et al., 2010). RIVA is also the only NOAC approved for secondary prevention of atherothrombotic events after acute coronary syndrome (ACS) (Alsaid et al., 2019). Regarding the prevention of ischemic events, RIVA has been able to highlight a protective effect in the ATLAS ACS 2-TIMI 51 Trial and the COMPASS Trial. The ATLAS ACS 2-TIMI 51 trial was a double-blind and placebo-controlled trial where 15,526 patients with recent ACS received two daily doses of 2.5 mg or 5 mg RIVA or placebo. This treatment was done for a mean of 13 months up to 31 months. It was shown that RIVA reduced risk of composite end point of death from cardiovascular causes, stroke or myocardial infarction in patients with a recent ACS, but the risk of major bleeding and intracranial hemorrhage was increased under RIVA treatment. The risk of fatal bleeding was not increased (Mega et al., 2012) (**Fig. 5**).

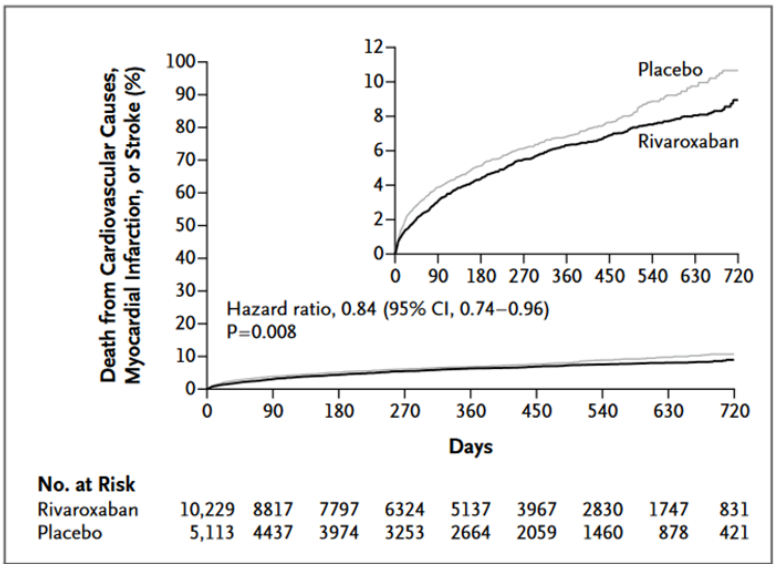

Figure 5: Cumulative incidence of the primary efficacy endpoint of the ATLAS ACS trial.

Shown are the deaths from cardiovascular cause, AMI or stroke in percentage, which are the reasons for the primary efficacy endpoint in the ATLAS ACS trial. The RIVA group contains patients with both doses (Mega et al., 2012).

The COMPASS trial investigated low-dose anticoagulation in patients with stable coronary heart disease (CHD) or arterial disease. In total, 27,395 patients were assigned to this study. The addition of 2 x 2.5 mg RIVA to an aspirin therapy prevented more cardiovascular deaths, AMIs and strokes, and even reduced all-cause mortality by 18 % after a median follow-up of 23 months, than aspirin alone (Alsaid et al., 2019) (**Fig. 6**).

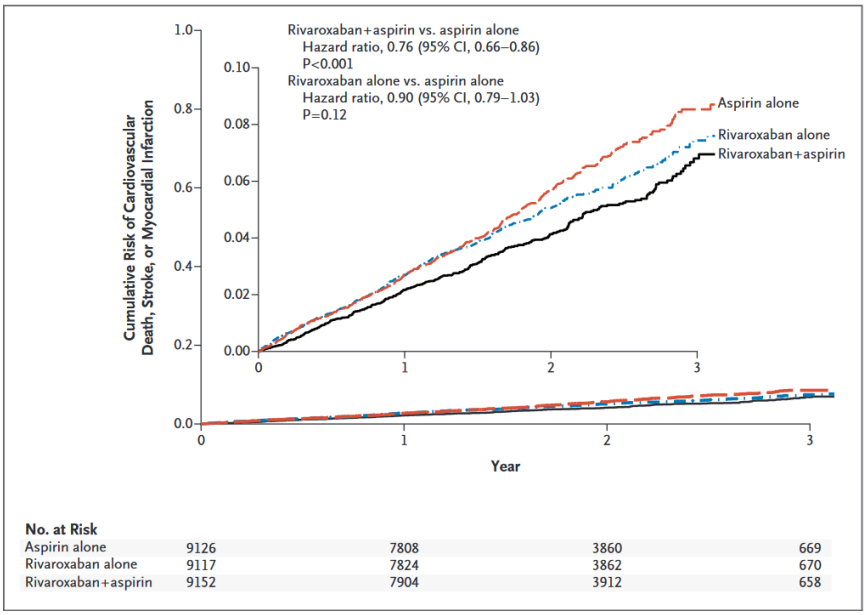

Figure 6: Cumulative incidence of the primary efficacy outcome of the COMPASS trial.

Shown is the risk of cardiovascular death, stroke or myocardial infarction. Participants in the COMPASS trial received RIVA in combination with aspirin, RIVA alone or aspirin alone (Eikelboom et al., 2017).

The COMMANDER HF trial, included 5022 patients with chronic HF, a left ventricular ejection fraction of ≤ 40 % and coronary artery disease (CAD). Patients received RIVA twice a day with 2.5 mg or placebo in addition to their standard treatment. The RIVA treated group of patients showed no significantly lower rate of death, myocardial infarction or stroke in comparison to the placebo group with worsening chronic HF, reduced left ventricular ejection fraction, CAD and no AF, as well as they show no significant different rehospitalization rates (Zannad et al., 2018) (**Fig. 7** and **8**).

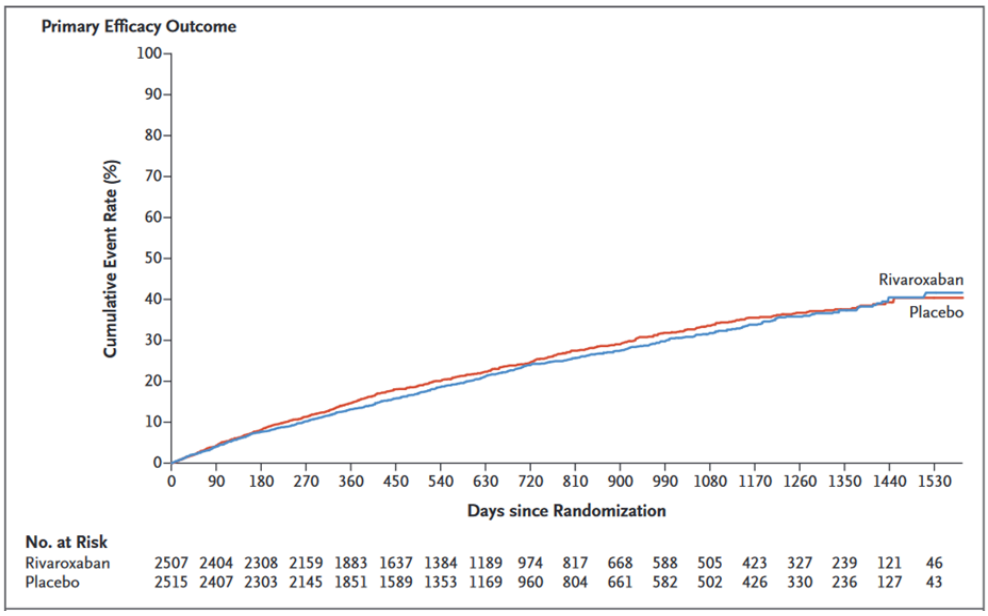

Figure 7: Primary efficacy outcome of the COMMANDER HF trial.

The cumulative event rate of death, stroke and AMI in percentage of patients participated in the COMMANDER HF trial in a Kaplan-Meier plot is shown (Zannad et al., 2018).

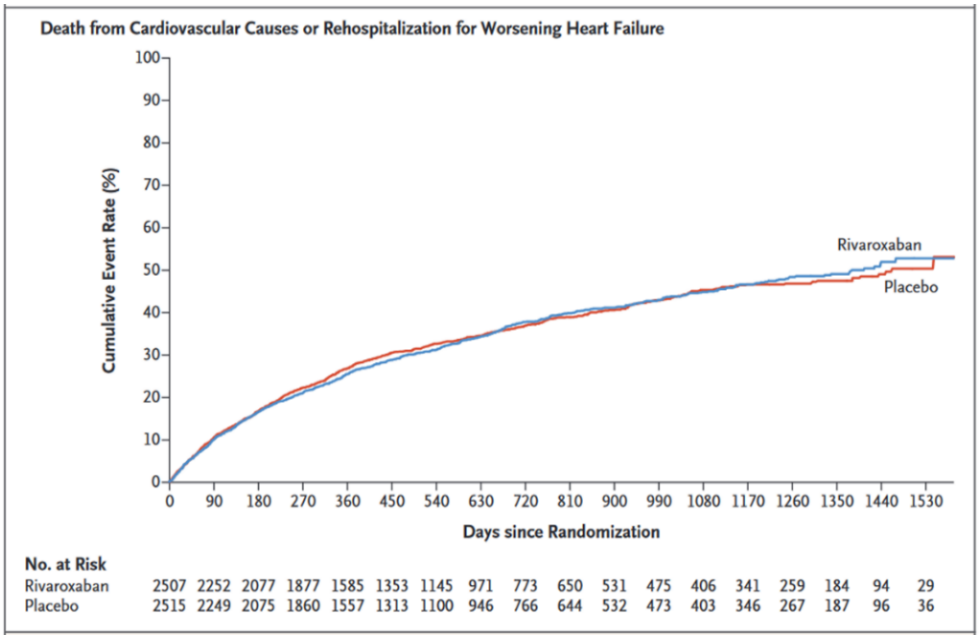

Figure 8: Death from cardiovascular causes or rehospitalization in the COMMANDER HF trial.

Shown are the cumulative event rate of death from cardiovascular causes or the rehospitalization for worsening heart failure (HF) in percentage in a Kaplan-Meier plot (Zannad et al., 2018).

1.4 Thromboinflammation

Next to thrombocytes, other cell types and their recruitment play an important role for the immune system's defense against infection, but also in the coagulation cascade and thrombus formation (von Bruhl et al., 2012). These are among others monocytes, macrophages and neutrophil granulocytes, which are often recruited by platelets after their activation. Platelets show a wide repertoire of mechanisms and when they are activated, like killing pathogens or promotion of pathogen clearance (Zhou et al., 2022). This process leads to activation of macrophages and neutrophil granulocytes, facilitating neutrophil extracellular trap (NET) formation. Inflammatory monocytes move to the inflammatory area. Next to the production of inflammatory cytokines, NETs provide local as well as to systemic inflammation (Kurihara et al., 1997). They have a high infiltration rate and can differentiate into inflammatory macrophages, which remove cell debris (Nahrendorf et al., 2007). A key protein for the initiation of coagulation via tissue activation upon cell injury, the protein ‘tissue factor’, is largely provided by monocytes. The formation of NETs by neutrophil granulocytes is also an important interaction mechanism between inflammation and coagulation (Papayannopoulos, 2018). These structures are like nets of fine chromatin fibers. Intracellular granular contents lead to the entrapment of both invading microorganisms and coagulation factors and platelets, providing a positive feedback mechanism for thrombus formation. In addition, the extracellular DNA structures form a negatively charged surface. By contact activation, coagulation factor XII initializes the coagulation cascade (Renne et al., 2007). This tissue and/or contact activation of the coagulation system may be amplified in inflammatory diseases, especially due to de-inflammatory cell decay, analogous to malignancies.

1.5 Aims of the thesis

Clinically, there is evidence of previously unknown and non-plasmatic effects of coagulation factors. For example, patients who have suffered a stroke while receiving NOACs show a low infarct severity, as well as a better clinical outcome compared with patients receiving VKA therapy or no anticoagulation (Meinel et al., 2019; Meinel et al., 2021). For patients with AMI, currently no clinical data exist on the extent to which the platelet-derived FXa signaling pathway and inhibition thereof affect infarct size, post ischemic thromboinflammation and left ventricular after AMI. A recently published study demonstrated that there is altered tissue inflammation and regeneration in the mouse AMI model upon NOAC administration, which is presumably due to altered activated Protein C (aPC) generation (Gadi et al., 2021). However, the underlying mechanism, in particular its effect on the proteome of platelets and leukocytes as effector cells of thromboinflammation, remains unclear.

In the context of the continued increased clinical use of NOACs, a fundamental understanding of its non-plasmatic effects beyond mere anticoagulation is essential. The aim of this thesis is to investigate if chronic in comparison to acute oral FXa inhibition of platelets influences the infarct size in AMI and in stroke and to investigate the underlying mechanism. Hypothetically, this occurs via a reduction in platelet granule secretion and consecutive thromboinflammation based on altered protein synthesis in megakaryocytes and platelets under oral FXa inhibition. The results should lead to a better understanding of the effect of FXa on platelets (**Fig. 9**). Based on this, the findings will contribute to the development of new treatment approaches for thromboinflammation based on modification of the platelet secretome. Understanding pathophysiological changes and how they can be influenced by pharmacotherapeutic principles is essential for new therapeutic approaches.

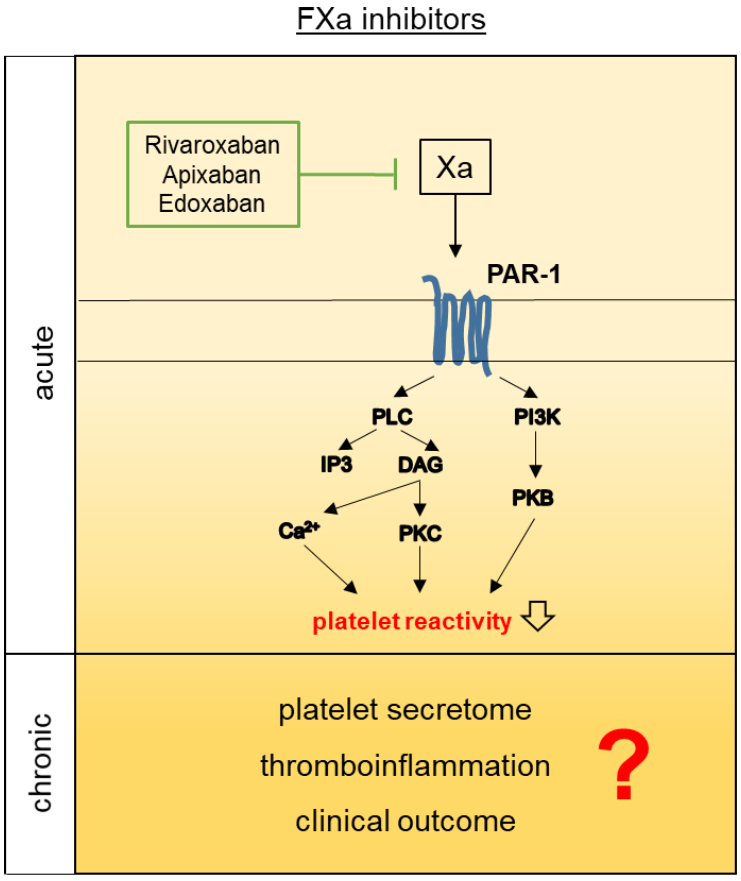

Figure 9: The impact of FXa inhibitors in acute and chronic setting.

Oral factor Xa (FXa) inhibitors reduce platelet reactivity by inhibiting FXa induced platelet activation of protease-activated receptor-1 (PAR1). PAR1 cleavage via FXa induces the activation of platelets via phospholipase C and phosphoinositide 3-kinase pathways. Chronic effects on platelet secretion, thromboinflammation and clinical outcome are poorly understood (adapted from Polzin et al, 2021).

2. Material and Methods

The materials used for the experiments as well as the manufacturers are listed below.

2.1 Material

2.1.1 Animals

The experimental animals used in this work were approved by the Landesamt für Natur, Umwelt- und Verbraucherschutz Nordrhein-Westfalen (LANUV NRW) under file number 81-02.04.2021.A001.

Male C57BL6/J mice obtained from Janvier Labs (53940 Le Genest-Saint-Isle, France) were used for this project. The animals were 11-13 weeks old and weighed 20-30 g. The experimental animals were kept and cared for by the specialized staff and on the premises of the Central Facility for Animal Research and Scientific Animal Welfare (ZETT) of Heinrich-Heine-University, Düsseldorf, Germany. All animals were kept according to the recommendations and specifications of the Federation of European Laboratory Animal Science Associations (FELASA) in a circadian 12 h day-night cycle at a room temperature (RT) of 22°C and a relative humidity of 50 %. Drinking water and food were available *ad libitum* to the animals.

2.1.1.1 Animal treatment

Mice were randomly divided into treatment and control groups. Chronic FXa inhibition was performed for five weeks. For this, RIVA was dissolved in phosphate-buffered saline (PBS) and administered every two days at a dose of 3 mg/kg body weight by oral gavage (Terry et al., 2016). Acute treatment was given at the same dosage for only two days. Animals from the control group received 1X PBS at the same interval.

2.1.2 Laboratory tools and equipment

2.1.2.1 Chemicals

Table 1: **Chemicals used for this study**

Chemicals	Company
Buprenorphine	Indivior, Chesterfield Court House (USA)
Bepanthen eye ointment	Bayer AG, Leverkusen
Bovine serum albumin	Sigma-Aldrich, St. Louis (USA)
BloxAll-Blocking solution	Vector laboratories, Peterborough (UK)
Chemiluminescent detection reagent (ECL)	Merck, Darmstadt
Citrate buffer (pH 6.0)	Thermo Fisher Scientific, Waltham (USA)
Collagen I	Sigma-Aldrich, St. Louis (USA)
Collagenase/Dispase	Sigma-Aldrich, St. Louis (USA)
Dulbecco's Modified Eagle's Medium	Sigma-Aldrich, St. Louis (USA)
DNaseI	Thermo Fisher Scientific, Waltham (USA)
Ethanol	VWR, Darmstadt
Evans Blue solution	Sigma-Aldrich, St. Louis (USA)
Fc-block reagent	Miltenyi Biotec, Bergisch Gladbach
Fetal calf serum	Sigma-Aldrich, St. Louis (USA)
Fibrillar collagen (5 µg/ml)	Chrono-Log Corporation, Havertown (USA)
Glycophorin A MicroBeads (130-050-501)	MACS Miltenyi Biotec, Bergisch Gladbach
Hematoxylin Gill II	Carl Roth, Karlsruhe
Isoflurane	CP-Pharma, Burgdorf
Ketamine	Zoetis, Berlin
Lysis Buffer	Zentralapotheke, Uniklinikum Düsseldorf
Mono-Poly-Resolving-Medium	Avantor, Radnor (USA)
NaCl 0.9 %	B.Braun, Melsungen
Octenisept	SCHÜLKE & MAYR, Norderstedt
Paraformaldehyde 4 %	Thermo Fisher Scientific, Waltham (USA)
Permanent mounting medium (H-5000)	Vector laboratories, Peterborough (UK)
PGI2, 500 ng/ml final concentration	Abcam, Cambridge (UK)
ProLong™ Diamond Antifade Mountant with DAPI	Thermo Fisher Scientific, Waltham (USA)
Rivaroxaban	ApexBio, Houston (USA)
Roticlear	Roth, Karlsruhe
Roti-Mount FluorCare (DAPI)	Roth, Karlsruhe
Sucrose	Sigma-Aldrich, St. Louis (USA)
Tissue Tek	Sakura Finetek, Umkirch
Triton X-100	Acros Organics, Waltham (USA)
Trypan blue	Sigma-Aldrich, St. Louis (USA)
Tween-20	Sigma-Aldrich, St. Louis (USA)
Xylazine	Bayer AG, Leverkusen
2,3,5-triphenyltetrazolium chloride solution	Sigma-Aldrich, St. Louis (USA)

2.1.2.2 Antibodies and primers

Table 2: Antibodies and primers used in this study

Antibody	Company
Anti-Histone3-antibody (ab1791)	Abcam, Cambridge (UK)
β-actin (13E5 Rabbit mAb HRP conjugated)	Cell Signaling, Danvers (USA)
CD3 APC	BioLegend, San Diego (USA)
CD4 PerCP/Cy5.5	BD Biosciences, Franklin Lakes (USA)
CD8 V500	BD Biosciences, Franklin Lakes (USA)
CD19 FITC	BioLegend, San Diego (USA)
CD45 MicroBeads	MACS, Miltenyi Biotec, Bergisch Gladbach
CD45 Pe-Cy7	BioLegend, San Diego (USA)
CD45 APC-Cy	BD Biosciences, Franklin Lakes (USA)
Donkey anti-goat Alexa488	Thermo Fisher Scientific, Waltham (USA)
Goat anti-Iba1	Abcam, Cambridge (UK)
Goat anti-mouse IgG-HRP conjugated	Bio-Rad Laboratories, Hercules (USA)
Goat anti-rabbit Alexa594	Thermo Fisher Scientific, Waltham (USA)
Goat anti-rat Alexa680	Thermo Fisher Scientific, Waltham (USA)
GPIb antibody (#R300)	Emfret, Eibelstadt
Human/mouse myeloperoxidase antibody	Bio-Techne, Minneapolis (USA)
IgG-control antibody (#C301), Emfret	Emfret, Eibelstadt
Ly6C APC	BD Biosciences, Franklin Lakes (USA)
Ly6G FITC	BioLegend, San Diego (USA)
phalloidin 488	Thermo Fisher Scientific, Waltham (USA)
Rabbit anti-CitH3	Abcam, Cambridge (UK)
Rabbit anti-goat Alexa647	Thermo Fisher Scientific, Waltham (USA)
Rat anti-Ly6G	Abcam, Cambridge (UK)
Rat anti-Mac-2	Cedarlane, Ontario (CAN)
Rat anti-mouse F4/80 PE	Bio-rad, Hercules (USA)
Rat anti-mouse Ly6G FITC	BD Biosciences, Franklin Lakes (USA)
TaqMan CD32 (Mm00438875_m1)	Thermo Fisher Scientific, Waltham (USA)
TaqMan CD16 (Mm00438882_m1)	Thermo Fisher Scientific, Waltham (USA)
TaqMan CD206 (Mm01329359_m1)	Thermo Fisher Scientific, Waltham (USA)
TaqMan GAPDH (Mm99999915_g1)	Thermo Fisher Scientific, Waltham (USA)
TaqMan IL-1β (Mm00434228_m1)	Thermo Fisher Scientific, Waltham (USA)
TaqMan IL-6 (Mm00446190_m1)	Thermo Fisher Scientific, Waltham (USA)
TaqMan IL 18 (Mm00434225_m1)	Thermo Fisher Scientific, Waltham (USA)
TaqMan TGF-β1 (Mm01178820_m1)	Thermo Fisher Scientific, Waltham (USA)
TaqMan Ym-1 (Mm04213363_u1)	Thermo Fisher Scientific, Waltham (USA)
vWF (1:1000; clone:M16.10A1)	Enzo Life Science, Farmingdale (USA)

2.1.2.3 Solutions

Table 3: Solutions used for this study

Solutions	Composition
DNase I-Mix	70 µl RDD Buffer + 10 µl DNase I stock
FACS buffer	500 ml 1X PBS, 10 ml FCS, 500 mg NaN_3
Percoll 100 %	100% Percoll (90 ml) with 10X PBS (10 ml)
Percoll 70 %	70% Percoll 100% (70 ml) with DMEM/FCS (30 ml)
Percoll 30 %	30% Percoll 100% (30 ml) with 1X PBS (70 ml)
Proteinase K- mixture	590 µl H_2O + 10 µl Proteinase K
RLT Mix	10 µl β-Mercaptoethanol (β-ME) + 1 ml RLT buffer
Sucrose 30 %	1X PBS, 300 g/l Sucrose (w/v)
Tyrode's Buffer	137 mM NaCl, 2.8 mM KCl, 12 mM NaHCO3, 5.5 mM glucose, 10 mM HEPES, pH = 6.5

2.1.2.4 Utensils

Table 4: Utensils used for this study

Utensils	Company
Aquasonic 100 gel	Parker Laboratories, Fairfield (UK)
Cannula 20 G, 0.9-40 mm	B.Braun, Melsungen
EDTA tubes	S-Monovette, Sarstedt
Electrode gel	Vyaire Medical, Höchberg
EzDNase synthesis kit	Thermo Fisher Scientific, Waltham (USA)
ImmPact DAB (SK-4105)	Vector laboratories, Peterborough (UK)
ImmPRESS- Goat Anti-Rat IgG (Mouse Adsorbed) Polymer Kit (MP-7444)	Vector laboratories, Peterborough (UK)
LEGENDplex mouse inflammatory panel	BioLegend, San Diego (USA)
LS Column	MACS, Miltenyi Biotec, Bergisch Gladbach
Microscope slides superfrost	Gerhard Menzel, Braunschweig
Microvettes 500	Saerstedt, Nümbrecht
MiniCollect Lithium Heparin	Greiner Bio-One, Kremsmünster (AUT)
QIAshredder	Qiagen, Hilden
RNeasy Mini Kit	Qiagen, Hilden
RNeasy Mini spin column	Qiagen, Hilden
Serotonin ELISA kit	Abcam, Cambridge (UK)
Vascular Occluder 10 mm, OC10	Kent scientific, Torrington (USA)
Vasofix Safety Cannula 20 G 1.1x25 mm	B.Braun, Melsungen
Veet depilatory cream	Reckitt Benckiser, Slough (UK)
0.1 M sodium citrate tubes EDTA tubes	S-Monovette, Sarstedt
21 G butterfly needle	Safety Multifly-Needle, Sarstedt
4-0 Prolene thread	Ethicon, Raritan (USA)
5-0 Prolene thread	Ethicon, Raritan (USA)
6-0 medium MCAO suture L910 PK10	Doccol corporation, Sharon (USA)
7-0 Prolene thread	Ethicon, Raritan (USA)
7-0 silk suture	Serag-Wiessner, Naila

2.1.2.5 Devices

Table 5: Devices used for this study

Devices	Company
Amersham ImageQuant 800	Cytiva, Marlborough (USA)
Animal operating table (50-1247)	Hugo Sachs, March
BD FACSverse Flow cytometer	BD Biosciences, Crystal Lakes (USA)
Bright field microscope Leica DM4000M	Leica Microsystems, Wetzlar
Centrifuge 5810 R (with swinging bucket Rotor with microplate adaptor)	Eppendorf, Hamburg
Confocal microscope LSM 800	ZEISS, O
Cryostat, Leica CM3050S	Leica Microsystems, Wetzlar
Cutting block	Kent Scientific, Torrington (USA)
Fluorescence microscope (DFC9000)	Leica Microsystems, Wetzlar
Light microscope DM6B	Leica Microsystems, Wetzlar
Millar catheter SPR-839, diameter 1.4F	ADInstruments, Sydney (AUS)
MiniVent Type 845	Hugo Sachs, March
Optical aggregometer (Model 700)	Chrono-Log Corporation, Havertown (USA)
Pressure calibration device (KAL 84)	Halstrup Walcher, Kirchzarten
Rectal thermometer (Testo 108)	Testo, Titisee-Neustadt
Rollerpump (RS232)	Ismatec, Grevenbroich
QuantStudio 7 Flex	Thermo Fisher Scientific, Waltham (USA)
Spectrophotometer DS-11-FX	DeNovix, Wilmington (USA)
Surface electrocardiogram (Powerlab 8/35)	ADInstruments, Sydney (AUS)
Vevo 3100	Fujifilm Visual Sonics, Toronto (CAN)
18-38 MHz MS400 transducer	Fujifilm Visual Sonics, Toronto (CAN)
30-70 MHz MS700 transducer	Fujifilm Visual Sonics, Toronto (CAN)

2.1.2.6 Software

Table 6: Software used for this study

Software	Company
Diskus View software	Technisches Büro Hilgers, Königswinter
Flow-Jo™	BD Biosciences, Franklin Lakes (USA)
GraphPad Prism	GraphPad Software Inc., San Diego (USA)
ImageJ	U.S. National Institutes of Health, Rockville (USA)
LabChart Pro7	ADInstruments, Sydney (AUS)
Leica Application Suite X (LASX)	Leica Microsystems, Wetzlar
LEGENDplex data analysis software	BioLegend, San Diego (USA)
VevoLab	Fujifilm Visual Sonics, Toronto (CAN)
ZEN blue, ZEN black software	ZEISS, Oberkochen

All other devices used corresponded to the usual laboratory standard.

2.2 Methods

2.2.1 Ischemia/reperfusion injury for induction of an acute myocardial infarction

The method of ischemia/reperfusion (I/R) injury is a surgical intervention for the induction of an AMI in mice (Polzin et al., 2022). Half an hour before the injury, the experimental animal received an analgesia with buprenorphine (0.1 mg/kg subcutaneous (s.c.). After 30 minutes, the anesthesia of the mouse was induced. The mouse was placed in an airtight chamber and anesthetized with 3 % Isoflurane in room air. A lack of reflexes between the mouse toes indicated complete anesthesia and the mouse was intubated afterwards with a Vasofix Safety Cannula (20 G 1.1 x 25 mm). The anesthesia of the intubated animal was performed continuously via MiniVent murine respirator with 2 % isoflurane in room air enriched with 40 % oxygen. To prevent cooling of the animal, the mouse was placed on a heated small animal operating table and the temperature was controlled permanently by a rectal thermometer. Furthermore, a surface electrocardiogram (ECG) was used to monitor the success of the surgery. In addition, Bepanthen eye ointment containing dexpanthenol was applied to the eyes to prevent drying of the cornea. Echocardiographic examinations prior to this procedure were done to have baseline data of the heart function. Because of this, the thorax was already depilated. After completion of all preparations, the thorax was opened between the third and fourth ribs and the heart was exposed. Ribs were opened and the heart was dissected free. The left anterior descending coronary artery (LAD) was undercut and looped with a 7-0 Prolene thread. Both ends of the suture were pulled through a thin plastic tubing, so that the plastic tubing stopped the blood flow through the artery and induced ischemia. After 30 minutes of ligation of the LAD, the reperfusion phase followed. The plastic tubing was removed and the ends of the suture were looped into a loose knot. The thread had to remain in the puncture site to allow subsequent infarct sizing afterwards. The ribs were closed with a 4-0 silk thread and the skin was sutured with 5-0 Prolene. After completion of the operation, the suture was disinfected with Octenisept. The mouse was extubated and kept under a heat lamp in a holding cage until complete awakening. Postoperatively, the mouse received buprenorphine (0.1 mg/kg s.c.) for analgesia, which was administered at 4 hour intervals in the light phase (7-19 h) and at night by drinking water (0.009 mg/ml) for a minimum of two and a maximum of three days, depending on the experimental protocol.

2.2.2 Closed-chest murine model of AMI

In platelet depleted mice, it was not possible to perform the above described open-chest I/R injury of AMI due to increased bleeding during the process. Alternatively, a closed-chest model of AMI was used for this experimental procedure with less risk of bleeding. Mice were anesthetized via intraperitoneal injection of ketamine (Ketanest, 100 mg/kg body weight) and xylazine (Rompun, 10 mg/kg body weight) 20 minutes before surgery. After intubation, the LAD was looped, but not ligated, with 7-0 silk suture which is passed through a thin plastic tubing, as described above. At the end of this procedure, the suture was stored under the skin of the mice. Five days later, platelet depletion was induced by intravenous injection of the tail vein with a GPIb antibody (2 µg/g) 24 h before an AMI was induced. Corresponding IgG-control antibody (2 µg/g, #C301) was used for control mice without depletion. After successful anaesthesia with isoflurane (2 vol%) AMI was induced by gently pulling the applied suture under the mice' skin until typical ST-elevation appeared on the ECG. After 30 minutes of LAD ligation, the suture war loosened and reperfusion was confirmed on the ECG. The mouse was extubated and kept under a heat lamp in a holding cage until complete awakening. Postoperatively, the mouse received buprenorphine (0.1 mg/kg s.c.) for analgesia, which was administered at 4 h intervals in the light phase (7-19 h) and at night by drinking water (0.009 mg/ml) for a minimum of two and a maximum of three days, depending on the experimental protocol.

2.2.3 Electrocardiogram (ECG)

ECG recording was performed during the whole process of the I/R injury to confirm an ischemia followed by a reperfusion of the mouse myocardium (Scofield et al., 2016). The ECG was recorded immediately after sufficient anesthesia of the animal via two clamping electrodes on each front paw as well as one on a hind paw. Electrodes were connected with the PowerLab (8/35), supported by the LabChart Pro 7 software.

2.2.4 Murine transthoracic echocardiography

To assess cardiac function, echocardiographic examinations were performed at defined time points before and after induction of AMI (Dannenberg et al., 2021). For this purpose, the experimental animal was placed in an airtight chamber and exposed to an air mixture of 3 % Isoflurane, 40 % oxygen and 57 % room air. After reaching an adequate depth of anesthesia, tested by a lack of inter-toe reflex, the animal was positioned supine on a pre-warmed derivation plate. Anesthesia was thereby maintained via a nasal mask containing 2 % Isoflurane, 40 % oxygen and 58 % room air. The animal was restrained at the extremities on

the ECG contact sites. For this purpose, a small amount of electrode gel was applied to the ECG contact sites in advance. Internal body temperature was controlled by a rectal thermometer and maintained at 37-38°C. Bepanthen eye ointment containing dexpanthenol was applied to prevent drying of the eyes. The vital signs of the mouse were monitored continuously. After completion of the preparations, Veet depilatory cream was applied in the thoracic region and depilated after a short exposure time. To ensure proper coupling of the transducer, pre-warmed Aquasonic 100 ultrasound gel was applied to the thorax without air bubbles. This was followed by imaging of the parasternal long axis (PSLA, (**Fig. 10**) and parasternal short axis (SAX) of the left ventricle using a high-resolution Vevo 3100 ultrasound unit and an 18-38 MHz MS400 transducer. After completion of the recordings, inhalation anesthesia was turned off and the experimental animal was returned to a holding cage, kept under a heat lamp until full awakening. The analysis was performed in the 3.2.6 VevoLab software. The endo- and epicardial boundaries were drawn manually, the stroke volume (µl) (SV) (formula 1), the cardiac output (ml/min) (CO) (formula 2), the average shortening (fractional shortening (%) (FS)) (formula 3) and the ejection fraction (%) (EF) (formula 4) as well as the end-systolic and end-diastolic volume (ESV and EDV) of the left ventricle, on the other hand, are measured and calculated automatically.

Formula 1 Calculation of the stroke volume:

$$SV\ (\mu l) = EDV\ (\mu l) - ESV\ (\mu l)$$

Formula 2 Calculation of the cardiac output:

$$CO\ \left(\frac{ml}{min}\right) = heartrate\ \left(\frac{1}{min}\right) * SV\ (\mu l) * 0.001$$

Formula 3 Calculation of the fractional shortening:

$$FS\ (\%) = \frac{EDV\ (\mu l) - ESV\ (\mu l)}{EDV\ (\mu l)} * 100$$

Formula 4 Calculation of the ejection fraction:

$$EF\ (\%) = \frac{SV\ (\mu l)}{EDV\ (\mu l)} * 100$$

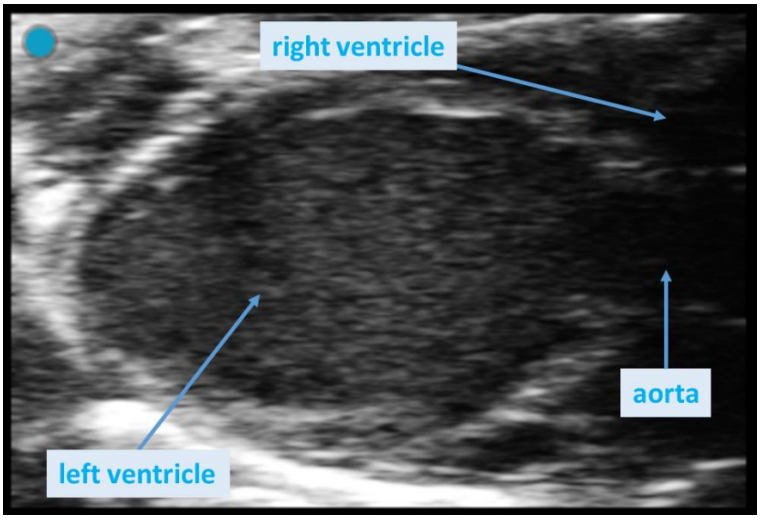

Figure 10: Exemplary echocardiographic image of a murine heart.

The left and the right ventricle and the aorta can be observed in this image. The image shows the parasternal long axis of a murine heart.

2.2.5 Transient middle cerebral artery occlusion

The transient middle cerebral artery occlusion (tMCAO) injury allows a targeted induction of a stroke in the mouse brain. After prior induction of anesthesia with 5 % isoflurane in an anesthesia chamber, the mouse received an inhalation anesthesia with nitrous oxide/oxygen (2:1) with isoflurane (2 vol.%), while lying on the operation table. For analgesia, a dose of buprenorphine (0.1 mg/kg; s.c) was administered subcutaneously 20-30 minutes before the procedure. In addition, the eyes are protected from dehydration with Bepanthen eye and nasal ointment. After sufficient anesthesia, the experimental animal is fixed lying on its back on an operating table warmed to 37°C and disinfected with Octenisept. Subsequently, the brain-supplying right carotid artery, the *Arteria carotis communis*, is exposed via a ventromedian skin incision of 10-15 mm in the neck. The bifurcation of the right carotid artery into the *A. carotis interna* and *externa* was visited and exposed as well (**Fig. 11**). This was followed by ligation of both the *A. carotis communis* and the *A. carotis externa* using 4-0 silk. Through a third suture the *A. carotis interna* was sutured, which temporarily cut off the blood supply to the vessel. A 6-0 medium MCAO suture was inserted via a small incision in the temporarily ligated vessel. The suture was advanced cephalad ward to the initial portion of the middle cerebral artery (MCA), which is occluded by the suture tip. The successful occlusion of the vessel was visible from the clinical assessment made using the Bederson score. Subsequently, the suture was fixed to the vessel, the skin was closed with a skin suture and the anesthesia was terminated. This process of waking up is especially important for the clinical evaluation, since the first conclusions about a successfully performed surgery on the basis of the "circling" could be

drawn. After 60 minutes, under renewed isoflurane anesthesia, the skin was reopened, the suture was pulled out and the neck vessel is closed so that blood flow in the middle cerebral artery is restored. Again, the skin was closed with suture and the anesthesia was terminated. The duration of anesthesia for inserting the suture was about 15 minutes and for pulling out the suture was about 10 minutes. Because the procedure was performed under anesthesia followed by analgesia, the stress for the animals was classified as moderate. Analgesia was provided every 4 hours with buprenorphine (0.1 mg/kg s.c.) in the light phase on the day of surgery and additionally it is provided continuously in the drinking water (0.009 mg/ml), to relieve wound pain (Gliem et al., 2012; Gliem et al., 2015). Mice were sacrificed 24 h post injury and brains were stained with 2,3,5-triphenyltetrazolium-chloride (TTC) staining, like described below. The experiments were performed with the assistance of Dr. Lilian Vornholz from the cardiovascular research laboratory of the University Hospital Düsseldorf and Dr. Goran Pavic from the Department of Neurology from the University Hospital Düsseldorf.

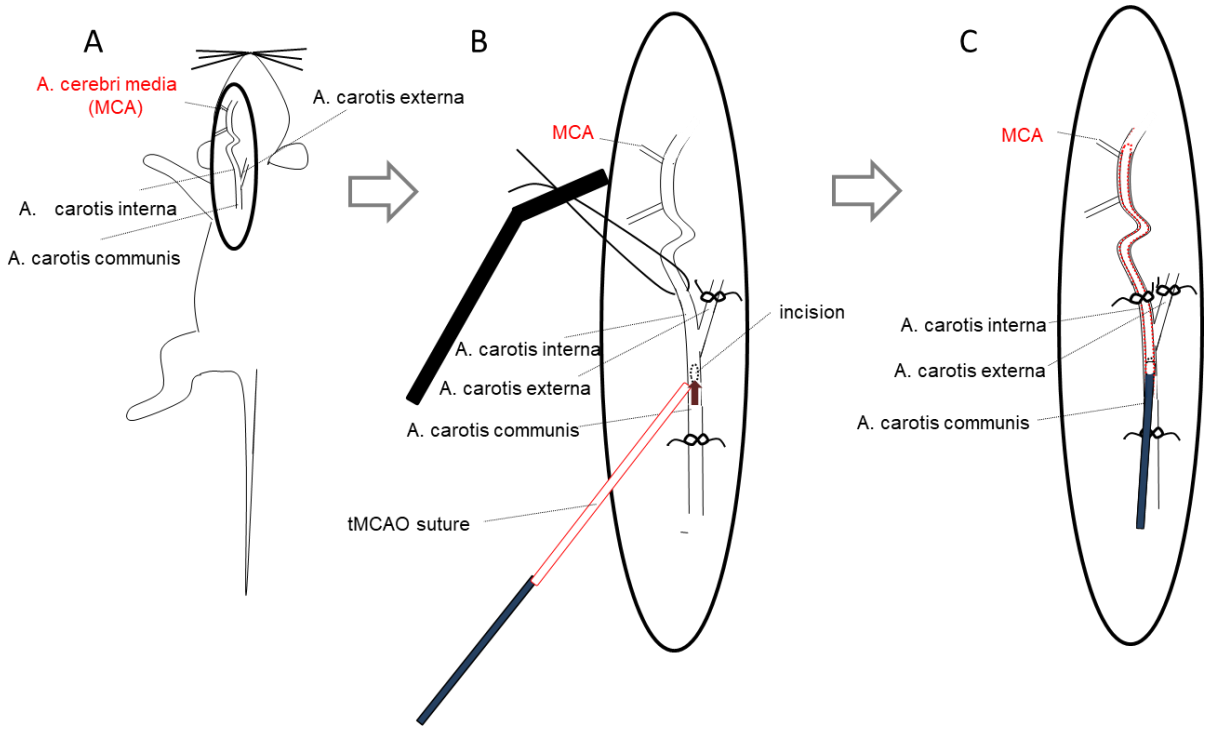

Figure 11: Schematic drawing of the surgical method of transient occlusion of the middle cerebral artery (tMCAO) for stroke induction in mice.

(A) A mouse is shown in the supine position, with the surgical area in focus. (B) surgical area: The *Arteria* (*A.) carotis communis* is shown in the lower section, which bifurcates into the *A. carotis externa* and *interna*. Following the *A. carotis interna* brainwards the *A. cerebri media* was shown labeled in red. After ligation of the *A. carotis communis* and *externa*, and snaring of the *A. carotis interna*, an incision was made in the common carotid artery through which the tMCAO suture was inserted. (C illustration of the inserted and fixed tMCAO suture occluding the middle cerebral artery (modified from doctoral thesis of Dr. Lilian Vornholz (Vornholz, 2019)).

2.2.6 Behavioral testing/ scoring in experimental stroke research

Each tMCAO-operated animal was examined after full awakening from anesthesia and 24 hours after surgery. This was done using a "score sheet" with predetermined termination criteria. The body weight, general condition and spontaneous behavior were assessed. A clinical neurological assessment was performed one hour and 24 hours postoperatively as well, using the Bederson score (Bieber et al., 2019). This involves placing the animals on a pad and observing their spontaneous movements.

Table 7: Neurological score according to Bederson for mice after transient middle cerebral artery occlusion.

Score	Description
0	no observable deficit
1	forelimb flexion
2	forelimb flexion and decreased resistance to lateral push
3	circling or turning around the longitudinal axis
4	circling and spinning around the cranial-caudal axis
5	no spontaneous movement

2.2.7 Flow-mediated dilatation

After 5 weeks of treatment with a FXa-inhibitor, the experimental animals underwent a flow-mediated dilatation (FMD) measurement (Heiss et al., 2008; Q. Chen et al., 2013). With this method, the endothelial function could be investigated. The mouse was placed in an airtight chamber with isoflurane (3 % by volume). When complete anesthesia has been achieved by checking the reflexes between the toes, the mouse was transferred to a heated examination table. While lying on the table the anesthesia was continued via face mask (isoflurane 2 vol.% in 40 % oxygen-enriched room air). The mouse extremities were fixed with adhesive tape on the tables ECG electrodes for the purpose of ECG derivation. Electrodes were covered with electrode gel before. The mouse body temperature was kept at 37°C, checked via application of a rectal thermometer. All hair on the left hind leg was removed with hair removal cream at the beginning of the examination. A vascular occluder (10 mm) was then applied for pressure-controlled occlusion of the femoral artery. To establish the necessary pressure in mmHg within the occluder, a pressure calibration device was used. To further enhance vascular imaging, bubble-free and pre-warmed Aquasonic 100 ultra sound gel was applied to the thigh. Noninvasive measurement of FMD was performed using a VEVO 3100 high-resolution

ultrasound device and a 30-70 MHz transducer (MS 700). During the sonographic measurement of FMD, the *A. iliaca externa* was searched and the vascular occluder then inflated to 300 mmHg, thereby occluding the arterial flow of the hind leg for exactly 5 minutes. After 5 minutes of occlusion, the hind leg was reperfused by releasing the previously applied pressure cuff. At 30-second intervals, native images of the *A. iliaca externa* were taken for further 5 minutes to document possible vasodilation. After completion of the recordings, the anesthesia was released. The animal was returned to the holding cage and kept under a heat lamp until complete awakening. Until further experiments can be performed on the animal, the animal is allowed a regeneration period of at least 24 hours. Post processing analyses were performed offline using the VevoLab 3.2.6. software.
After a recovery period of at least 24 hours, invasive blood pressure measurement can be performed in the same mouse using a Millar catheter. Since a spatial union of both methods is not possible, the pressure-volume measurement cannot be performed immediately afterwards. For this reason, the mice are allowed to recover.

2.2.8 Pressure-volume measurement

The method for pressure-volume measurement in the mouse allows accurate monitoring of hemodynamic parameters in the aorta and the heart via catheter (Zhao et al., 2011; Erkens et al., 2015). Thirty minutes before starting the preparation, the animal received analgesic buprenorphine (0.1 mg/kg bw , i.p.). For induction of anesthesia, the mouse was placed in an airtight chamber with isoflurane (3 vol.% in room air enriched with 40 % oxygen). Anesthesia was maintained via a nasal mask (2 vol.% isoflurane). After sufficient anesthesia, fixation of the experimental animal was performed lying on its back on an operating table warmed to 37°C. A lack of reflexes between the mouse toes indicated complete anesthesia. Skin incision with a length of approximately 1.5 cm was done ventrally on the right side of the neck at the level of the larynx, followed by exposure of the *A. carotis communis* with careful sparing of surrounding vessels and nerves, especially the vagus nerve. The *A. carotis communis* was ligated immediately proximal to the carotid bifurcation with 5-0 silk. The position of a vascular clamp approximately 1-2 cm proximal to the vascular ligation followed. Careful incision of the vessel wall in the area of the vessel site previously eliminated from blood circulation by ligation and vascular clamping was performed. After opening of the cranially positioned vascular clamp, the catheter was carefully advanced until the corresponding aortic blood pressure signal was recorded (**Fig. 12**). The systolic (P_{sys}), diastolic (P_{dias}) and mean arterial pressure (MAP) were recorded.

Mean arterial pressure (MAP) calculations were performed as follows:

Formula 5 Calculation of the mean arterial pressure (MAP):

$$MAP\ (mmHg) = P_{dias}(mmHg) + \frac{1}{3}\ (P_{sys}\ (mmHg) - P_{dias}\ (mmHg))$$

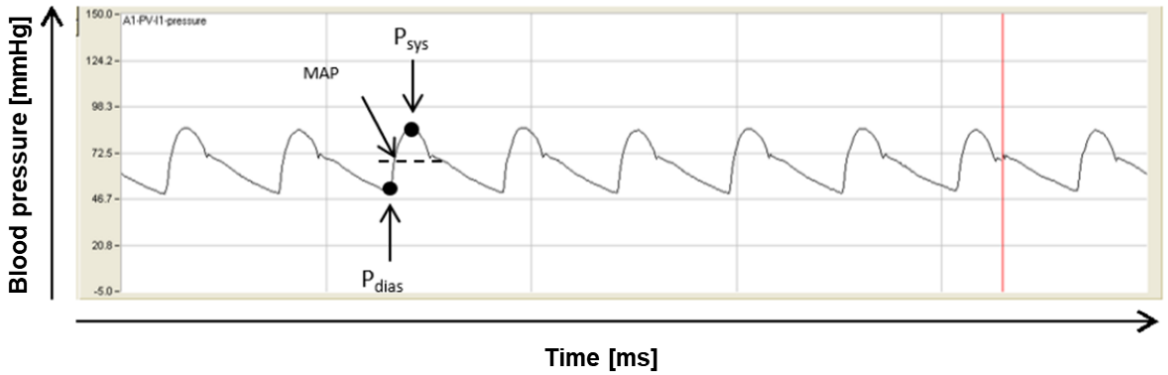

Figure 12: Blood pressure curve of a mouse measured with a Millar catheter system.

This figure shows an example of a section of a blood pressure trace recorded in a mouse using a Millar catheter system. P_{sys}= systolic arterial blood pressure, P_{dias}= diastolic arterial blood pressure, MAP= mean arterial blood pressure (Vornholz, 2019).

The catheter was removed and the common carotid artery was ligated proximal to the incision site with 5-0 silk. The isoflurane supply was increased to 5 vol.% and anesthesia was thus deepened. Finally, the animal was killed by exsanguination through final blood sampling and simultaneous organ removal.

2.2.9 Blood collection from mice

The experimental animal was weighed and anesthetized according to its weight with ketamine (Ketanest, 100 mg/kg, i.p.) and xylazine (Rompun, 10 mg/kg, i.p.). With adequate depth of anesthesia and a lack of the inter-toe reflex, the animal was positioned on the table and blood was extracted from the retro bulbar sinus via a heparinized glass cannula (Van Herck et al., 2001). Blood was collected in MiniCollect Lithium Heparin tubes for fluorescence activated cell sorting experiments and inverted properly to avoid clotting of blood components until the experiments started. Murine blood, which was needed to perform proper blood count, was collected in EDTA microvettes 500.

2.2.10 Transcardial perfusion

A transcardial perfusion was used to prepare the brains either for fluorescence activated cell sorting or histology and the hearts only for histology (Gage et al., 2012; Wu et al., 2021). This method ensures that no resting cells in the smallest blood vessels of an organ give false results, because only tissue resident cells should be investigated. The experimental animals were weighed and anesthetized according to the weight with ketamine (Ketanest 100 mg/kg, i.p.) and xylazine (Rompun 10 mg/kg, i.p.). The reflexes of the mice were controlled via pinching the toes to check the depth of the anesthesia. They were fixed on a styrofoam board afterwards and the abdominal cavity was opened with a scissor upwards to the sternum until the heart was exposed. Subsequently, the perfusion needle was stung in the left ventricle and the right atrial auricle was cut open. To flush the heart and remove all blood, even from the smallest vessels, 1X PBS was passed through the body's circulatory system for 10 minutes with the aid of a roller pump. After only clear fluid left the perforated atrial auricle and the liver was fully decolorated, hearts, which were used for histological analysis, were cut out carefully and put in 15 ml falcon tubes, filled with 5 ml of 4 % paraformaldehyde (PFA). After fixing the hearts over night at 4°C, they were transferred to falcon tubes with 30 % sucrose in 1X PBS and stored until they sink.

For brains which were used for histological investigations the body was flushed for a second time with another additional solution. The flushing solution was 4 % PFA to fix the tissue for around 20 minutes. When the tissue became firm, brains were removed and post fixed in a falcon tube filled with 4 % PFA overnight in the refrigerator. After post fixation, the brains were transferred to a falcon tube containing 30 % of sucrose in 1X PBS and stored until they sink. Sucrose serves as a dehydration agent to remove all water from the tissue and to cryoprotect the brains.

2.2.11 Fluorescence Activated Cell Sorting (FACS)

Flow cytometry enables the counting and analysis of individual cell populations within a sample. With the aid of fluorescent dyes, it is possible to label a wide variety of cells within a sample and then sort and analyze them. The fluorescent dyes are coupled to specific antibodies, which in turn can bind to specific surface structures of cells.

2.2.12 FACS of inflammatory cells in murine blood

After collecting blood from the retro bulbar sinus of a mouse, 900 µl of Mono-Poly-Resolving-Medium were added to 500 µl of blood. The tubes were centrifuged with 300 g at RT for 45 minutes without brake. Afterwards, the obtained cells were washed one time with 1X PBS and centrifuged with 500 g at 4°C for 10 minutes. The supernatant was discarded and the obtained cells were resuspended with Lysis Buffer and incubated for 10 minutes at RT, followed by another centrifugation step with the same previous conditions. The cell pellet was resuspended with 400 µl of 1X PBS and incubated at 4°C for 20 minutes in the dark, with the following antibodies: CD45-PE-Cy7 (Phycoerythrin) to detect leukocytes, CD19-FITC (fluoresceinisothiocyanate) for B-cells and CD3-APC for T-cells. CD3 and CD19 were gated from CD45. To detect T-helper cells CD4-PerCP/Cy5.5 was used and for T-killer cells CD8-V500. Ly6G-FITC to detect the granulocytes was gated from CD45 and divided in Ly6G+ and Ly6G-. Ly6C-APC was gated from Ly6G- for the inflammatory monocytes represented as Ly6C++ and the non-inflammatory monocytes were represented as Ly6C+ (**Fig. 13**). All previous antibodies were diluted 1:100 in 1X PBS and distributed regarding the FACS panels. Two hundred µl of every sample were stained with 50 µl of antibodies mix with 1X PBS. The incubated samples were centrifuged for 10 minutes with 500 g at 4°C. Finally, the pellets were resuspended with 200 µl 1X PBS and measured with BD FACSVerse™ flow cytometer. Data were processed and analysed using Flow-Jo™ software.

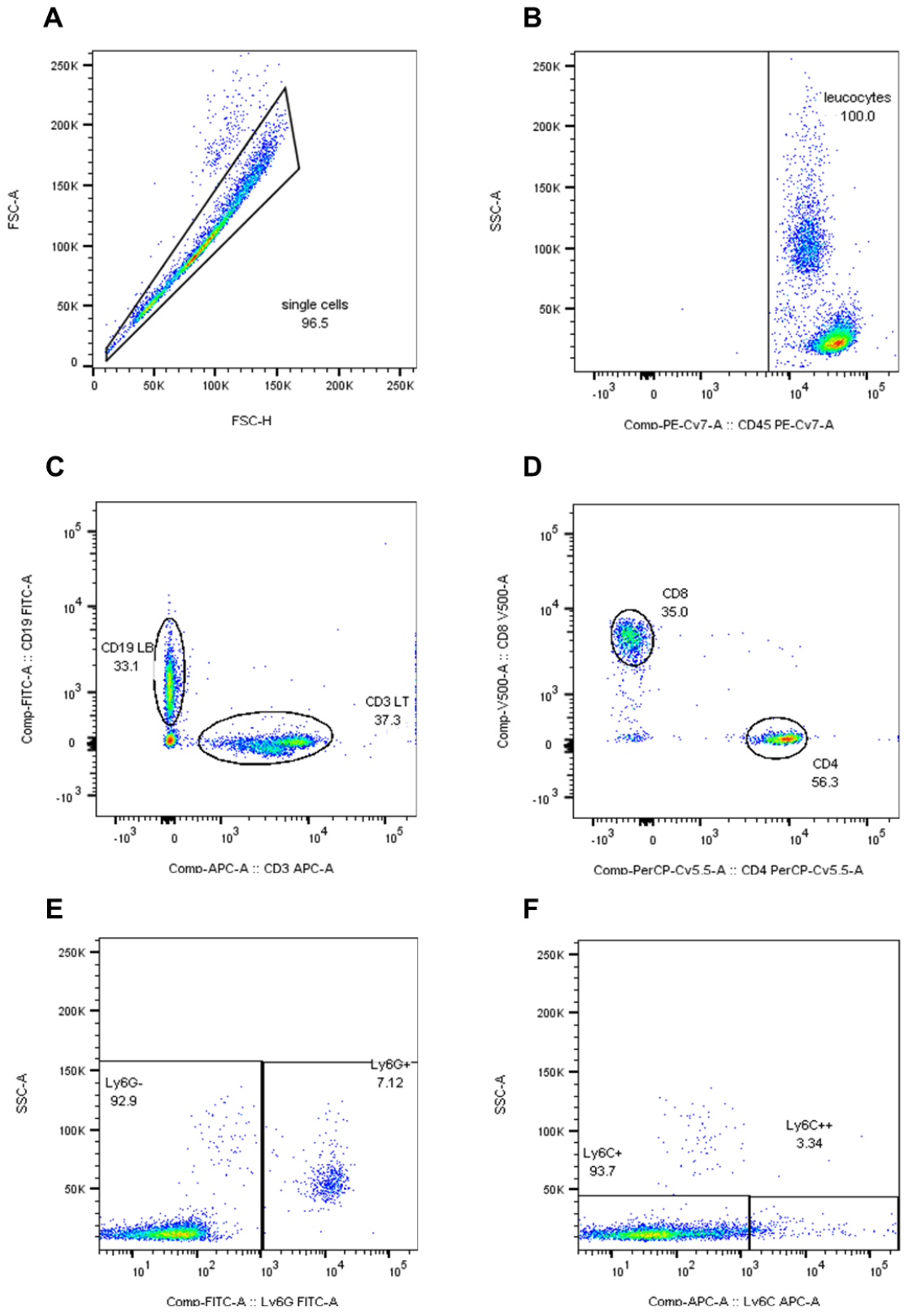

Figure 13: Gating strategy for FACS of inflammatory cells in murine blood.

(A) The panel shows all recorded cells. (B) To detect leukocytes, CD45 was gated. (C) CD19 and CD3 were used to divide between B-cells and T-cells. CD3 and CD19 were gated from CD45. (D) To detect T-cells CD3 was used. Further division of T-cells in T-helper cells via CD4 and T-killer cells via CD8 was done. (E) Ly6G for granulocytes was gated from CD45 and divided in $Ly6G^{+}$ and Ly6G-. (F) Ly6C was gated from $Ly6G^{-}$ for the inflammatory monocytes represented as $Ly6C^{++}$ and the non-inflammatory monocytes were represented as $Ly6C^{+}$.

2.2.13 FACS of intracerebral leukocytes

To remove all circulating cells in the brain vessels and to investigate only tissue resident cells, a transcardial perfusion with 1X PBS (**Fig. 14**) was used to prepare brains for FACS analysis. The perfused brain was removed from the scull carefully and divided via medial incision into two parts using a scalpel. The anterior side was discarded in each case and the posterior side was again divided into two parts. These left parts of the infarcted side and the contralateral side were used for further examination (Chu et al., 2014). Each well of a 24-well plate was filled with 625 µl Dulbecco's Modified Eagle's Medium (DMEM) and 10 % fetal calf serum (FCS). Brain samples were then added to the wells and homogenized with scissors. Additional mixing was performed using a syringe with a cannula (20 G, 0.9-40 mm). 125 µl Collagenase/Dispase (10 mg/ml) was added to the tissue mixture. The 24-well plate was then incubated for 45 minutes at 37°C in an incubator. After the incubation period, 25 µl DNase I (10 mg/ml) was added and everything was thoroughly resuspended. Another incubation step was done for 45 minutes at 37°C. Afterwards the cell suspension was transferred to a 15 ml falcon tube and washed with 5 ml DMEM/FCS. The mixture was then transferred to a 70 µm cell strainer and the collected liquid was centrifuged for 10 minutes with 300 g and at 4°C. The supernatant was discarded afterwards. Cells were taken up in a total of 5 ml of 70 % Percoll. First, 500 µl of 70 % Percoll were added to the cells and everything was homogenized with a pipette. Then, the remaining 4.5 ml of 70 % Percoll were added to the same tube. To create a gradient, another layer of Percoll was added very carefully. This had a concentration of 30 % Percoll. To perform a density centrifugation, the cells were centrifuged for 25 minutes with 1200 g at RT. The acceleration was adjusted at 7 and the brake at 0. The centrifuge was cooled down to 4°C beforehand and then upregulated to RT due to vibration. After centrifugation, the myelin layer was removed with a Pasteur pipette and approximately 3 ml of the interphase were also aspirated. The remaining liquid was filled up to 10 ml with DMEM/FCS. Furthermore, another step of centrifugation was performed for 15 minutes with 500 g at 4°C. The supernatant was discarded afterwards and the pellet was washed in FACS buffer (500 ml 1X PBS, 10 ml FCS, 500 mg NaN_3). After another centrifugation for 10 minutes with 300 g at 4°C, the supernatant was also discarded and the pellet was taken up in 500 µl FACS buffer. The cell number was determined afterwards by using Trypan blue 0.4 % (1:1). The counted cells were diluted to 3 ml with FACS buffer and distributed to FACS tubes. Each FACS tube was filled up to 2 ml with FACS buffer. Tubes were then centrifuged at 300 g for 10 minutes at 4°C. The supernatant was discarded and 25 µl Fc-block reagent (1:25) was added to all tubes and vortexed. Cells were incubated for 15 minutes at 4°C. The tube was then filled up to 2 ml with FACS buffer. Centrifugation was repeated for 10 minutes at 300 g and 4°C and the supernatant was discarded. Coupled antibodies were added (25 µl each with a dilution of 1:50) and incubated for 30 minutes at 4°C. The used antibodies were: Rat anti

Mouse F4/80 PE coupled for microglial detection, rat anti-mouse Ly6G FITC coupled for detection of granulocytes and CD45 APC-Cy7 (Allophycocyanin-cyanin) coupled for detection of leukocytes 2 ml FACS buffer were added and vortexed thoroughly. Tubes were centrifuged for 10 minutes at 300 g and 4°C. The supernatant was discarded, and cells were dissolved in 500 µl FACS buffer. Briefly, the cells of brain suspension were analysed with the BD FacsVerse™ flow cytometer. A loose gate was drawn to exclude the cell debris in the left corner of the FSC-A/SSC-A plot. Single cells were gated using the FSC-H/FSC-A plot. Dead cells were identified as 4',6-diamidino-2-phenylindol+ (DAPI+) and excluded in the analysis. CD11b+ and Ly6G- leukocytes were further differentiated into monocytes and macrophages (Mo/Mp) with a high CD45 expression (CD45++) and microglia with a lower CD45 expression (CD45+). Granulocytes were gated as Ly6G+ and Ly6C-. All values were shown as percentages of all living cells. Data were processed and analysed using Flow-Jo™ software.

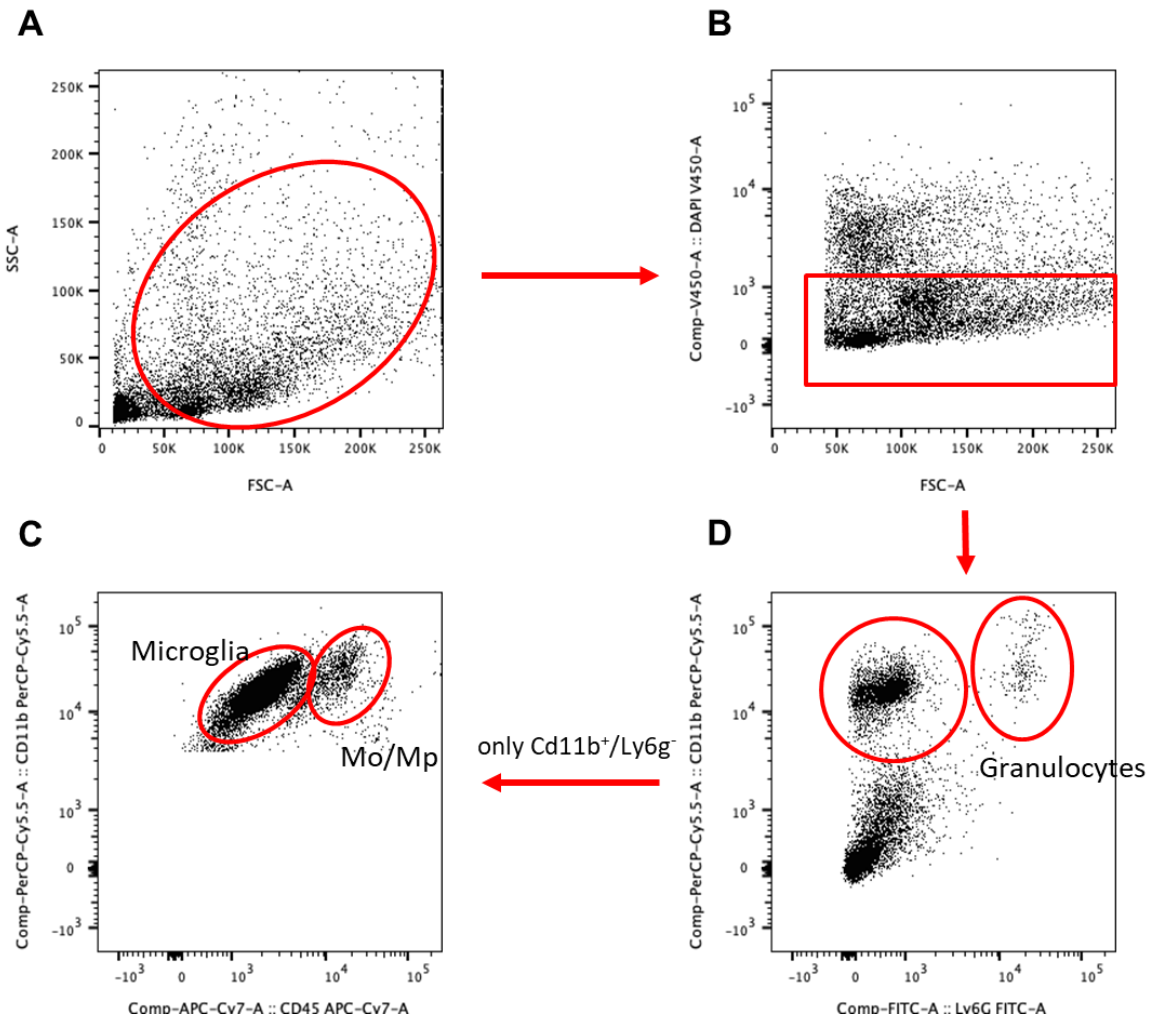

Figure 14: Gating strategy for FACS of intracerebral leukocytes in murine brains after tMCAO.

(A) A loose gate was drawn to exclude the cell debris in the left corner of the FSC-A/SSC-A plot. (B) Single cells were gated using the FSC-H/FSC-A plot and dead cells were identified as 4',6-Diamidino-2-phenylindol+ (DAPI+) and excluded in the analysis. (C) CD11b+ and Ly6G- leukocytes were further differentiated into monocytes and macrophages (Mo/Mp) with a high CD45 expression (CD45++) and microglia with a lower CD45 expression (CD45+). (D) Granulocytes were gated as Ly6G+ and Ly6C-. All values were shown as percentages of all living cells.

2.2.14 Real time polymerase chain reaction (qPCR) of murine brains after tMCAO

Ribonucleic acid (RNA) was isolated from infarcted brain hemispheres with the RNeasy Mini Kit. A maximum of 30 mg per sample was used to avoid overloading of the RNeasy spin column. The brain hemispheres were disrupted by using a TissueRuptor. The lysate was homogenized in 300 µl RLT buffer (10 µl β-Mercaptoethanol (β-ME) + 1 ml RLT buffer). Following, 400 µl of the lysate was transferred into QIAshredder and centrifuged for two minutes at 13200 g. The supernatant (300 µl) was transferred into a fresh 1.5 ml tube and 600 µl of Proteinase K- mixture (590 µl H2O + 10 µl Proteinase K) were added. After a ten-minute

incubation at 55°C, the sample was centrifuged for three minutes at 10000 g. Accordingly, 900 µl of the supernatant was transferred into a fresh 2 ml tube and 450 µl of 96-100 % absolute ethanol were added. The mixture was vortexed thoroughly and 700 µl were then transferred to RNeasy Mini spin column, where the RNA bound to the silicate column. After centrifugation of the column at 10000 rpm for 15 seconds, the flow-through was discarded. Also the remainder of the mixture, approximately 650 µl, were transferred to the columns and centrifuged at 10000 rpm for 15 seconds. 350 µl of RW1 buffer was added to the column and centrifuged at 10000 rpm for 15 seconds. Furthermore, 80 µl DNase I-Mix (70 µl RDD Buffer + 10 µl DNase I stock) were put directly onto the silicate column and incubated for 15 minutes at RT. Subsequently 350 µl RW1 buffer was added to the column and the tube was centrifuged at 10000 rpm for 15 seconds. Two times of adding 500 µl RPE buffer to the column and centrifugation at 10000 rpm for 15 seconds followed. 500 µl RPE buffer were added to the column and it was centrifuged at 10000 rpm for two minutes. A new collection tube was placed under the column and was centrifuged empty at 13200 g for one minute. The column was placed in a new and labeled 1.5 ml tube and 30-50 µl RNase free water was pipetted directly into the silicate column and incubated for five minutes. With the next centrifugation step of 10000 rpm for one minute, the column was eluted. For RNA quality and quantity control a maximum of 5 µl was transferred into a new tube and measured afterwards with a spectrophotometer. Afterwards the RNA was reverse transcribed with the SuperScript IV VILO Master Mix with ezDNase synthesis kit. To remove a possible genomic deoxyribonucleic acid (gDNA) contamination from template RNA, ezDNase was used in the first step. A digestion-reaction-mix was prepared, containing 1 µl of 10X ezDNase buffer, 1 µl ezDNase enzyme, a varied volume of template RNA (1 pg to 2.5 mg total RNA) an was filled up to 10 µl with nuclease-free water, for one sample. The solution was gently mixed and incubated at 37°C for two minutes. After that the reaction was briefly centrifuged and placed on ice. Into the reaction tube, 4 µl of SuperScript IV VILO Master Mix and 6 µl nuclease-free water were added. The tube was gently vortexed and incubated at 25°C for 10 minutes, followed by an incubation at 50°C for 10 minutes and another incubation step at 85°C for 5 minutes. The created cDNA was used for real time PCR with the QuantStudio 7 Flex. The qPCR was performed using the following protocol: preheating up to 95°C, followed by 40 amplification cycles: 20 seconds at 95°C, 20 second at 60°C. Real time PCR was conducted with TaqMan Fast Advanced Master Mix and pre-manufactured primers. Data were analyzed as x-fold change with the $2^{-\Delta\Delta CT}$ method. Glycerinaldehyde-3-phosphate-dehydrogenase (GAPDH) was used as housekeeping gene. TaqMan primers used: GAPDH (Mm99999915_g1), TNF (Mm00443258_m1), CD16 (Mm00438882_m1), CD32 (Mm00438875_m1), TGF-β1 (Mm01178820_m1), CD206 (Mm01329359_m1), Ym-1 (Mm04213363_u1), IL-1β (Mm00434228_m1), IL-6 (Mm00446190_m1), IL 18 (Mm00434225_m1).

2.2.15 LEGENDplex inflammatory assay

The analysis of inflammatory cytokines was performed with the LEGENDplex mouse inflammatory panel (13-plex). The panel allows simultaneous quantification of 13 mouse cytokines, including IL-1α, IL-1β, IL-6, IL-10, IL-12p70, IL-17A, IL-23, IL-27, CCL2 (MCP-1), IFN-β, IFN-γ, TNF-α, and GM-CSF. For the inflammatory assay, platelet poor plasma from mice 24 hours or five days post AMI was generated via centrifugation. Whole blood was collected in heparinized tubes and centrifuged for 10 minutes at 800 g. Afterwards, the supernatant was transferred in a new 1.5 ml tube and centrifuged for 1 minute at 5000 g. Platelets and plasma were divided during this step and the platelet poor plasma was transferred in a new tube and subsequently used for this assay.

Prior to start, the lyophilized standard cocktail was reconstituted with 250 µl assay buffer. It was mixed and rested at RT for 15 minutes. Afterwards, the seven standards were prepared. Six tubes, C1-C6, were labeled and 37.5 µl assay buffer were pipetted into each one. The top standard was prepared in tube C7. A 1:4 dilution of the top standard was prepared by transferring 12.5 µl of the top standard C7 to the C6 tube. This was the C6 standard. In the same manner, a serial 1:4 dilution was performed to obtain C5, C4, C3, C2 and C1 standards. 37.5 µl of assay buffer was used as the 0 pg/ml standard C0. Following the standard preparation, the lyophilized Matrix C was dissolved in 5 ml assay buffer and reconstituted for 15 minutes. The wash buffer was prepared afterwards by mixing 47.5 ml deionized water with 2.5 ml of 20x Wash buffer. Standards and samples were running as duplicates and a polypropylene V-bottom plate was used. Next, the samples were diluted 2-fold with Assay Buffer before testing by dilution of 50 µl sample with 50 µl buffer. To each standard well 12.5 µl of Matrix C and 12.5 µl standard were added. The sample wells were filled with 12.5 µl Assay Buffer and 12.5 µl of each diluted plasma sample. Mixed beads were vortexed for 30 seconds and 12.5 µl of mixed beads were added to each well. The total volume was 37.5 µl in each well after beads addition. After adding all ingredients, the plate was wrapped with aluminum foil to protect samples from light and was shakes at 800 rpm on an orbital shaker at 4°C over night. A centrifugation step followed at 600-700 g for five minutes by using a centrifuge with swinging bucket rotor (G.H 3.8) with microplate adaptor. Immediately after centrifugation, the supernatant was discarded by quickly inverting the plate. By dispensing 180 µl of Washing Buffer into each well, the plate was washed once via shaking the plate at 600-700 g for one minute. The plate was centrifuged afterwards at 600-700 g for 5 minutes and the supernatant was discarded. 12.5 µl of the detection antibodies were added to each well. The plate was sealed with a plate sealer and covered with aluminum foil to protect it from light and placed on a shaker at 800 rpm for 1 hour at RT. Afterwards 12.5 µl of SA-PE were added to each well directly, without a washing step in between. The plate was sealed with a

plate sealer and covered with aluminum foil again and placed on a shaker at 800 rpm for another 30 minutes at RT. A centrifugation step followed at 600-700 g for 5 minutes. Immediately after centrifugation, the supernatant was discarded by quickly inverting the plate. 120 µl of 1X Wash Buffer were added to each well and beads were resuspended by pipetting. The samples were read on the flow cytometer. Before the assay started, 60 µl of the C7 well was measured to make sure the maximum PE signal did not exceed values above 10^5. The voltage in PE was adjusted if needed. Resuspension was performed manually after every vertical row for optimal resuspension of the beads. The assay FCS files were analyzed by using BioLegend's LEGENDplex data analysis software.

2.2.16 Histology

2.2.16.1 Analysis of infarct sizes using 2,3,5-triphenyltetrazolium chloride staining

This staining method is used to determine the infarct size of murine hearts and brains 24 hours after I/R. For this purpose, the experimental animal was weighed and anesthetized according to the weight with ketamine (Ketanest 100 mg/kg, i.p.) and xylazine (Rompun 10 mg/kg, i.p.). At adequate depth of anesthesia (lack of inter-toe reflex), the animal was killed by final blood withdrawal and the heart was removed. The heart was immediately transferred to ice cold sodium chloride 0.9 % (NaCl) for preparation. The cardiac fat and other tissues were removed from the heart, except an approximately five-millimeter-long part of the ascending aorta. The aorta was then secured to a cannula and the heart was flushed with isotonic saline solution until only clear fluid drops out. A 7-0 silk suture was used afterwards to close the LAD at the site where the loose suture had remained after the I/R operation (**Fig. 15**). This suture could then be removed. A 0.1 % Evans Blue solution, which was dissolved in isotonic saline solution was injected into the heart through the cannula until the myocardium turned blue. Excess solution was rinsed with isotonic saline solution. After the staining process, the heart was tightly wrapped in commercial cling film and frozen at -20°C. Subsequently after freezing for approximately three hours, the heart was divided into six one millimeter thin sections with start from the apex. The sections were weighed and transferred to 1.5 ml tubes contained a 1 % 2,3,5-triphenyltetrazolium chloride solution (TTC). Slices were incubated at 37°C for five minutes. The healthy tissue converted TTC to a red dye (Redfors et al., 2012). Following the incubation period, images of the heart sections were taken by using a Leica DM6B light microscope. Analysis of the images was performed by Diskus View software.

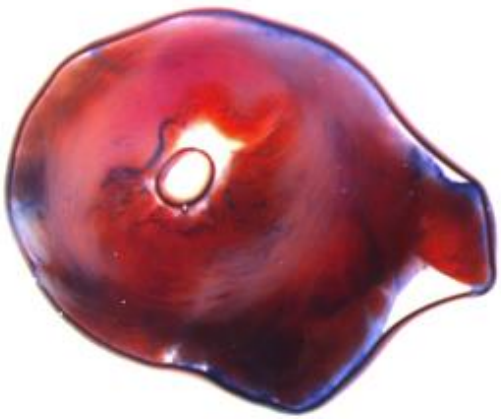

Figure 15: Example image of a heart section after TTC staining.

The Evans Blue stained area was not affected by ischemia. TTC-stained area in red was affected by ischemia, but is still healthy. The white part is unstained, affected by ischemia and the tissue is dead. The part which is red and white is the area at risk (AAR), the area of ischemia.

For TTC staining of murine brains, the mouse was dissected. For this purpose, the mouse was first decapitated and the skull was opened dorso-medially from the eyes to the neck. The opening of the scalp started from the vertebral canal by means of scissors through lateral cuts. The top of the skull was carefully dissected with forceps. After removing the brain, the cerebrum was cut transversely from rostral to caudal into 2 mm thick sections by using a cutting block. Each slice was stained individually in 1 % TTC solution at 37°C for 5 minutes in the dark. The sections were placed on a glass slide in an ascending order from rostral to caudal and Images of the brain sections were taken by using a Leica DM6B light microscope. The determination of infarct sizes was performed according to Kleinschnitz et al. Vital tissue was red, while avital tissue was pale or unstained (**Fig. 16**).

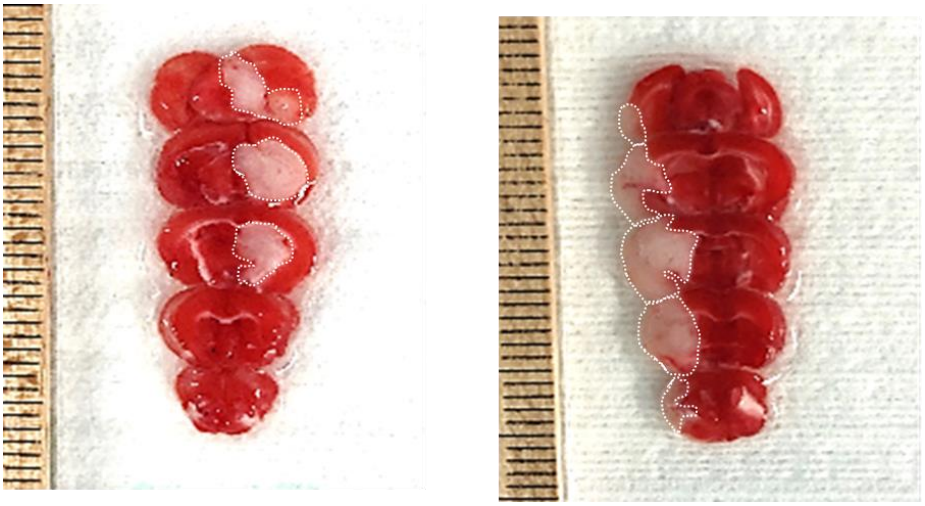

Figure 16: Triphenyl-tetrazolium chloride (TTC)-stained brain of a mouse, 24 hours after transient occlusion of the middle cerebral artery (tMCAO).

Five TTC-stained transverse sections of the mouse brain were imaged 24 hours after tMCAO. The section thickness was 2 mm. Vital tissue is stained red in, whereas dead areas (here: right hemispheric, thalamic, hypothalamic and cortical) remained unstained (outlined in white).

2.2.16.2 Immunohistochemical staining and quantification

2.2.16.2.1 Hearts

Mice were sacrificed five days after AMI and transcardial perfused with cold 1X PBS and processed like described in Polzin et al. (2023). After removing the hearts, they were fixed overnight in 4 % PFA. Post fixation the hearts were dehydrated and embedded in paraffin wax. The tissue was cut in 5 µm thin sections using a Leica CM 3050S microtome and put on microscope superfrost slides. Heart sections were deparaffinized two times for 5 minutes in Roticlear and rehydrated two times for 3 minutes in 100 % ethanol. Afterwards slides were put in 96 % and 70 % for 1 minute each and 3 minutes in aqua dest. followed by a heat-induced epitope retrieval (HIER) by using a citrate buffer (pH 6.0). After the epitope retrieval, BloxAll-Blocking solution was used for blocking the sections. Next, they were blocked with 2.5 % goat serum and afterwards incubated with primary antibodies at 4°C overnight. Primary antibodies used were: rat anti-Ly6G (1:100) and rat anti Mac-2 (1:1000). Following the ImmPRESS- Goat Anti-Rat IgG (Mouse Adsorbed) Polymer Kit was used for Ly6G and Mac-2 staining. For visualization the ImmPact DAB (SK-4105) detection system was used. Sections were counterstained with hematoxylin Gill II and mounted with permanent mounting medium. Images of stained sections were done by using a Leica DM4000M bright field microscope with 20x magnification. Five randomly chosen fields of 100 µm x 100 µm each, were imaged with the LASX software of one heart section and analyzed by using ImageJ software.

To investigate NET formation in murine hearts, rabbit anti-CitH3 (1:200) at 4°C overnight was used as first primary antibody. After washing, goat anti-rabbit Alexa594 (1:1000) was used as secondary antibody for one hour at RT. CitH3 stained sections were then incubated with a rat anti-Ly6g antibody (1:100) overnight at 4°C, followed by washing three times in washing solution the next day and an incubation with the secondary antibody goat anti-rat Alexa680 (1:1000) for one hour at RT. After incubation, the slides were washed and mounted with ProLong™ Diamond Antifade Mountant with DAPI. Images of stained sections were done by using a Leica-DFC9000 fluorescence microscope with 40x magnification. Five randomly chosen fields of 100 µm x 100 µm each, were imaged with the LASX software of one heart section and analyzed by using ImageJ software.

2.2.16.2.2 Brains

Mice were sacrificed at 24 h after tMCAO and perfused with icecold 1X PBS followed by 4 % PFA. Brains were removed, post fixed in 4 % PFA overnight and dehydrated in 30 % sucrose until they sank down. Afterwards they were embedded in Tissue-Tek and cut into 25 µm frozen cryosections by using a Leica CM3050S cryostat. Slices of the brains with infarcted area were put on microscope superfrost slides. Brain sections were defrosted for 20 minutes and rehydrated in 1X PBS for 10 minutes. Sections were washed in washing solution (1X PBS containing 0.5 % BSA , 0.1 % Tween-20) three times for five minutes each and permeabilized in washing solution containing 0.3 % Triton X-100. After three times washing with washing solution, sections were blocked with 10 % goat serum for one hour. Post blocking, the brain tissue was incubated with either goat anti-Iba1 (1:100) or rabbit anti-CitH3 (1:200) primary antibodies at 4°C overnight. After washing in washing solution, sections were incubated with secondary antibodies for one hour at RT. The following secondary antibodies were used: Rabbit anti-goat Alexa647 (1:1000) and goat anti-rabbit Alexa594 (1:1000). Iba1 incubated sections were then washed and mounted with ProLong™ Diamond Antifade Mountant with DAPI. CitH3 stained sections were then incubated with a rat anti-Ly6g antibody (1:100) overnight at 4°C, followed by washing three times in washing solution the next day and an incubation with the secondary antibody goat anti-rat Alexa680 (1:1000) for one hour at RT. After incubation the slides were washed and mounted with ProLong™ Diamond Antifade Mountant with DAPI. Images of stained sections were done by using a Leica fluorescence microscope (Leica-DFC9000) with 20x magnification (Polzin et al., 2023). Five randomly chosen fields of 300 µm x 300 µm each, were imaged with the LASX software of one heart section for Iba1 staining and analyzed by using ImageJ software. Five randomly chosen fields of view were selected for the NET staining and analyzed by using ImageJ software.

2.2.17 Human samples

The experiments were conformed to the Declaration of Helsinki and were approved by the ethics committee of the Ludwig-Maximilians-University Munich (LMU) and Heinrich-Heine-University Düsseldorf (study no. 6072R, registration ID 2017074372). In an open, prospective design, patients with chronic FXa-inhibition with RIVA or apixaban due to atrial fibrillation were recruited at the LMU hospital. Patients with hematological disorders, as well as active hematological malignancy, severe renal insufficiency with dialysis and under the age of 18 were excluded from the study. All experiments with human blood were done in collaboration with the working group of PD Dr. med. Tobias Petzold at LMU.

2.2.17.1 Human blood collection and platelet isolation

Patients had venous blood drawn from a cubital using a 21 G butterfly needle. Blood samples were collected in 2.9 ml 0.1 M sodium citrate tubes and 2.6 ml EDTA tubes and prepared as described in Thienel et al. (2023). For platelet isolation, citrate anticoagulated blood was centrifuged with 90 g for 20 minutes at RT. Afterwards, Platelet rich plasma (PRP) was diluted 1:10 in modified Tyrode's buffer substituted with prostaglandine (PGI2, 500 ng/ml final concentration). PRP was centrifuged at 450 g for ten minutes at RT and the obtained platelet pellet was resuspended in Tyrode's buffer (pH = 7.4). Highly purified platelets were used for proteome analyses. A magnetic activated cell sorting (MACS) based negative isolation kit was used to purify platelets. Before running over a LS Column, platelet suspension was incubated with CD45 MicroBeads and glycophorin A MicroBeads. Cells were centrifuged at 2,500 g for 5 minutes and resuspended in lysis buffer. Immediately after resuspension, cells were frozen in liquid nitrogen.

2.2.17.2 Serotonin release after platelet activation

To analyze the serotonin release platelets were firstly activated using aggregometry following the protocol from Thienel et al. (2023). Washed platelets were used for light transmission aggregometry (LTA) with a final concentration of 100.000 PLTs/µl. Platelets were resolved in a total volume of 300 µl Tyrode's Buffer (pH 7.4) with 1 mM Mg^{2+} and Ca^{2+}. Aggregation was induced by 2 µM U46619, 5 µg/ml fibrillar collagen and 0.1 U/ml thrombin. Six minutes after stimulation and full aggregation, platelet supernatant was retained. Serotonin level was quantified using commercially available ELISA kit performed according to the manufacturer's protocol.

2.2.17.3 Platelet vWF content after activation

To analyze vWF content platelets were firstly activated using aggregometry like described above and in the method part of Thienel et al. (2023). Six minutes after stimulation and full aggregation, aggregated platelets were retained, lysed and subjected to immunoblotting. The following antibodies were used to incubate the blotting membrane (PVDF): antibody against vWF (1:1000; clone:M16.10A1) and horse radish peroxidase (HRP)-coupled secondary antibody (Goat anti-mouse IgG-HRP conjugated). Quantification of the Western blot signals on the membrane were detected by Amersham ImageQuant 800 after addition of chemiluminescent detection reagent. Antibodies for the loading controls, used in this experiment, were an antibody against β-actin (1:1000, 13E5 Rabbit mAb HRP conjugated) or GAPDH (1:1000).

2.2.17.4 Platelet granule distribution

Coverslips were coated with 50 µg/ml rat tail collagen I for 1 hour at 37° C and washed afterwards with 1X PBS. Used stimuli for the highly purified platelets were 0.1 U/mL thrombin and 10 µg/ml fibrillar collagen. Afterwards platelets were seeded on the coated coverslips. Different time points were used, where platelets were fixed with 4 % PFA, permeabilized with 0.5 % Triton X-100 and stained with phalloidin 488 (1:1000) and vWF. Time points were 8, 15 and 30 minutes. Images were acquired by confocal microscopy (ZEISS LSM 800 confocal microscope) and analyzed by ZEN blue, ZEN black software (Thienel et al., 2023).

2.2.17.5 Human thrombi

After surgical intervention coronary human thrombi were stored at -80°C. Afterwards they were embedded in Tissue-Tek and cut into 10 µm frozen cryosections by using a Leica CM3050S cryostat. Sections of the thrombi were put on superfrost microscope slides and stored at -20°C. Before staining, the sections were defrosted for 20 minutes and fixed in 4 % PFA for another 15 minutes. Sections were washed three times with washing solution for five minutes each. Afterwards, they were permeabilized in washing solution containing 0.3 % Triton X-100 for 15 minutes. After three times of washing with washing solution, sections were blocked with 10 % BSA in washing solution for 15 minutes. Post blocking, the thrombi sections were incubated with two primary antibodies, Anti-Histone3-antibody (1:100, ab1791) and human/mouse myeloperoxidase (MPO) antibody (1:20), at 4°C overnight. After washing in washing solution, sections were incubated with secondary antibodies for one hour at RT. The following secondary antibodies were used: donkey anti-goat Alexa488 and goat anti-rabbit Alexa594 (both 1:1000). Sections were washed afterwards in 1X PBS and mounted with ProLong™

Diamond Antifade Mountant with DAPI. Images of stained sections were done by using a Leica-DFC9000 fluorescence microscope with 40x magnification. Five randomly chosen fields of 100 µm x 100 µm each, were imaged with the LASX software of one thrombus section for NETs staining and analyzed by using ImageJ software.

2.2.17 Statistics

All statistical studies and figures were analyzed and generated with GraphPad Prism software by means of one-way analysis of variance (ANOVA), two-way ANOVA, independent sample *t*-test and mixed-effects analysis was used for detailed comparisons. At the beginning of each analysis, the data were tested for normal distribution. The Kolmogorov-Smimof test, Shapiro-Wilk test, q-q plots and histograms were used for this purpose. Normally distributed data were examined with unpaired or paired t-tests, depending on the dependence of the variables. paired t-tests, depending on the dependence of the variables. For non-normally distributed data, the Wilcoxon test (dependent) or Mann-Whitney U test (independent) were used to analyze the data. All statistics reportings can be found in the supplementary. Statistical tests were two-tailed and parametric. Significance for comparisons: * $p \leq 0.05$; ** $p \leq 0.01$; *** $p \leq 0.001$; **** $p \leq 0.0001$. Results are presented as mean ± SD.

3. Results

3.1 Acute myocardial infarction in mice

3.1.1 Infarct sizes of TTC stained murine hearts 24 h post I/R

TTC staining is used to determine the infarct sizes of murine hearts 24 h after an ischemia reperfusion injury. In this experimental setup, control mice were treated with a vehicle. Mice with FXa-inhibitor treatment received it either for two days (acute) or for five weeks (chronic) in two days' intervals before I/R injury. Infarct sizes of mice with acute FXa-inhibition (41.71 ± 3.90 %) show no significant differences in comparison to control mice (41.39 ± 6.3 %), which were treated with a vehicle. A significant reduction of the infarct size of mice with chronic FXa-inhibition (33.37 ± 4.71 %) can be observed by the comparison with control mice and acute treated mice (ANOVA; $F_{2, 27} = 8.751$, $p \leq 0.01$; **Fig. 17 A**). These differences can be seen macroscopically in figure 13 C, where example pictures of TTC stained heart slices are shown. The dead white tissue is significantly smaller in the right picture of a chronically treated mouse. Another parameter which was analyzed after TTC staining is the myocardial area at risk (AAR/LV %). Figure 13 B shows no significant differences in the AAR/LV [%] values between the three groups (ANOVA, $F_{2, 26} = 0.2445$, all $p \geq 0.05$, n.s.).

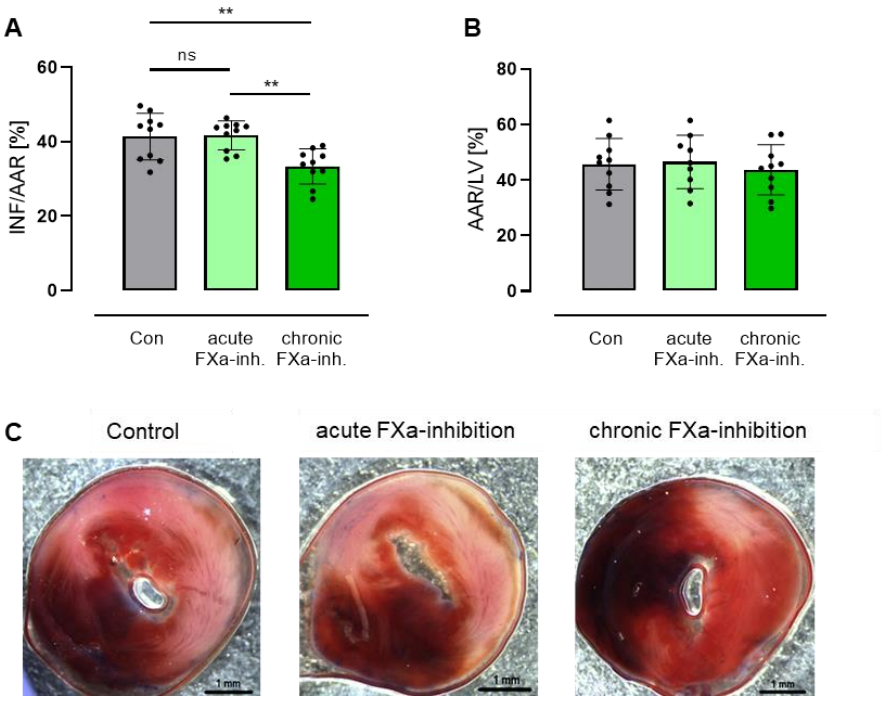

Figure 17: Infarct sizes of 2,3,5-triphenyltetrazolium chloride stained hearts 24 h post I/R.

(A) The infarct size was significantly smaller in mice treated chronically with a FXa-inhibitor (activated factor X) in comparison to control animals (Con) and acute treated mice. (B) The AAR/left ventricle shows no differences between all groups. Shown are means ± SD of all animals, control (n= 10), acute FXa-inhibition (n= 10) and chronic FXa-inhibition (n= 10). Stars above the bars indicate statistically significant differences between means by ANOVA. (C) Example pictures of heart slices, stained with 2,3,5-triphenyltetrazolium chloride (TTC). Stars above the bars indicate statistically significant differences between means.

3.1.2 Murine transthoracic echocardiography 24 h post I/R

In order to examine the heart function after I/R injury, an echocardiography of the mice hearts was performed the next day before TTC staining. Heart rates (HR) of all three groups (control mice (526.20 ± 60.84 [1/min]); acute FXa-inhibition (533.22 ±43.89 [1/min]); chronic FXa-inhibition (505.60 ± 47.56 [1/min])) were not significantly different what indicates, that FXa-inhibition had no influence on this parameter (ANOVA, $F_{2, 27}$ = 0.7826, all p > 0.05, n.s.; **Fig. 18 A**). Another measured parameter was the EF, which is measured as a percentage of the total amount of blood in the heart that is pumped out with every heartbeat. The chronic FXa-inhibitor treatment of mice post I/R (39.20 ± 2.59 %) leads to significantly increased EF in comparison to control mice (33.72 ± 2.91 %) and acute FXa-inhibitor treated mice (34.23 ± 3.61 %) (ANOVA, $F_{2,27}$ = 9.722, p ≤ 0.01; **Fig. 18 B**). Echocardiographic recording of the stroke volume (SV) is used to refer to the volume of blood ejected from the left ventricle during a heartbeat. Even in the analysis of the SV, the chronically treated group of mice (25.12 ± 2.25 µl) had a significant increased SV in comparison to the control group (22.80 ± 2.05 µl) and the acute treated group (21.51 ± 1.87 µl) of experimental animals (ANOVA, $F_{2,27}$ = 7.854, p ≤ 0.01; **Fig. 18 C**).

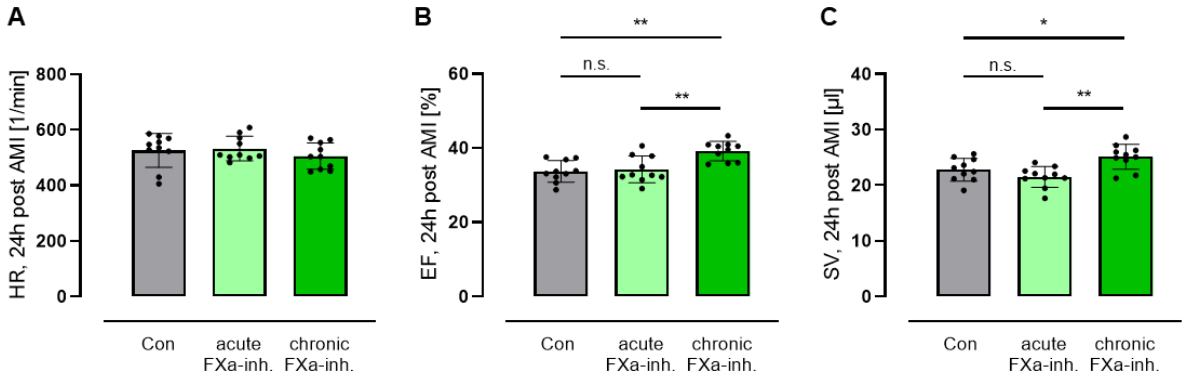

Figure 18: Transthoracic echocardiography of murine hearts 24 h post I/R.

(A) Heart rate (HR) of control (Con) and FXa-inhibitor (activated factor X) treated mice (acute and chronic treatment) during echocardiography. No significant differences can be observed. (B) The ejection fraction (EF) of control and acute FXa-inhibitor treated mice is not significantly different. Significant differences can be noticed between control and chronically treated mice. Under chronic FXa-inhibition the EF was significantly higher. Even between both treated groups, the EF was significantly higher under chronical treatment. (C) No significant differences in the stroke volume (SV) can be observed between the control group and the acute treated mice. Mice under chronic FXa-inhibitor treatment show a significant higher SV in comparison to control and acute treated mice. Shown are means ± SD, control (n= 10), acute FXa-inhibition (n= 10) and chronic FXa-inhibition (n= 10). Stars above the bars indicate statistically significant differences between means by ANOVA.

3.1.3 FACS of inflammatory cells in murine blood 24 h post I/R

Blood from control mice and chronically FXa-inhibitor treated mice was collected 24 h after I/R injury to investigate the inflammatory response to the AMI in the circulation. The blood was stained with antibodies and measured via FACS. To detect inflammatory cells, like leukocytes, within the blood, CD45 was gated to detect all of them (not shown). CD19 and CD3 were used to divide leukocytes in B-cells and T-cells and were gated from CD45. Figure 19 A shows no significant difference in the percentage of B-cells between the control group (38.43 ± 10.58 %) and the FXa-inhibitor treated group (37.47 ± 6.61 %) of experimental animals analyzed by *t*-test ($t(10) = 0.19$, $p \geq 0.05$). No significant differences can be observed in the percentage of CD3 positive cells ($CD3^+$), all T-cells, between the control (24.47 ± 2.27) and the chronically FXa-inhibitor treated group (22.83 ± 4.31 %) ($t(10) = 0.82$, $p \geq 0.05$; **Fig. 19 B**). From the whole population of $CD3^+$ cells, the percentage of $CD4^+$, the T-helper cells, within this population was gated. Figure 15 C shows a significant higher percentage of $CD4^+$ cells gated from $CD3^+$ cells in FXa-inhibitor treated mice (56.48 ± 2.47 %) than in the control group (53.33 ± 1.97 %) ($t(10) = 2.44$, $p \leq 0.05$). Another cell population gated from the whole T-cell population are $CD8^+$ T-killer cells. A significant reduction of $CD8^+$ cells in FXa-inhibitor treated animals (34.83 ± 2.30) is detected then in the control group (38.18 ± 2.14 %) ($t(10) = 2.61$, $p \leq 0.05$; **Fig. 19 D**). Another part of leukocytes in the context of inflammation are granulocytes, respectively $Ly6G^+$ cells. These cells were gated from CD45 and were divided in $Ly6G^+$ and $Ly6G^-$ cells. Within the $Ly6G^+$ positive cells no significant difference, in the FXa-inhibitor treated group (17.30 ± 9.25 %) in comparison to the control group (10.81 ± 5.26 %) was detected ($t(10) = 1.49$, $p \leq 0.05$; **Fig. 19 E**). From $Ly6G^-$ cells, Ly6C was gated for the non-inflammatory monocytes which were represented as $Ly6C^+$ cells in figure 15 F. The percentage of $Ly6C^+$ cells does not differ significantly between control mice (83.37 ± 1.96 %) and FXa-inhibitor treated mice (81.82 ± 2.41 %) ($t(10) = 1.22$, $p \leq 0.05$). No significant differences could be observed in the inflammatory monocytes, represented as $Ly6C^{++}$, either. The percentages of these cells, between control group (6.34 ± 1.59 %) and chronically FXa-inhibitor treated mice (6.99 ± 0.88 %), are shown in figure 19 G ($t(10) = 0.87$, $p \leq 0.05$).

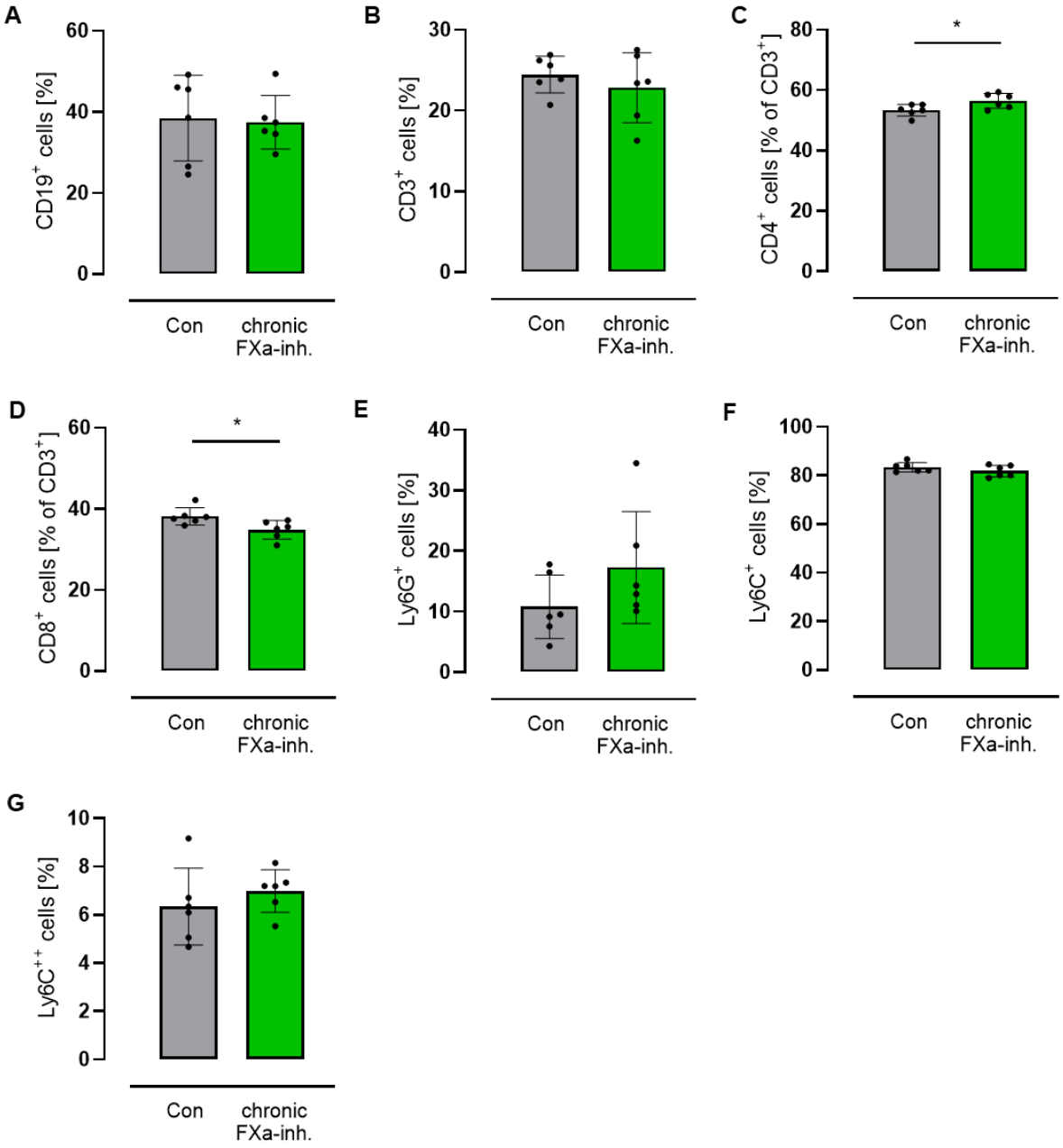

Figure 19: FACS of inflammatory cells in murine blood 24 h post I/R.

(A) The percentage of leukocytes in the blood samples of the control group and the chronically FXa-inhibitor treated group of mice do not differ significantly. (B) The percentage of CD3 positive cells ($CD3^+$) represent all T-cells within the sample of the two experimental groups and does not differ. (C) T-helper cells were identified via CD4 and a higher percentage of these cells is observed in chronically FXa-inhibitor treated mice in comparison to control mice. (D) T-killer cells were identified via CD8 and the chronically FXa-inhibitor treated group shows a significant lower percentage of T-killer cells in in comparison to the control group. (E) Ly6G staining for granulocytes show no significant difference between groups. (F) Ly6C was gated from $Ly6G^-$ cells for the non-inflammatory monocytes represented as $Ly6C^{++}$. No significant differences are found between both groups. (G) The inflammatory monocytes were represented as $Ly6C^+$ and show no significant differences between control and FXa-inhibitor treated groups. Shown are means ± SD, control (n= 6) and chronic FXa-inhibition (n= 6). Stars above the bars indicate statistically significant differences between means by *t*-test.

3.1.4 LEGENDplex inflammatory assay of mice plasma 24 h post I/R

Analysis of circulating inflammatory cytokines in murine plasma 24 h after AMI was done with the LEGENDplex inflammatory assay. Different known thromobinflammation related cytokines were measured and compared between FXa-inhibitor treated mice and control mice. The control group (3.5 ± 1.23 pg/ml) shows a significantly higher amount of interleukin-1 alpha (IL-1α) in comparison to the acute FXa-inhibitor treated group (1.86 ± 1.15 pg/ml) and the chronically FXa-inhibitor treated group of mice (1.96 ± 0.48 pg/ml) (ANOVA, $F_{2,19} = 6.75$, $p \leq 0.001$; **Fig. 20 A**). No significant differences in the amount of interleukin-1 beta (IL-1β) are observed between groups (control: 2.84 ± 1.42 pg/ml vs. acute FXa-inh.: 1.42 ± 0.48 pg/ml vs. chronic FXa-inh.: 3.56 ± 3.30 pg/ml; ANOVA, $F_{2,18} = 1.12$, $p \geq 0.05$; **Fig. 20 B**) as well as in the amount of interleukin-6 (IL-6), which is responsible to regulate inflammatory processes (control: 12.83 ± 7.16 pg/ml vs. acute FXa-inh.: 8.29 ± 5.51 pg/ml vs. chronic FXa-inh.: 8.14 ± 2.59 pg/ml; ANOVA, $F_{2,20} = 2.02$, $p \geq 0.05$; **Fig. 20 C**). Figure 20 D shows the amount of interleukin-12p70 (IL-12p70) in samples of control mice (1.76 ± 1.65 pg/ml), acute FXa-inhibitor treated mice (0.83 ± 0.43 pg/ml) and chronically FXa-inhibitor treated mice (1.10 ± 0.68 pg/ml) with no significant differences between groups (ANOVA, $F_{2,20} = 1.23$, $p \geq 0.05$). Three other interleukins were measured with the LEGENDplex assay. Interleukin-17A levels (IL-17A) show no significant difference (ANOVA, $F_{2,17} = 1.35$, $p \geq 0.05$; **Fig. 20 E**) in control mice (1.55 ± 0.55 pg/ml) in comparison to acute FXa-inhibitor treated mice (1.12 ± 0.56 pg/ml) and chronic FXa-inhibitor treated mice (1.26 ± 0.35 pg/ml), as well as interleukin-23 levels (IL-23) (control: 285.2 ± 227.2 pg/ml vs. acute FXa-inh.: 145.9 ± 47.06 pg/ml vs. chronic FXa-inh.: 350.6 ± 216.5 pg/ml; ANOVA, $F_{2,17} = 1.09$, $p \geq 0.05$; **Fig. 20 F**). The last measured interleukin was interleukine-27 (IL-27), which does not show significant differences between control mice (189.90 ± 178.7 pg/ml), acute FXa-inhibitor treated mice (322.4 ± 405.6 pg/ml) and chronically treated mice (96.67 ± 81.71 pg/ml) (ANOVA, $F_{2,19} = 1.55$, $p \geq 0.05$; **Fig. 20 G**). Another measured cytokine is the monocyte chemotactic protein 1 (MCP-1), which is produced by monocytes, memory T-cells and dendritic cells during inflammatory processes. Between the three investigated groups, no significant difference is seen in the amount of MCP-1 in the samples (control: 13.3 ± 6.32 pg/ml vs. acute FXa-inh.: 5.60 ± 4.91 pg/ml vs. chronic FXa-inh.: 13.37 ± 7.13 pg/ml; ANOVA, $F_{2,22} = 2.89$, $p \geq 0.05$; **Fig. 20 H**). The amount of granulocyte-macrophage colony-stimulating factor (GM-CSF) does not differ significantly within the samples between control mice (3.05 ± 1.91 pg/ml), acute FXa-inhibitor treated mice (2.39 ± 1.49 pg/ml) and chronic FXa-inhibitor treated mice (2.75 ± 1.35 pg/ml) (ANOVA, $F_{2,22} = 0.29$, $p \geq 0.05$; **Fig. 20 I**). Figure 20 J shows the amount of interferon beta (IFN-β), which is secreted by macrophages and fibroblasts, between control animals (20.40 ± 10.43), acute FXa-inhibitor treated mice (29.80 ± 27.52) and chronic treated animals (73.73 ± 71.85). No significant differences are noticed between groups (ANOVA, $F_{2,21} = 3.10$, $p \geq 0.05$). Another member of

the interferon family was also investigated. In figure 20 K the amount of interferon gamma (IFN-ɣ) is shown and no significant differences are detected between groups (control: 1.27 ± 0.58 pg/ml vs. acute FXa-inh.: 1.03 ± 0.29 pg/ml vs. chronic FXa-inh.: 1.14 ± 0.54 pg/ml; ANOVA, $F_{2,21} = 0.38$, $p \geq 0.05$). The cytokine tumor necrosis factor alpha (TNFα) is known to be involved in almost all inflammatory processes and is secreted by monocytes and macrophages. In this analysis the plasma samples of control mice (3.86 ± 2.11 pg/ml), acute FXa-inhibitor treated mice (4.57 ± 1.73 pg/ml) and chronically FXa-inhibitor treated mice (4.58 ± 1.67 pg/ml) show no significant differences in their amount of TNF-α 24 h post I/R (ANOVA, $F_{2,21} = 0.43$, $p \geq 0.05$; **Fig. 20 L**).

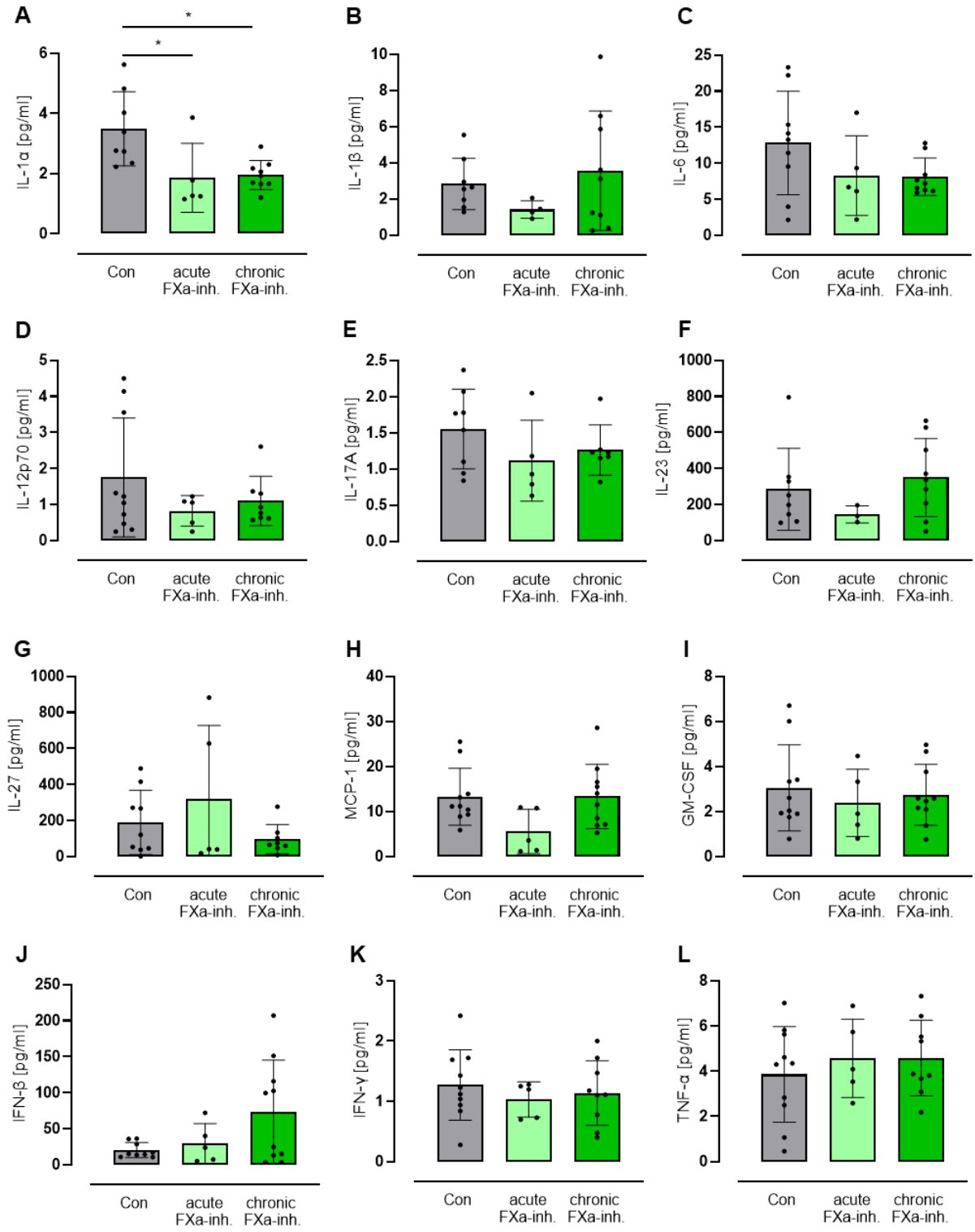

Figure 20: LEGENDplex inflammatory assay of mice plasma 24 h post I/R.

Figures show inflammatory cytokines measured by LEGENDplex inflammatory assay in the plasma of mice 24h post I/R. (A) Interleukin-1 alpha (IL-1α) is higher in control mice than in treated mice. No significant differences were observed in the amounts of (B) Interleukin-1 beta (IL-1β), (C) Interleukin-6 (IL-6), (D) Interleukin-12p70 (IL-12p70), (E) Interleukin-17A (IL-17A), (F) Interleukin-23 (IL-23), (G) Interleukin-27 (IL-27), (H) monocyte chemotactic protein-1 (MCP-1), (I) granulocyte-macrophage colony-stimulating factor (GM-CSF), (J) Interferon alpha (INF-α), (K) Interferon gamma (INF-ɣ) and (L) tissue necrosis factor alpha (TNF-α). Shown are means ± SD, control (n= 8-10), acute FXa-inhibition (n= 3-5) and chronic FXa-inhibition (n= 8-10). Stars above the bars indicate statistically significant differences between means by one-way ANOVA.

3.1.5 LEGENplex inflammatory assay of mice plasma five days post I/R

Next to the measurements of cytokines in mouse blood 24 h post I/R, plasma samples from mice five days post I/R were analyzed as well with the LEGENDplex inflammatory assay. The same thromobinflammation related cytokines were measured and compared between FXa-inhibitor treated mice and control mice. The control group (1.80 ± 0.63 pg/ml) shows no significant differences in the amount of IL-1α in comparison to the acute FXa-inhibitor treated group (1.76 ± 0.68 pg/ml) and the chronically FXa-inhibitor treated group of mice (2.81 ± 1.91 pg/ml) (ANOVA, $F_{2,19} = 1.82$, $p \geq 0.05$; **Fig. 21 A**). Significant differences in the amount of IL-1β are observed in the chronic FXa-inhibitor treated group (7.84 ± 8.80) in comparison to the control group (1.21 ± 0.58 pg/ml) and the acute FXa-inhibitor treated group (1.42 ± 0.48 pg/ml) (ANOVA, $F_{2,19} = 4.117$, $p \leq 0.05$; **Fig. 21 B**) as well as in the amount of IL-6 (control: 3.13 ± 1.27 pg/ml vs. acute FXa-inh.: 3.58 ± 3.22 pg/ml vs. chronic FXa-inh.: 7.97 ± 5.14 pg/ml; ANOVA, $F_{2,19} = 4.60$, $p \leq 0.05$; **Fig. 21 C**). **Figure 21 D** shows the amount of IL-12p70 in samples of control mice (0.42 ± 0.25 pg/ml), acute FXa-inhibitor treated mice (1.05 ± 1.00 pg/ml) and chronically FXa-inhibitor treated mice (0.54 ± 0.32 pg/ml) with no significant differences between groups (ANOVA, $F_{2,18} = 2.331$, $p \geq 0.05$). Three other interleukins were measured with the LEGENDplex assay. IL-17A shows no significant difference in its amount (ANOVA, $F_{2,19} = 2.02$, $p \geq 0.05$; **Fig. 21 E**) in control mice (0.99 ± 0.42 pg/ml) in comparison to acute FXa-inhibitor treated mice (1.34 ± 0.77 pg/ml) and chronic FXa-inhibitor treated mice (1.59 ± 0.65 pg/ml), as well as IL-23 (control: 107.1 ± 80.69 pg/ml vs. acute FXa-inh.: 183.8 ± 118.1 pg/ml vs. chronic FXa-inh.: 272.8 ± 359.1 pg/ml; ANOVA, $F_{2,15} = 1.25$, $p \geq 0.05$; **Fig. 21 F**). The last measured interleukin was IL-27, which does not show significant differences between control mice (563.1 ± 368.2 pg/ml), acute FXa-inhibitor treated mice (140.0 ± 119.0 pg/ml) and chronically treated mice (242.4 ± 265.4 pg/ml) (ANOVA, $F_{2,14} = 3.25$, $p \geq 0.05$; **Fig. 21 G**). No significant differences are seen in the amount of MCP-1 in control mice samples (6.43 ± 5.57 pg/ml) in comparison to acute FXa-inhibitor treated (15.13 ± 8.85 pg/ml) and chronic FXa-inhibitor treated mice (8.73 ± 4.22 pg/ml) (ANOVA, $F_{2,18} = 3.38$, $p \geq 0.05$; **Fig. 21 H**). The amount of GM-CSF does not differ significantly within the samples between control mice (1.79 ± 0.81 pg/ml), acute FXa-inhibitor treated mice (2.21 ± 1.03 pg/ml) and chronic FXa-inhibitor treated mice (2.20 ± 1.19 pg/ml) (ANOVA, $F_{2,19} = 0.49$, $p \geq 0.05$; **Fig. 21 I**). Figure 21 J shows the amount of IFN-β between control animals (24.58 ± 15.33 pg/ml), acute FXa-inhibitor treated mice (33.80 ± 21.99 pg/ml) and chronic treated animals (16.22 ± 4.70 pg/ml). No significant differences are noticed between groups (ANOVA, $F_{2,19} = 1.67$, $p \geq 0.05$). In figure 21 K the amount of IFN-ɣ is shown and significant differences are detected between groups (ANOVA, $F_{2,19} = 3.83$, $p \leq 0.05$). The chronically treated group (2.91 ± 1.93 pg/ml) shows higher amount of IFN-ɣ in comparison to the control group (1.15 ± 0.37 pg/ml) and the acute FXa-inhibitor treated group (1.78 ± 1.34 pg/ml). The amount of TNF-α in the

plasma samples of chronically FXa-inhibitor treated mice (4.74 ± 1.15 pg/ml) show a significant higher amount of TNF-α five days post I/R in comparison to plasma from control mice (2.63 ± 0.95 pg/ml) and acute FXa-inhibitor treated mice (3.13 ± 1.70 pg/ml) (ANOVA, $F_{2,19} = 5.60$, $p \leq 0.05$; **Fig. 21 L**).

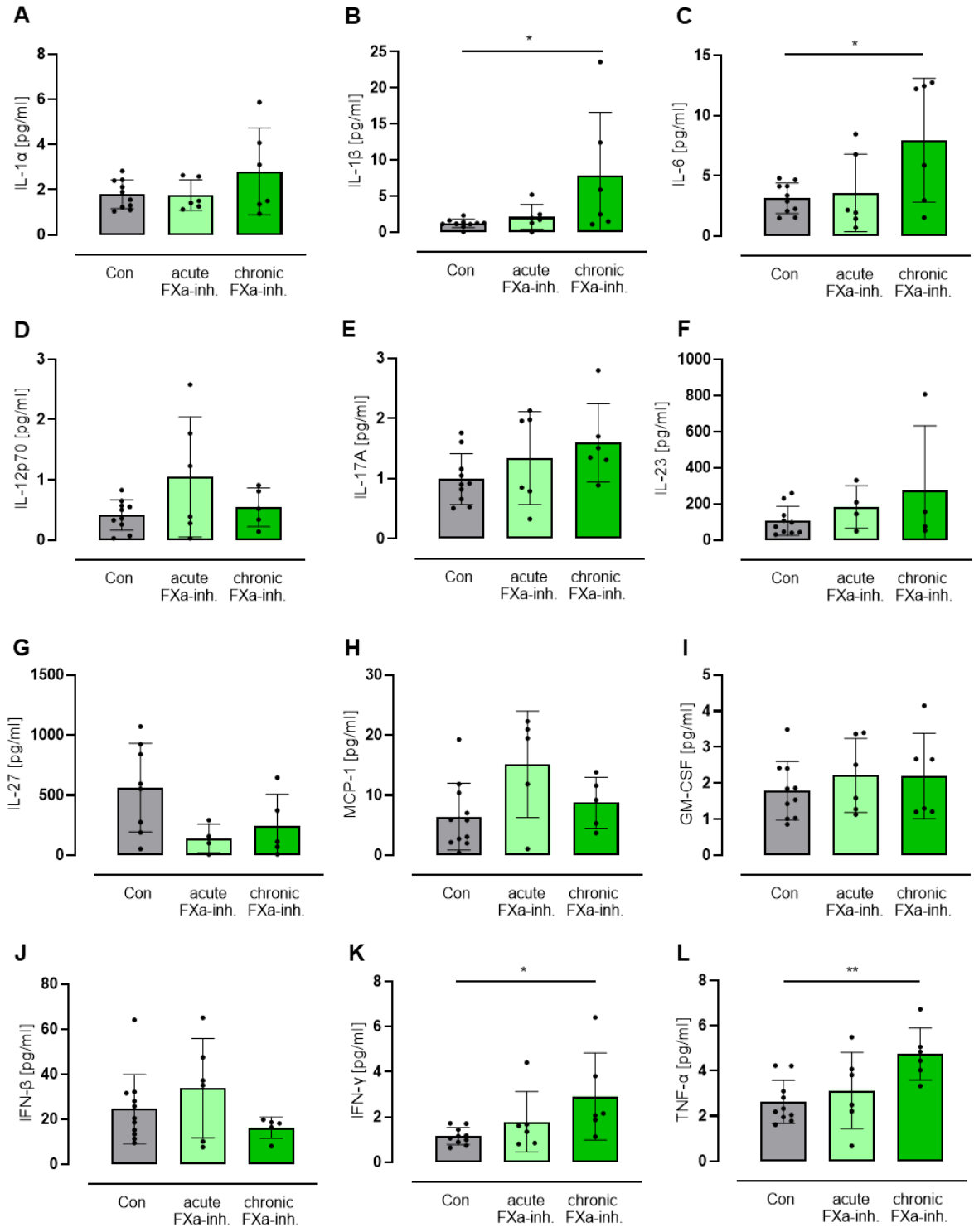

Figure 21: LEGENDplex inflammatory assay of mice plasma five days post I/R.

Figures show inflammatory cytokines measured by LEGENDplex inflammatory assay in the plasma of mice 24h post I/R. (A) Interleukin-1 alpha (IL-1α) is higher in control mice than in treated mice. No significant differences were observed in the amounts of (B) Interleukin-1 beta (IL-1β), (C) Interleukin-6 (IL-6), (D) Interleukin-12p70 (IL-12p70), (E) Interleukin-17A (IL-17A), (F) Interleukin-23 (IL-23), (G) Interleukin-27 (IL-27), (H) monocyte chemotactic protein-1 (MCP-1), (I) granulocyte-macrophage colony-stimulating factor (GM-CSF), (J) Interferon alpha (INF-α), (K) Interferon gamma (INF-ɣ) and (L) tissue necrosis factor alpha (TNF-α). Shown are means ± SD, control (n= 8-10), acute FXa-inhibition (n= 3-5) and chronic FXa-inhibition (n= 8-10). Stars above the bars indicate statistically significant differences between means by one-way ANOVA.

3.1.6 Histological analysis of mouse hearts five days post I/R

After an AMI, the inflammatory process within the tissue is of great importance for the subsequent outcome. Different types of inflammatory cells, like neutrophils and macrophages, support healing processes of injured tissue (Feng et al., 2022). Five days after an I/R injury, the number of neutrophils, respectively Ly6G positive cells, is significantly decreased in chronically FXa-inhibitor treated mice (8.70 ± 2.71) in comparison to the control group (11.62 ± 1.89) and acute treated mice (17.10 ± 2.17). Compared to the control group and the chronically treated group, the number of Ly6G positive cells is significantly higher in infarcted tissue of acute FXa-inhibitor treated mice (ANOVA, $F_{2,20} = 23.01$, $p \leq 0.0001$; **Fig. 22**).

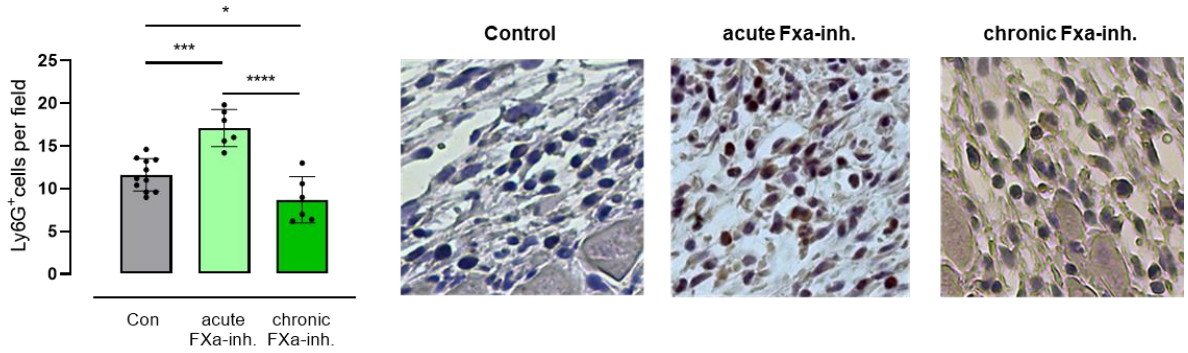

Figure 22: Histological analysis of neutrophils in infarcted mouse hearts five days post I/R.

The number of Ly6G positive cells is significantly lower in the chronically FXa-inhibitor treated group in comparison to the control and acute treated group. Compared to the control and the chronically treated group, the acute FXa-inhibitor treated group show a significantly higher number of Ly6G positive cells. Shown are means ± SD, control (n= 11), acute FXa-inhibition (n= 6) and chronic FXa-inhibition (n= 6). Stars above the bars indicate statistically significant differences between means by ANOVA. Size of exemplary histological images 100 x 100 µm.

Another cell type which regulates inflammation and scar formation are cardiac macrophages. The pro-inflammatory macrophages support clearance of matrix and debris via phagocytosis of dead cells (Ross et al., 2021). Histological analyses in this study show a significantly lower number of macrophages, Mac2 positive cells, in infarcted mice hearts of chronic FXa-inhibitor treated mice (11.77 ± 2.65) in comparison to control (17.13 ± 2.08) and acute FXa-inhibitor (22.60 ± 2.73) treated mice. Compared to the other groups, acute FXa-inhibitor treated mice show a significantly higher amount of Mac2 positive stained cells (ANOVA, $F_{2,21} = 30.85$, $p \leq 0.0001$; **Fig. 23**).

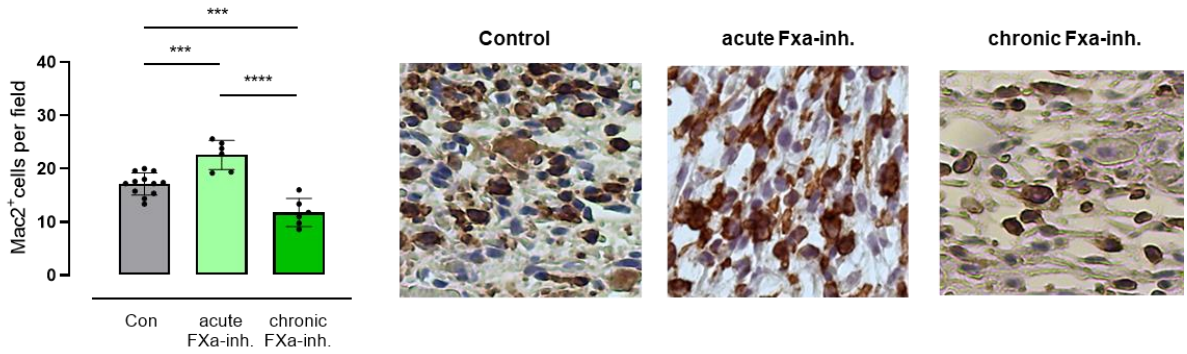

Figure 23: Histological analysis of macrophages in infarcted mouse hearts five days post I/R.

The number of Mac2 positive cells is significantly lower in the chronically FXa-inhibitor treated group in comparison to the control and acute treated group. Compared to the control and the chronically treated group, the acute FXa-inhibitor treated group show a significantly higher number of Mac2 positive cells. Shown are means ± SD, control (n= 12), acute FXa-inhibition (n= 6) and chronic FXa-inhibition (n= 6). Stars above the bars indicate statistically significant differences between means by ANOVA. Size of exemplary histological images 100 x 100 µm.

One of the neutrophil functions is forming NET. NETs have pro-thrombotic properties by stimulating fibrin deposition. Because of this the number of NETs has also been evaluated in this study. The number of NETs in infarcted heart tissue is significantly reduced in mice treated chronically with FXa-inhibitor (2.37 ± 0.46) in comparison to control mice (3.50 ± 0.58) and acute treated mice (3.20 ± 0.57). No significant differences are observed between control and acute FXa-inhibitor treated mice (ANOVA, $F_{2,19} = 8.21$, $p \leq 0.001$; **Fig. 24**).

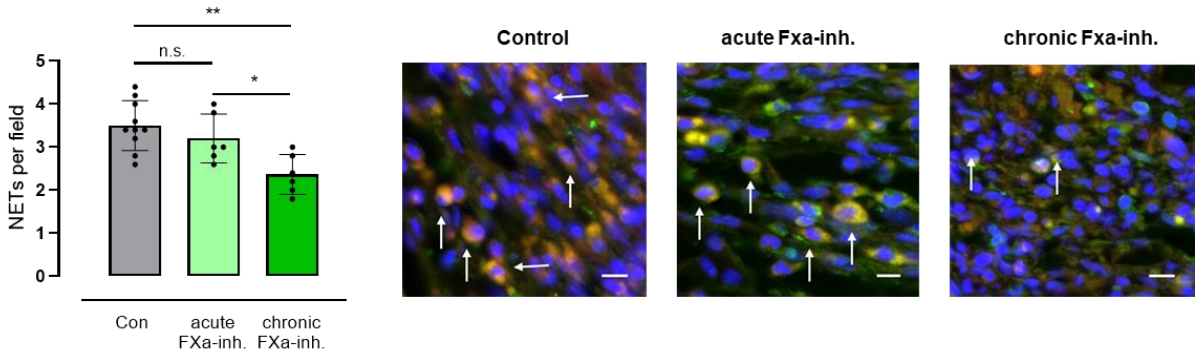

Figure 24: Histological analysis of neutrophil extracellular traps in infarcted mouse hearts five days post I/R.

The number of NETs is significantly lower in the chronically FXa-inhibitor treated group in comparison to the control and acute treated group. Comparison between control and acute FXa-inhibitor treated group shows no significant differences in the number of NETs. Shown are means ± SD, control (n= 10), acute FXa-inhibition (n= 6) and chronic FXa-inhibition (n= 6). Stars above the bars indicate statistically significant differences between means by ANOVA. Size of exemplary histological images 100 x 100 µm at 40x magnification and scale bar = 10 µm.

3.2 tMCAO in mice

Next to the investigation of possible effects of FXa-inhibitor treatment in the context of AMI, another investigated scenario was the effect of FXa-inhibitor treatment in stroke of mice which underwent a tMCAO injury. These mice received the same amounts of acute or chronic FXa-inhibitor like mice in the AMI group (paragraph 2.1.1.1).

3.2.1 Infarct sizes of TTC stained murine brains 24 h post tMCAO

TTC staining could not only be used for determining the infarct sizes of murine hearts. It is also a valid method for infarct size measurement of infarcted brains after an ischemic stroke. To investigate the effect of acute and chronic FXa-inhibitor treatment in mice which underwent a tMCAO injury, brains were removed 24 h after and stained with TTC. A significant bigger infarct volume of mice under acute FXa-inhibitor treatment (27.14 ± 3.69 %) was observed in comparison to control mice with tMCAO (20.29 ± 4.40 %) and chronically FXa-inhibitor treated mice (20.18 ± 5.87 %; ANOVA, $F_{2,22}$ = 6.42, p ≤ 0.05; **Fig. 25 A**). Also the macroscopic examination of the example pictures of TTC stained brain sections in figure 25 B shows that most of the tissue in the infarcted hemisphere is white and therefore dead.

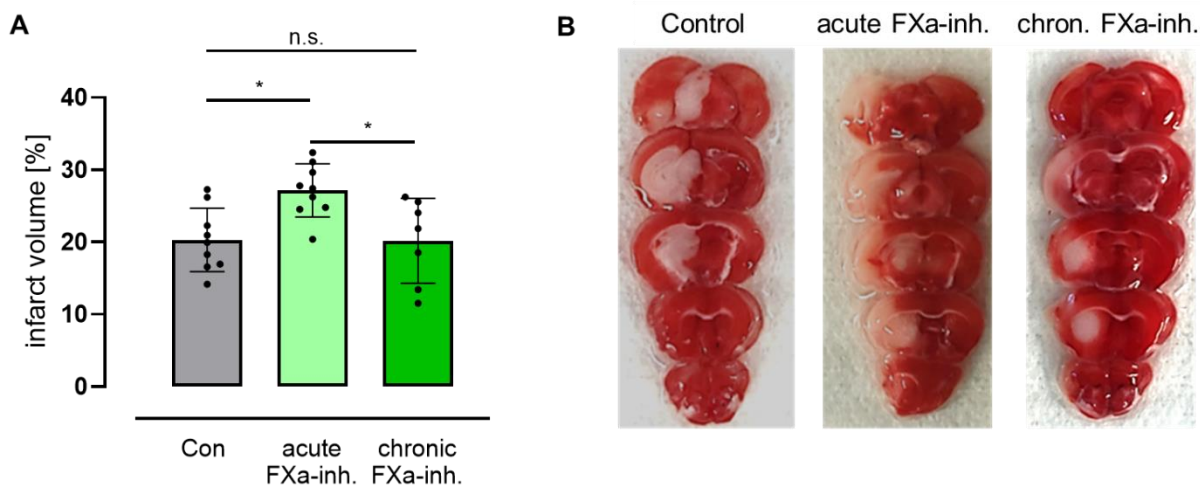

Figure 25: 2,3,5-triphenyltetrazolium chloride (TTC)-stained cerebrum of a mouse after transient occlusion of the middle cerebral artery (tMCAO).

A) Infarct volume of TTC stained infarcted brains 24 h after tMCAO injury. Shown are means ± SD, control (n= 9), acute FXa-inhibition (n= 9) and chronic FXa-inhibition (n= 7). Stars above the bars indicate statistically significant differences between means by one-way ANOVA. B) Five TTC-stained sections (2 mm thickness each) of the cerebrum of a mouse were imaged 24 hours after tMCAO. Vital tissue stained red in this staining. Not vital areas remained unstained (white). Stars above the bars indicate statistically significant differences between means by one-way ANOVA.

3.2.2 FACS of intracerebral leukocytes in murine brains 24 h post tMCAO

The inflammatory response after an injury is essential for the outcome after an ischemic event. In this study, brains were removed after 24 h post tMCAO and the percentages of intracerebral leukocytes, like granulocytes, microglia and monocytes/macrophages were measured via FACS. All groups do not show significant differences in their percentages of granulocytes (Control: 2.21 ± 1.52 % vs. acute FXa-inhibitor 1.57 ± 0.67 % vs. chronic FXa-inhibitor 1.34 ± 1.22 %; ANOVA, $F_{2,18} = 1.00$, $p \geq 0.05$; **Fig. 26 A**). The percentage of monocytes/macrophages (Mo/Mp) after chronic FXa-inhibitor treatment is reduced, but does not differ significantly between the control group (6.02 ± 3.7 %), the acute treated group (6.04 ± 2.93 %) and the chronically FXa-inhibitor treated group (3.35 ± 4.68 %; ANOVA, $F_{2,18} = 2.00$, $p \geq 0.05$; **Fig. 26 C**). Significant differences could be observed in the percentage of microglia in brain tissues. The percentage of microglia in brains of the chronic FXa-inhibitor treated group (23.06 ± 1.25 %) was significantly decreased in comparison to the control (30.56 ± 5.40 %) and the acute FXa-inhibitor treated group (27.24 ± 3.52 %; ANOVA, $F_{2,18} = 6.89$, $p \leq 0.01$; **Fig. 26 B**). Chronic FXa-inhibitor treatment reduces the percentage of activated microglia in the infarcted brains.

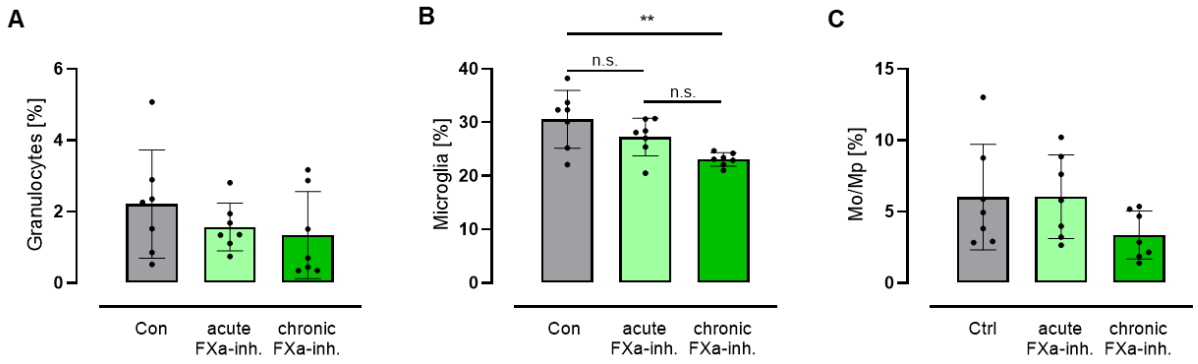

Figure 26: FACS of intracerebral leukocytes of mice brains 24 h after tMCAO.

A) The percentage of granulocytes in brain tissue after tMCAO does not differ significantly between groups of control (n= 7), acute FXa-inhibitor (n= 7) and chronic FXa-inhibitor treated mice (n= 7). B) Percentage of microglia of chronic FXa-inhibitor treated mice (n= 7) is significantly reduced in comparison to control mice (n= 7) and acute FXa-inhibitor treated mice (n= 7). C) A reduction of monocytes/macrophages could be seen in chronic FXa-inhibitor treated mice in comparison to control (n= 7) and acute FXa-inhibitor treated mice. Stars above the bars indicate statistically significant differences between means by one-way ANOVA.

3.2.4 qPCR of murine brains 24 h post tMCAO

To investigate, if the FXa-inhibitor treatment had an influence on the RNA expression in infarcted hemispheres, a qPCR was performed. Different genes were observed in this experiment. GAPDH was used as the housekeeping gene (Joshi et al., 2022) and all values refer to the mean value of the control group. The RNA expression of TNF-α was lower in control mice (1.02 ± 0.16) in comparison to acute FXa-inhibitor treated group (1.48 ± 0.42) and chronically FXa-inhibitor treated mice (1.52 ± 0.59, ANOVA, $F_{2,15} = 2.55$, $p \geq 0.05$; **Fig. 27 A**), but showed no significant difference. RNA-expression of CD16 as a pro-inflammatory factor (Hamzei Taj et al., 2016), showed also no significant difference between the groups (control 1.06 ± 0.39 vs. acute FXa-inh. 0.95 ± 0.41 vs. chronic FXa-inh. 0.98 ± 0.29; ANOVA, $F_{2,15} = 0.15$, $p \geq 0.05$; **Fig. 27 B**). A reduction of the RNA expression, but not a significant one, of another pro-inflammatory factor, CD32, a marker for the classic phenotype of microglia (M1) (Hamzei Taj et al., 2016), could be observed in mice brains of the chronic FXa-inhibitor treated group (0.87 ± 0.18) in comparison to the control group (1.09 ± 0.5) and the acute FXa-inhibitor treated group (1.1 ± 0.44; ANOVA, $F_{2,15} = 0.64$, $p \geq 0.05$; **Fig. 27 C**). The RNA expression of TGF-β1, which is known for its neuroprotective effects in cerebral ischemia (Dhandapani et al., 2003) shows no significant difference between the control group (1.14 ± 0.62), the acute FXa-inhibitor treated group (1.07 ± 0.39) and the chronic FXa-inhibitor treated group (1.08 ± 0.52; ANOVA, $F_{2,15} = 0.03$, $p \geq 0.05$; **Fig. 27 D**). The expression of the mannose receptor, CD206, which is typically expressed on matured macrophages (Wright et al., 2021), showed no significant difference between all groups (control 1.10 ± 0.50 vs. acute FXa-inh. 1.09 ± 0.52 vs. chronic FXa-inh. 1.09 ± 0.60; ANOVA, $F_{2,15} = 0.00$, $p \geq 0.05$; **Fig. 27 E**) in the infarcted hemispheres. Another marker, Ym1, which is, among others, physiologically expressed in microglia of the mouse brain (Ponomarev et al., 2007) is known to be expressed in the brain under pathological conditions in microglia (Kumar et al., 2013; Kang et al., 2022) and in neutrophils (Cuartero et al., 2013; Kang et al., 2022). In this setting Ym1 showed no significant different expression pattern between the control group (0.94 ± 0.74), the acute FXa-inhibitor treated group (1.15 ± 0.68) and the chronic FXa-inhibitor treated group (0.93 ± 0.58; ANOVA, $F_{2,15} = 0.20$, $p \geq 0.05$; **Fig. 27 F**). Furthermore, the cytokine IL-1β, which is released under physiological conditions by different cell types in the healthy CNS (Hewett et al., 2012), showed no significant differences between all groups (control 1.45 ± 1.26 vs. chronic FXa-inh. 1.22 ± 0.69), whereas a slight reduction was observed in the acute FXa-inhibitor treated group (0.72 ± 0.31; ANOVA, $F_{2,15} = 1.16$, $p \geq 0.05$; **Fig. 27 G**). Another cytokine in the CNS is IL-6, which showed no significant differences in its RNA expression pattern in the infarcted hemispheres of control mice (1.63 ± 1.81), acute FXa-inhibitor treated mice (1.81 ± 1.1) and chronic FXa-inhibitor treated mice (2.35 ± 1.13; ANOVA, $F_{2,15} = 0.44$, $p \geq 0.05$; **Fig. 27 H**). The last measured gene expression was the one of interleukin 18 (IL-18), which is constitutively

expressed in different cell types. Expression of IL-18 was slightly increased in the control group (1.04 ± 0.3) in comparison to the acute FXa-inhibitor treated group (0.86 ± 0.17) and the chronic FXa-inhibitor treated group (0.82 ± 0.22), but no significant difference was observed (ANOVA; $F_{2,15}$ = 1.48, p ≥ 0.05; **Fig. 27 I**).

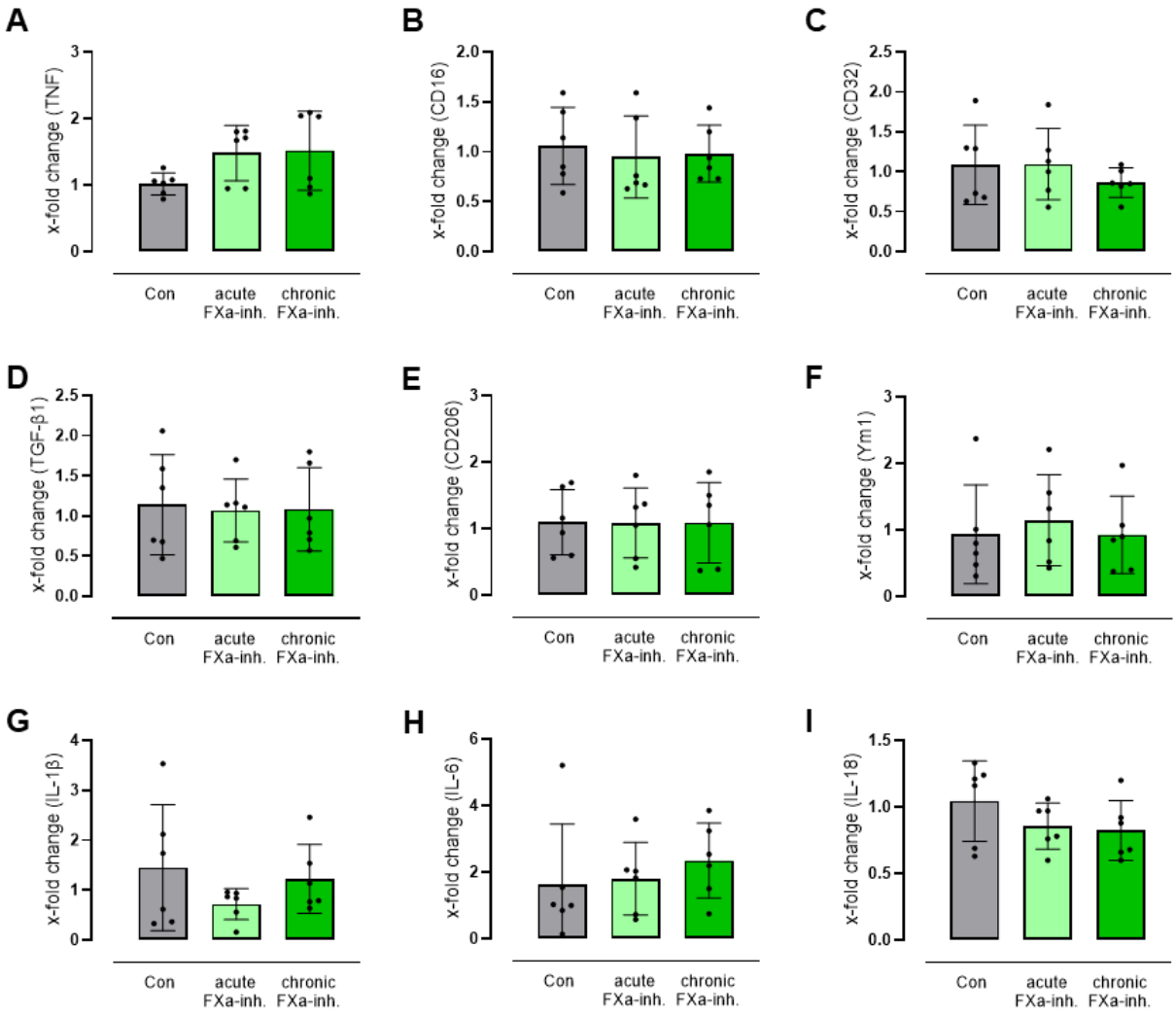

Figure 27: Polymerase chain reaction (qPCR) of murine brains 24 h post tMCAO.

The expression of different genes in the control group, the acute FXa-inhibitor treated group and the chronic treated group was compared. Nine different genes were investigated and no significant difference between them was shown. Next to tumor necrosis factor (TNF) and CD16, CD32, transforming growth factor (TGF) and CD206 were measured in qPCR, as well as Ym1, interleukin-1β (IL-1β), interleukin-6 (IL-6) and interleukin-18 (IL-18). Statistical differences between means were measured by one-way ANOVA (all groups n=6).

3.2.5 Histological analysis of mouse brains 24 h post tMCAO

Next to NETs in murine hearts, they were also investigated in mouse brains 24 h after tMCAO surgery. Figure 28 A shows, that the number of NETs per field is significantly higher in acute FXa-inhibitor treated mice (5.65 ± 0.19) in comparison to control mice (4.10 ± 0.60) and chronic FXa-inhibitor treatment (4.75 ± 0.19; ANOVA, $F_{2,9} = 16.78$, $p \leq 0.001$). Exemplary pictures of NET staining are shown in the upper row of figure 24 C. Another important parameter in the context of inflammation is the infiltration of the injured tissue with macrophages. A specific cell type, the microglia, have the function of macrophages in the central nervous system (CNS). The staining of microglia gives an overview of the activation of this macrophage population in the brain. For this purpose, the ionized calcium binding adaptor molecule 1 (Iba1) was stained. In comparison to control mice (5.94 ± 0.55) and chronic FXa-inhibitor treated mice (5.88 ± 0.60) the acute FXa-inhibitor treated group of mice (8.63 ± 0.43) shows a significant higher number of $Iba1^+$ cells in the infarcted hemisphere (ANOVA, $F_{2,9} = 34.84$, $p \leq 0.0001$; **Fig. 28 B**). Exemplary pictures of Iba1 staining are shown in the lower row of figure 28 C.

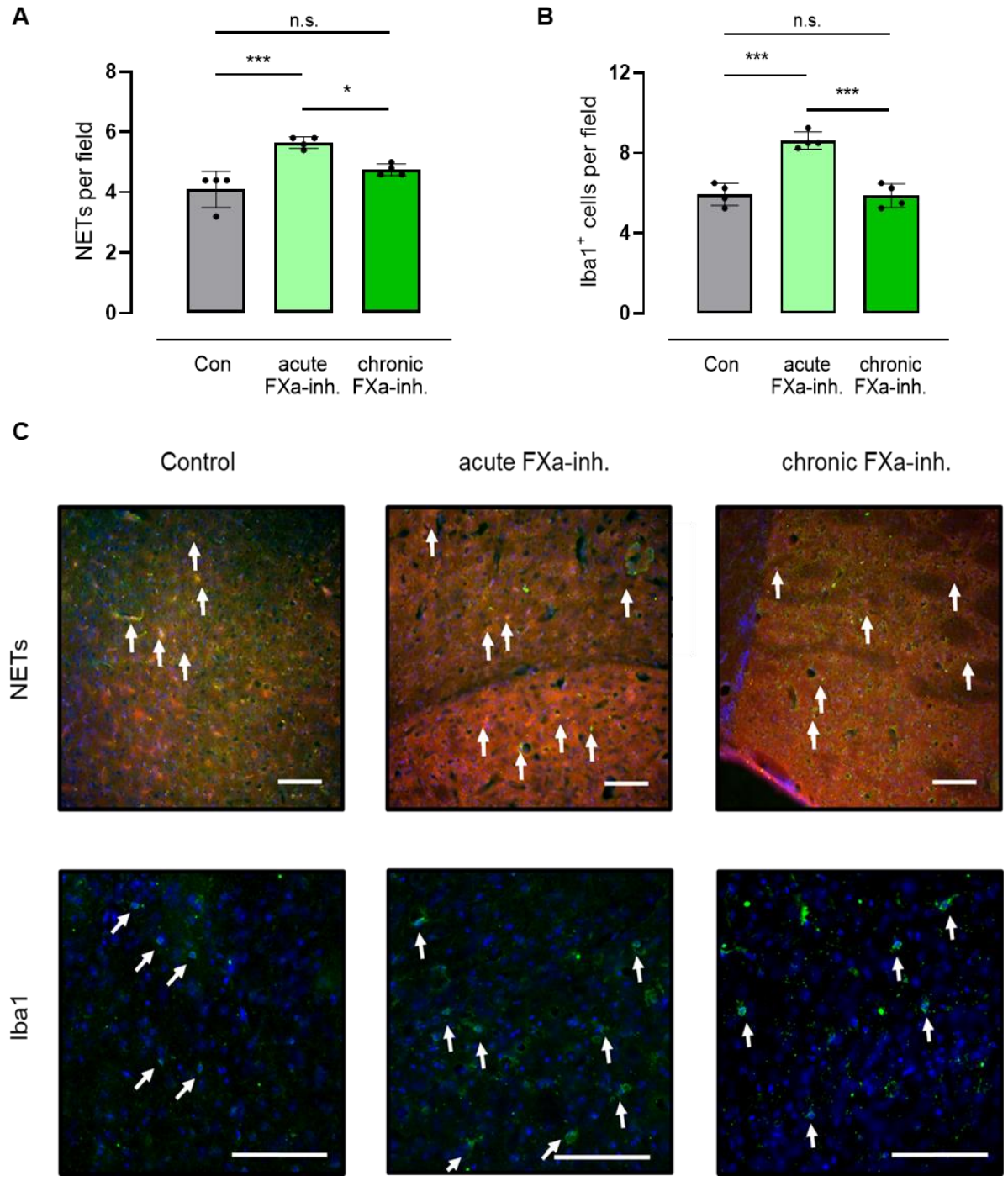

Figure 28: Histological analysis of neutrophil extracellular traps and activated microglia in infarcted mouse brains 24 h post tMCAO.

A) The number of NETs is significantly lower in the acute FXa-inhibitor treated group in comparison to the control and chronically treated group. Comparison between control and chronic FXa-inhibitor treated group shows no significant differences in the number of NETs. Shown are means ± SD, control (n= 4), acute FXa-inhibition (n= 4) and chronic FXa-inhibition (n= 4). B) The number of Iba1 positive cells is significantly lower in the acute FXa-inhibitor treated group in comparison to the control and chronically treated group. Comparison between control and chronic FXa-inhibitor treated group shows no significant differences in the number of Iba1 positive cells. Shown are means ± SD, control (n= 4), acute FXa-inhibition (n= 4) and chronic FXa-inhibition (n= 4). Stars above the bars indicate statistically significant differences between means by ANOVA. C) upper row: NET staining and size of exemplary histological images was one field at 20x magnification and scale bar = 100 µm. Lower row: Iba1 staining and size of exemplary histological images was 300 x 300 µm at 20x magnification and scale bar = 100 µm.

3.3 Effect of FXa inhibition in depleted mice

To find out, if platelets, as the first population which migrates to the infarcted myocardium, play a significant role in the reduction of infarct sizes of chronic FXa inhibition after 24 h, mice were platelet depleted via a specific monoclonal antibody directed against mouse GPIbα (CD42b). This leads to thrombocytopenia in the injected mice. The infarct size of mice with FXa-inhibitor treatment (26.95 ± 4.5 %) was significantly lower in comparison to the control group (43.32 ± 6.18 %). This effect was blunted by platelet depletion (control group depleted: 33.36 ± 5.2 % vs. FXa-inhibitor treated group depleted (33.02 ± 5.78 %) (ANOVA, $F_{1,28}$ = 17.31, p ≤ 0.0001; **Fig. 29 A**). The area at risk of the left ventricle did not differ between mice without FXa inhibition and depletion (49.43 ± 10.35 %), mice with chronic FXa-inhibitor treatment (46.64 ± 8.54 %), mice without FXa-inhibitor treatment but with depletion (46.47 ± 12.02 %) and mice with FXa-inhibitor treatment and depletion (45.06 ± 6.82 %) (ANOVA, $F_{1,28}$ = 0.04, p ≥ 0.05; **Fig. 29 B**). The depletion of mice did not have a significant effect on the heart rate 24 h post AMI (control group: 534.1 ± 55.77 1/min vs. FXa-inhibitor treated mice 505.5 ± 51.33 1/min vs. control group depleted: 490.5 ± 28.97 1/min vs. FXa-inhibitor treated mice with depletion: 516.2 ± 28.39 1/min; ANOVA, $F_{1,28}$ = 3.19, p ≥ 0.05; **Fig. 29 C**). Echocardiographic assessment of the mice 24 h after AMI show a significant better EF 24 h post AMI in mice with FXa-inhibitor treatment (43.40 ± 4.73 %) in comparison to control mice without any treatment (35.14 ± 5.66 %). The blunted effect of depletion was also observed in the EF and no significant differences were observed in mice with depletion (39.55 ± 5.92 %) and mice with FXa-inhibitor treatment and depletion (40.37 ± 5.75 %) (ANOVA, $F_{1,28}$ = 3.62 p ≥ 0.05; **Fig. 29 D**). this pattern was observed as well in the measurement of the SV. FXa-inhibitor treated mice showed a significant higher SV 24 h post AMI (30.89 ± 4.27 µl) in comparison to mice without any treatment (24.64 ± 3.47 µl). The beneficial effect of chronic FXa inhibition on cardiac function after AMI disappeared in platelet depleted mice with FXa-inhibitor treatment (25.20 ± 4.17 µl) and in mice with depletion without FXa-inhibitor treatment (24.96 ± 5.47 µl) (ANOVA, $F_{1,28}$ = 3.72, p ≥ 0.05; **Fig. 29 E**). The positive effect of chronic FXa-inhibitor treatment was blunted in platelet depleted mice.

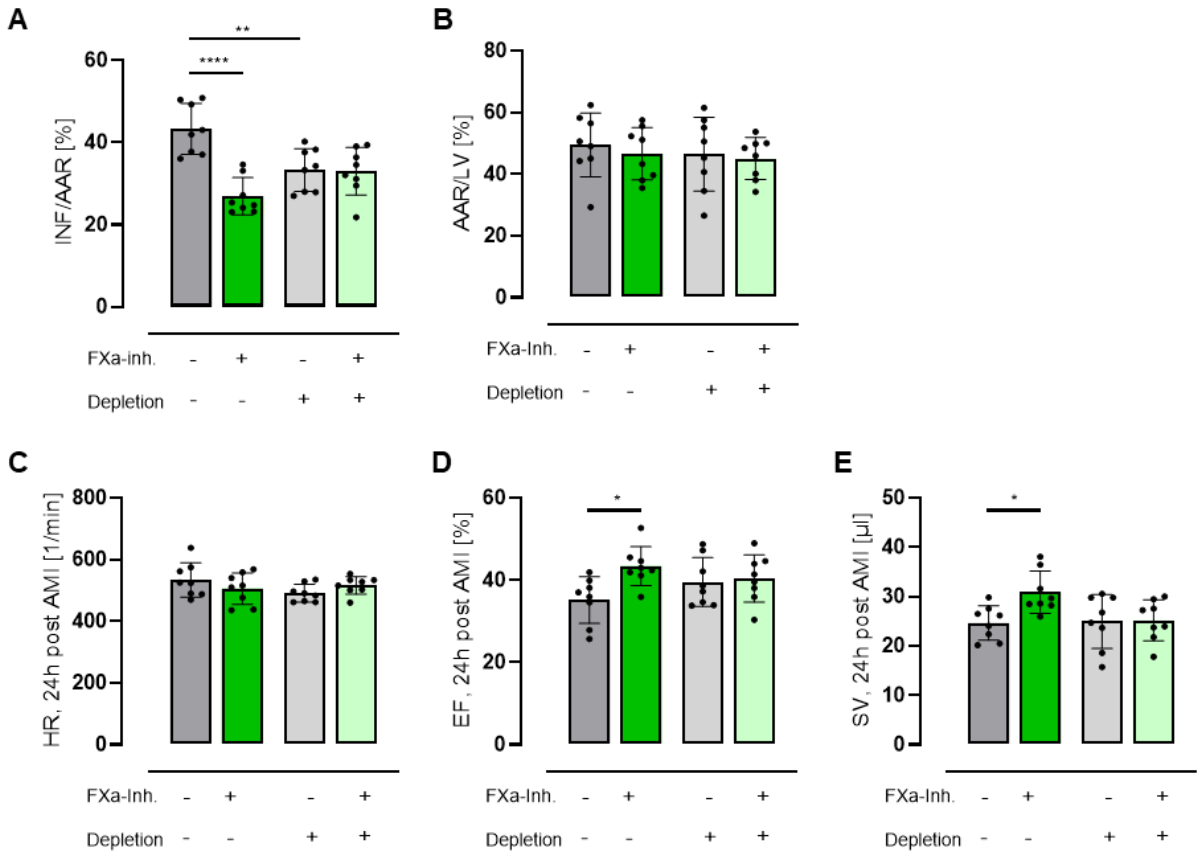

Figure 29: Effect of FXa inhibition of infarct size 24 h after AMI in platelet depleted mice.

A) Infarct size reduction of chronic FXa inhibition 24h after AMI was blunted by platelet depletion. C-E) This was also confirmed by the echocardiographic assessment of the mice 24h after AMI. The beneficial effect of chronic FXa inhibition on cardiac function after AMI disappeared in platelet depleted mice (all groups n=8). Shown are means ± SD. Statistical differences between means were measured by two-way ANOVA.

3.4 Effect of chronic FXa-inhibitor treatment on blood composition

FXa-inhibitors have an anticoagulatory effect on blood. To test whether the chronic treatment of mice with a FXa-inhibitor changes, next to the function, also the composition of blood components and if so, what is the underlying mechanism, was also investigated in this study. Blood from control mice and chronically treated mice was collected. These mice did not undergo any surgical process, to avoid the impact of inflammatory responses. Control mice (1542 ± 110) and chronically FXa-inhibitor treated mice (1525 ± 48) do not differ significantly in the number of platelets ($t(8) = 0.32$, $p \geq 0.05$; **Fig. 30 A**) and also the platelet volumes are not significantly different (control: 5.56 ± 0.36 µm³ vs. chron. FXa-inhibitor: 5.36 ± 0.22 µm³ ; $t(8) = 1.07$, $p \geq 0.05$; **Fig. 30 B**). Another important cell type in this study are white blood cells (WBC), which play a major role in inflammatory responses. Both groups, control (2.40 ± 0.69) and chronically FXa-inhibitor treated one (3.12 ± 1.26), do not differ significantly in the number of WBC ($t(8) = 1.12$, $p \geq 0.05$; **Fig. 30 C**). There are different components grouped under the

category of white blood cells. These cell types do not show significant differences in their numbers of cells: neither the number of lymphocytes (control 1.78 ± 0.43 vs. chronic FXa-inhibitor 2.44 ± 0.97; $t(8) = 1.39$, $p \geq 0.05$; **Fig. 30 D**) nor the number of monocytes (control 0.08 ± 0.08 vs. chronic FXa-inhibitor 0.10 ± 0.07; $t(8) = 0.41$, $p \geq 0.05$; **Fig. 30 E**) or the number of granulocytes (control: 0.54 ± 0.34 vs. chronic FXa-inhibitor: 0.58 ± 0.24; $t(8) = 0.22$, $p \geq 0.05$; **Fig. 30 F**). These findings suggest that the FXa-inhibitor treatment of mice over five weeks has no effect on the composition of blood samples.

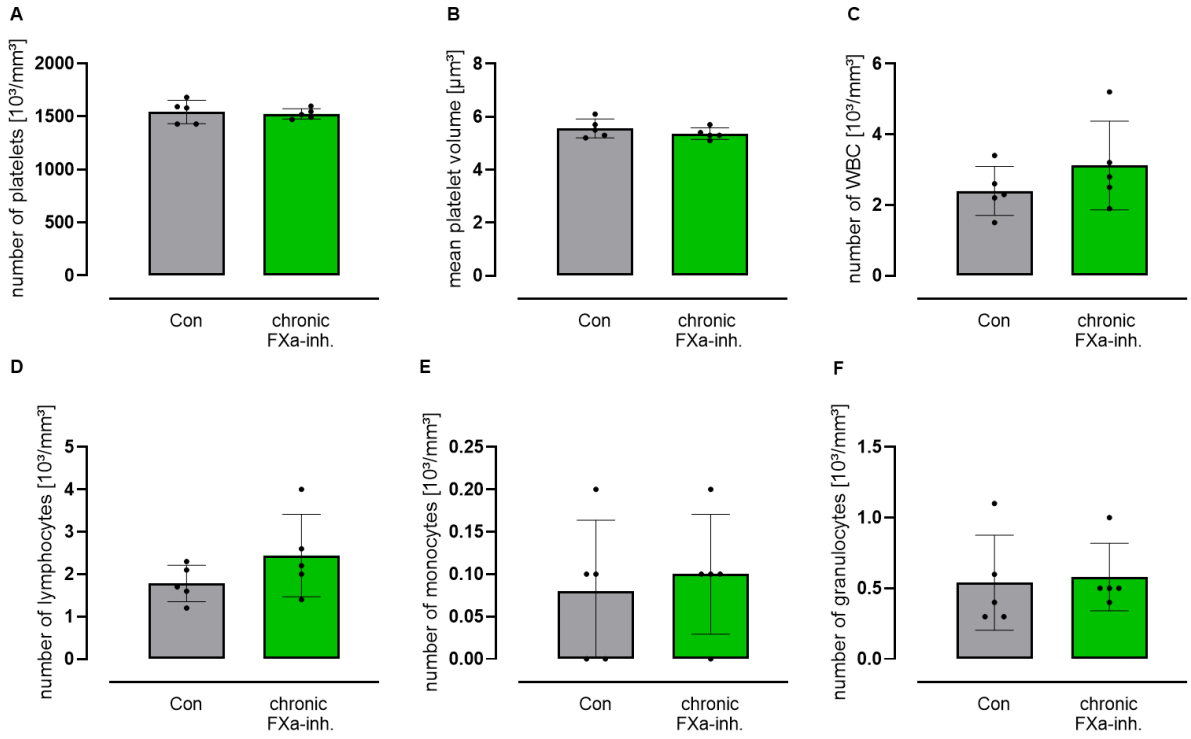

Figure 30: Effect of chronic FXa-inhibitor treatment on blood composition.

Shown are numbers or volume of different blood components from control mice and chronically FXa-inhibitor treated mice. (A) The number of platelets does not show significant differences between groups. (B) Sizes of platelets are not significantly different between groups. (C) The number of white blood cells (WBC) in general and of the different WBC components, like lymphocytes (D), monocytes (E) and granulocytes (F) do not differ significantly between groups. Shown are means ± SD, control (n= 5) and chronic FXa-inhibition (n= 5). Significant differences between means were calculated by *t*-test.

3.4.1 Effect of chronic FXa-inhibitor treatment on endothelial function

To investigate if the treatment with a FXa-inhibitor has an effect on endothelial function, the blood pressure in control mice and chronic FXa-inhibitor treated mice was measured via Millar catheter system. Two parameter were measured: the systolic pressure (P_{sys}) and the diastolic pressure (P_{dias}). With these two values, the MAP was calculated. No significant differences in the P_{sys} of control mice (90.62 ± 8.95 mmHg) in comparison to chronic FXa-inhibition (89.42 ± 4.10 mmHg; $t(8) = 0.27$, $p \geq 0.05$; **Fig. 31 A**) and in the P_{dias} (control: 62.84 ± 9.84 mmHg vs. chron. FXa-inh. 61.64 ± 1.86 mmHg; $t(8) = 0.27$, $p \geq 0.05$; **Fig. 31 B**) are observed. The calculated MAP shows no significant differences between both experimental groups (control: 81.36 ± 9.15 mmHg vs. chron. FXa-inh. 80.16 ± 3.24 mmHg; $t(8) = 0.28$, $p \geq 0.05$; **Fig. 31 C**). Another measured parameter during the blood pressure measurement was the heart rate, which did not differ significantly between groups (data not shown). The chronic treatment with a FXa-inhibitor has no effect of the endothelial function in the context of blood pressure and heart rate.

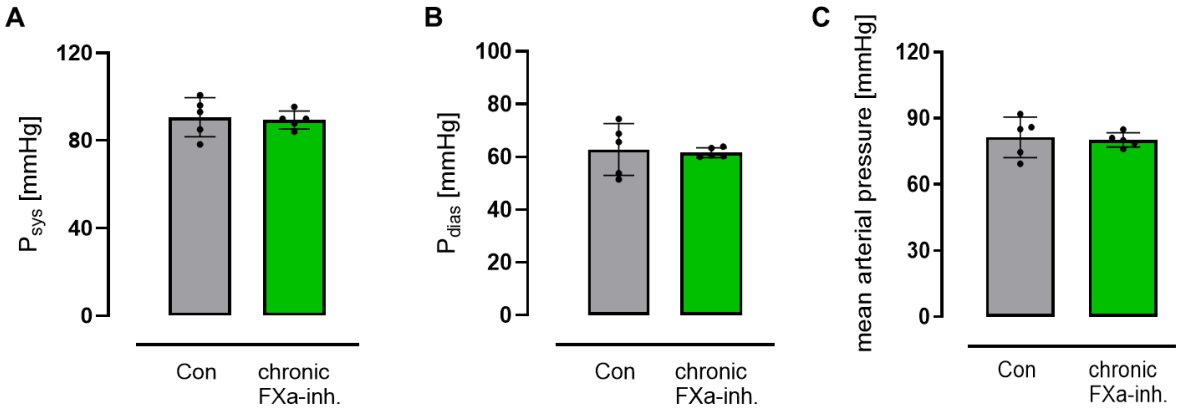

Figure 31: Blood pressure of control mice and mice under chronic FXa-inhibitor treatment.

Shown are (A) systolic (P_{sys}) and (B) diastolic pressure (P_{dias}) of mouse blood, measured in the carotid artery of control mice and mice which were treated chronically for five weeks with a FXa-inhibitor. The mean arterial pressure was calculated from P_{sys} and P_{dias} Shown are means ± SD, control (n= 5) and chronic FXa-inhibition (n= 5). Significant differences between means were calculated by *t*-test.

Another experiment in this study, to examine the influence of chronic FXa-inhibitor treatment on the endothelium and its function, was the measurement of the flow-mediated dilatation. The *Arteria iliaca externa* in the mouse hind limb was occluded with a vascular occluder for five minutes and reperfused afterwards for another five minutes. The measured dilatation during these ten minutes does not differ significantly between the control group and the group of mice treated chronically with a FXa-inhibitor (**Fig. 32**).

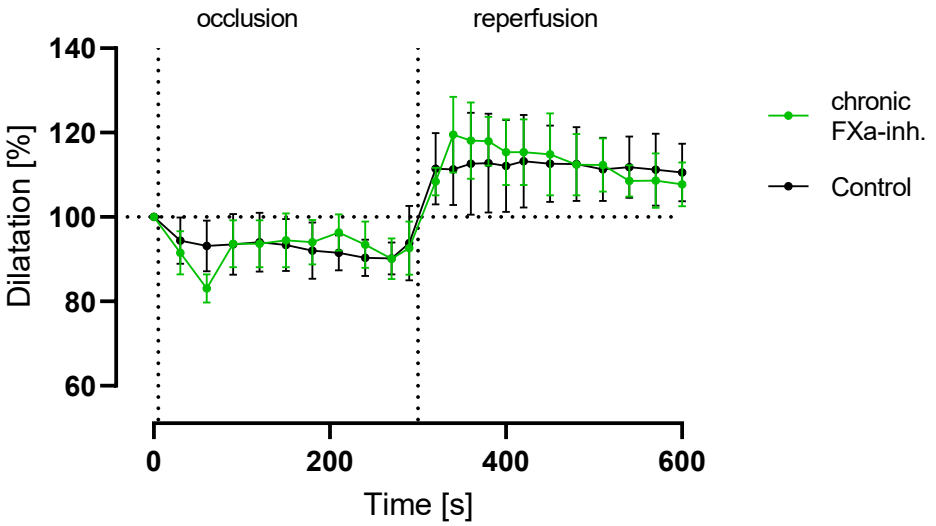

Figure 32: Flow-mediated dilatation of the *A. iliaca externa* in control mice and chronic FXa-inhibitor treated mice.

The dilatation of the *A. iliaca externa* during the occlusion and reperfusion phase was recorded and showed no significant difference between control group (n=9) and chronic FXa-inhibitor treated group (n=5). Shown are means ± SD of control and chronic FXa-inhibition. Significant differences between means were calculated by mixed-effects analysis.

3.5 Human samples

In collaboration with the working group of PD Dr. med. Tobias Petzold from LMU, human samples were also investigated. The experiments were performed by Dr. Petzold's working group. Collection of human coronary thrombi and all histological analyses were done at the University Hospital Düsseldorf.

3.5.1 RNA and proteome analyses of human platelets

In these experiments, the direct effects of FXa on platelets in the setting of acute atherothrombosis were elaborated. To investigate the role of the FXa-platelet axis and its inhibition in the chronic setting, analyses of the platelet proteome as well as the platelet transcriptome were performed. To avoid interindividual differences as confounding factors, a matched platelet proteome analysis by quantitative mass spectrometry and a matched RNA sequencing of the individual patients were performed in patients with AF or flutter with temporary oral anticoagulation (FXa inhibitor) during and four weeks after completion of FXa inhibitor intake (**Fig. 33 A**). This analyses identified 2128 differentially expressed RNAs and 601 differentially expressed proteins. To reduce the intrinsic limitations of quantitative proteomic analysis, especially with regard to less highly expressed or membrane-bound proteins, a pooled analysis of the proteomic as well as RNA sequencing data was performed (**Fig. 33 B**). The present analysis includes only genes that showed similar changes at RNA and protein levels. Subsequently, a Gene Ontology Enrichment Analysis (GO enrichment analysis) was performed, in which differentially regulated signaling pathways were identified. FXa inhibition essentially led to a downregulation of genes at the RNA and protein level (**Fig. 33 B**). In particular, signaling pathways involved in vesicle formation (i.e. membrane trafficking) and vesicle transport were found (**Fig. 33 C**). Among the genes most clearly regulated at the protein and RNA levels under FXa inhibition was vesicle associated membrane protein-8 (VAMP-8) of the soluble N-ethylmaleimide-sensitive factor attachment receptor (v-SNARE) family (**Fig. 33 D**). An altered protein biosynthesis of platelet by blockade of non-plasmatic FXa action was found.

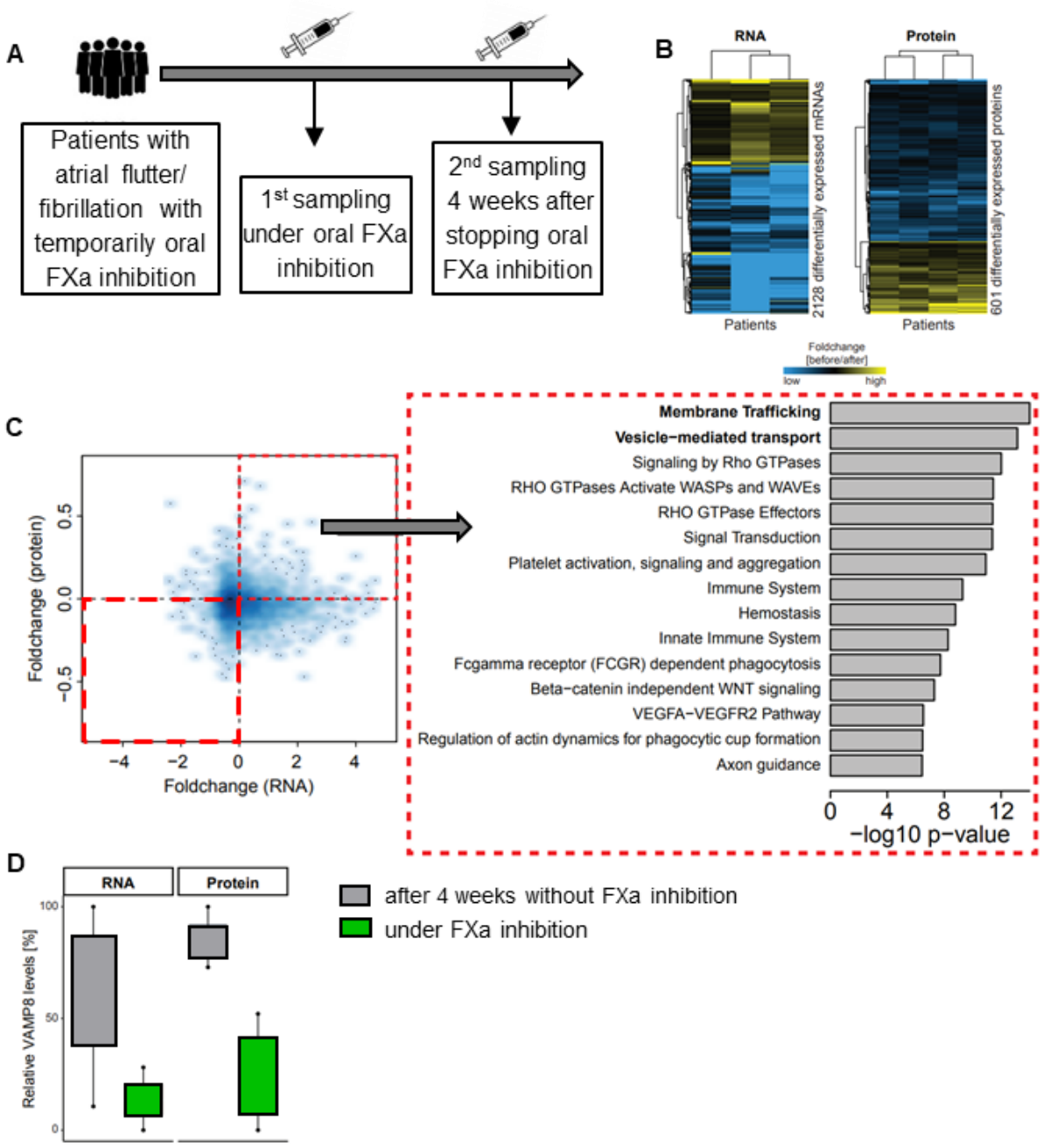

Figure 33: Proteome and RNA analyses of human platelets under oral FXa inhibition.

(A) The flowchart shows the included patient: a high-purity platelet population was isolated from patients with temporary oral factor Xa inhibition under and 4 weeks after discontinuation. (B-C) Proteome and RNA expression analysis with pooled Gene Ontology enrichment analysis. GO enrichment analysis was performed only for genes that showed similar changes at the RNA and protein levels (red frame). Indication of the most upregulated signaling pathways under FXa inhibition (apixaban). (D) A downregulation of VAMP-8 under direct FXa inhibition at the protein level was observed. Data sets shown were generated from 4 patients under or after discontinuation of apixaban (n=4).

To test the functional relevance of proteomic changes under pharmacotherapeutic inhibition with regard to platelet vesicular function, degranulation experiments were performed. Here, washed platelets from patients under chronic FXa inhibition were compared with age- and sex-matched controls. This revealed markedly reduced secretion for the α-granule protein vWF (**Fig. 34 A**) and serotonin stored in dense granules (**Fig. 34 B**) from platelets after stimulation with different agonists, like U46619, a TXA_2 analogon, collagen and thrombin. No evidence was found for differential loading of platelets with vWF or serotonin (data not shown). Differences with respect to platelet aggregation were not found, suggesting residual vesicle secretion required for platelet aggregation (**Fig. 34 C**).

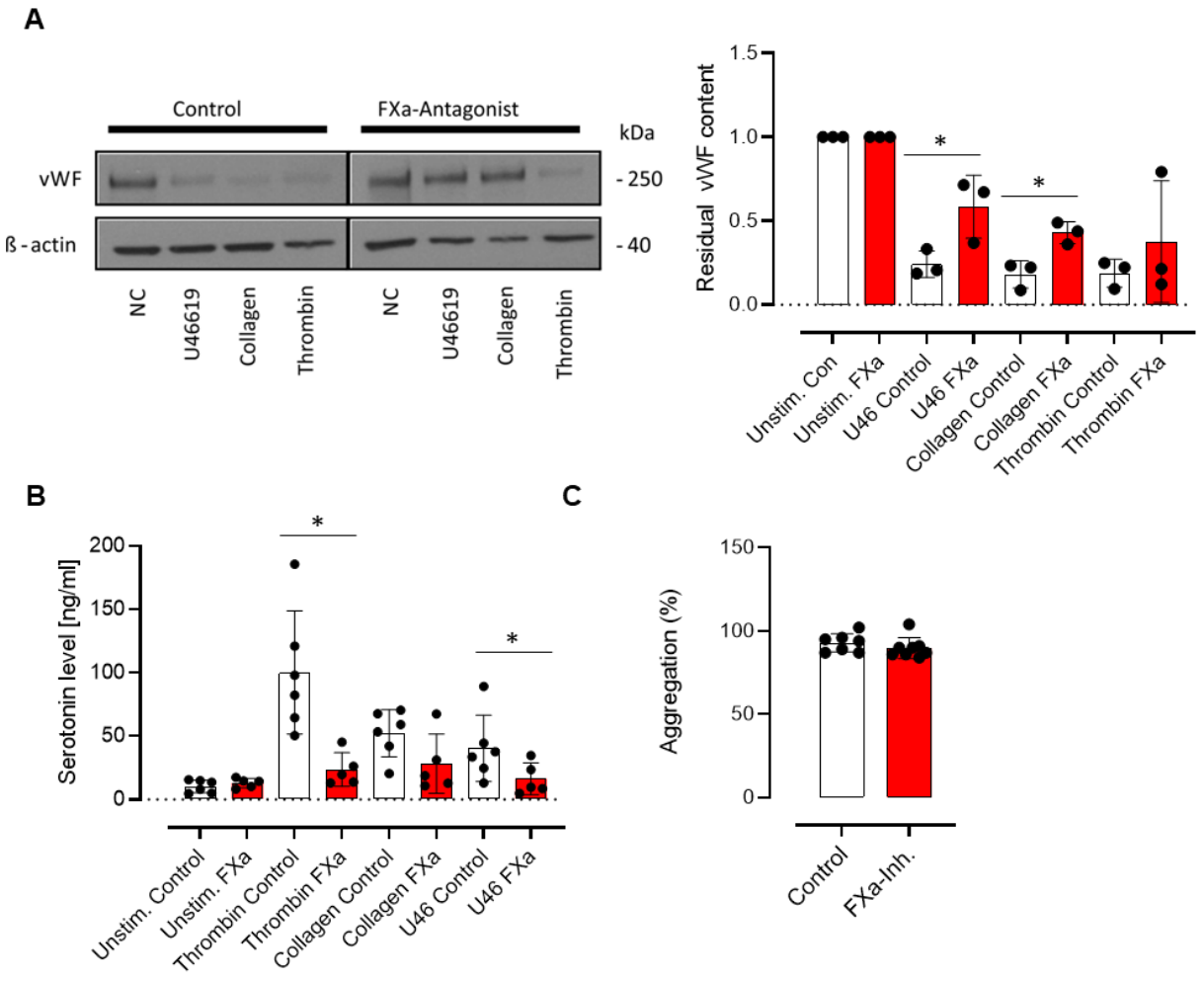

Figure 34: Effect of chronic FXa inhibition on platelet function and pharmacological inhibition.

(A) Secretion assay in patients with chronic oral inhibition of factor Xa (apixaban) and controls. Determination of residual vWF factor in aggregated platelets by Western blotting after stimulation with the indicated agonists. β-Actin serves as a loading control. (B) Serotonin release after platelet aggregation for the indicated agonists in chronic factor Xa inhibitor patients (n=5; apixaban) and controls (n=6), significance levels are indicated. (C) Light transmission aggregometry in washed platelets (WP) from patients on chronic oral FXa therapy or controls after collagen stimulation (n=8 for apixaban, n=7 for controls).

In platelets and their precursors, megakaryocytes, VAMP proteins (including VAMP-3, VAMP-8) regulate the endocytosis of plasma proteins, the formation and transport of intracellular granules, as well as their secretion (Sharda et al., 2018). In this context, the VAMP-3 protein plays an essential role in the endocytosis of plasma and membrane proteins into endosomes and in granule distribution (Lowenstein, 2017). To investigate the influence of FXa inhibition on these processes, the number of vesicles as well as their distribution were analyzed in thrombin-stimulated platelets (**Fig. 35 A**). Compared with platelets from non-anticoagulated patients, an increased number of VAMP-3 positive vesicles with a central distribution pattern within the cell was found (**Fig. 35 B-D**), demonstrating the functional relevance of chronic FXa inhibition on vesicle formation and transport.

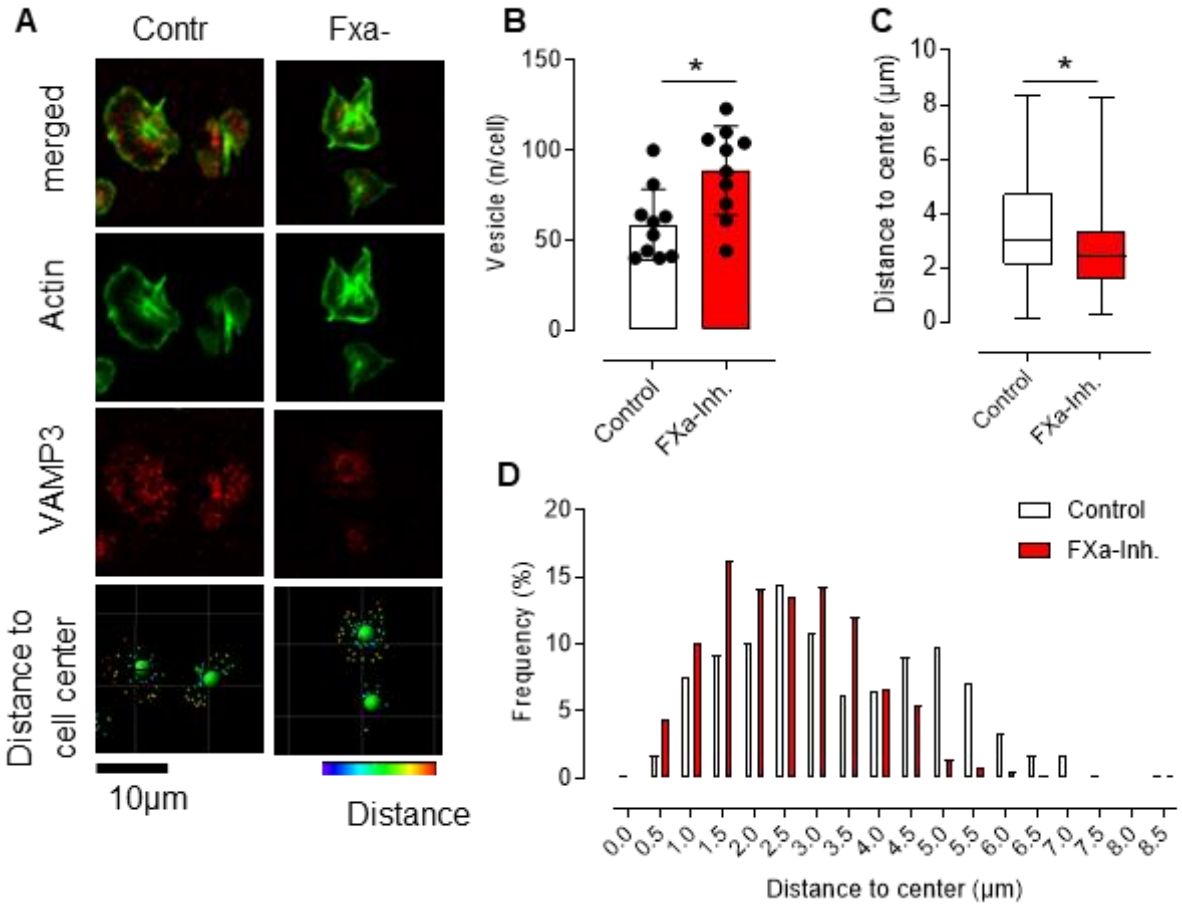

Figure 35: Effect of chronic FXa inhibition on VAMP-3 in human platelets.

Analysis of VAMP-3 positive membrane compartment (vesicles) in patients under chronic oral FXa inhibition (apixaban) and healthy controls (n=2 per group). (A) Immunofluorescence images of thrombin-stimulated platelets (red: VAMP-3, green: phalloidin). Representative images are shown. Scale corresponds to 10 µm. (B) Quantification of the number as well as (C) the mean vesicle distance to the calculated cell center (subfigure A; green sphere). (D) Distance distribution histogram of VAMP-3 positive vesicles within the cell. Symbols represent individual cells (B); significance levels (*p*-values) are indicated.

3.5.2 Histological analysis of NETs in human thrombi

Next to the experiments with human platelets, human coronary thrombi were collected after interventions. Thrombi of patients under FXa inhibitor treatment and people without any FXa inhibitor intake were compared. Significant differences in the number of NETs could be investigated between the control group (2.64 ± 0.52) and the FXa inhibitor treated group of patients (0.68 ± 0.23). Under FXa inhibitor treatment, patients show a significantly reduced number of NETs in coronary thrombi ($t(8) = 7.75$, $p < 0.0001$; **Fig. 36 A** and **B**).

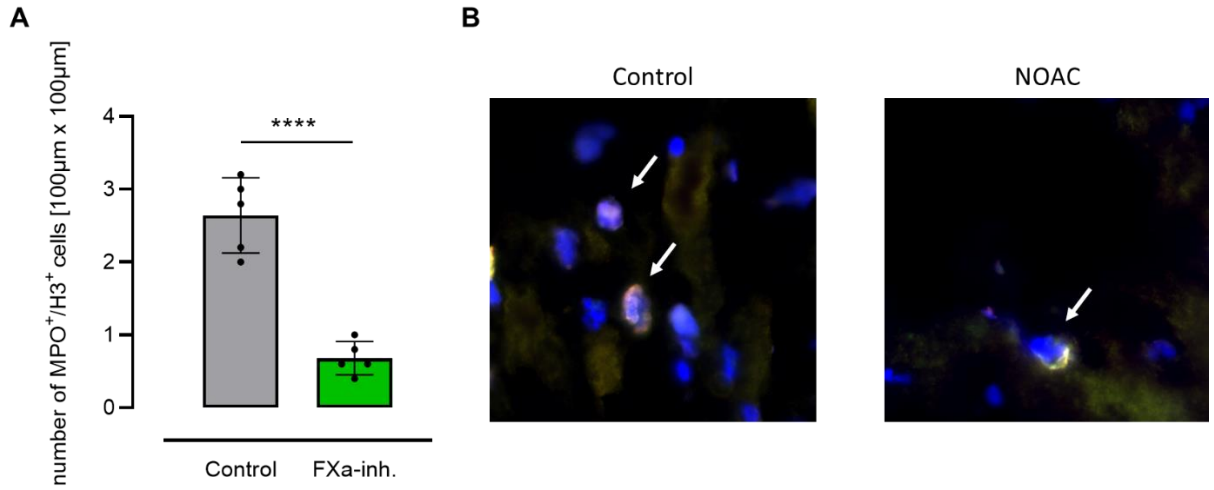

Figure 36: Histological analysis of neutrophil extracellular in human coronary thrombi.

A) The number of NETs is significantly lower in the FXa-inhibitor treated group of patients in comparison to the control group. B) Histological staining of NETs in control and NOAK treated patients. Shown are means ± SD, control (n= 5), FXa-inhibition (n= 5). Significant differences between means were calculated by *t*-test.

To sum the humans experiments up, it could be shown, that chronic oral inhibition of FXa leads to a reduction of platelet biosynthesis and presumably also megakaryocyte biosynthesis of membrane trafficking proteins and thus to altered granule secretion and localization. As well as mice, human show significant thromboinflammation under FXa-inhibitor treatment and have a better outcome after an acute event.

4. Discussion

4.1 Main findings

In this thesis, a novel platelet-derived anti-thromboinflammatory effect of long-term FXa inhibition is revealed, which improves the outcome after AMI and stroke. The three main findings of this thesis are:

1. The chronic, but not the acute oral FXa inhibition, improves the outcome after AMI and stroke in mice experiments
2. A reduced platelet-driven thromboinflammation and NET formation was revealed as the underlying mechanism
3. Chronic FXa-inhibition results in a reduced synthesis of VAMP proteins with a following blocked platelet degranulation

4.2 Clinical relevance

The use of NOACs has been increasing in the past years. These drugs are the first choice for preventing thrombotic complications, especially strokes, in patients with AF (Kirchhof et al., 2016). Different inhibitors of FXa, like RIVA, apixaban or edoxaban are approved. Also one FIIa inhibitor, dabigatran, is available. These inhibitors show reduced bleeding complications in comparison to the long known VKAs. Nevertheless, there was evidence of differences between NOACs and VKAs in the incidence of MI (Connolly et al., 2009; Granger et al., 2011; Patel et al., 2011; Gibson et al., 2016; Cannon et al., 2017; Lopes et al., 2019), which was surprising, because ultimately both classes of drugs address the same point, FXa, of the coagulation cascade. This is consistent with clinical evidence from the main trials in which patients with oral FXa inhibition had numerically lower rates of ischemic events.

The experiments in this thesis are influenced by the three main studies on RIVA treatment in CAD and HF: the ATLAS ACS trial, the COMPASS trial and the COMMANDER HF trial. The ATLAS ACS trial (**Fig. 5**) investigated the effect of RIVA in patients with recent ACS (Mega et al., 2012). ACS is the result of coronary atherosclerosis with overlaid thrombosis (Singh et al., 2023). The hypothesis of this trial was that RIVA in low doses can improve the cardiovascular outcome in humans with ACS, which includes patients with STEMI, NSTEMI or unstable angina. In total, 15,526 patients with ACS received a RIVA dose of 2.5 mg or 5 mg twice a day for a mean of 13 and a maximum of 31 months. A combination of death due to cardiovascular causes, myocardial infarction or stroke was set as the primary endpoint. In the ATLAS ACS

trial, RIVA decreased the number of primary endpoints in comparison with the placebo over time. These improvements were observed in the 2.5 mg group and also in the 5 mg group, where every group got doses twice a day. Interestingly, a bigger survival benefit was found in the 2 x 2.5 mg group. Nevertheless, the risk of major bleeding and intracranial haemorrhage under RIVA was increased in comparison to the placebo. Between both RIVA treated groups rates of major bleeding was lower in patients with the 2.5 mg dose than in the 5 mg dose group (1.8 % vs. 2.4 %, p = 0.12), significantly lower rates of minor bleeding could be observed in the group which received low dose RIVA (0.9 % vs. 1.6 %, p = 0.046), bleeding requiring medical attention (12.9 % vs. 16.2 %, p <0.001) and fatal bleeding (0.1% vs. 0.4%, p = 0.04) (Mega et al., 2012). The findings and results in this thesis agree with the results of the ATLAS ACS trial: Also in the mice experiments a low chronic dose of RIVA improved cardiac outcome after AMI. However, in our experiment setup RIVA administration was started before the deliberately induced event and not before a naturally occurring AMI. In the “Cardiovascular Outcomes for People Using Anticoagulation Strategies” (COMPASS) trial, 27,395 randomly assigned stable cardiovascular disease (CVD) patients received either RIVA 2.5 mg twice a day plus 100 mg aspirin once a day, 5 mg RIVA twice a day or 100 mg aspirin alone once a day (Eikelboom et al., 2017). A combination of cardiovascular death, stroke or MI was the primary outcome. Even when patients with cardiovascular disease receive drugs to prevent other upcoming events, 5 to 10 % have another event each year (Bhatt et al., 2010; Eikelboom et al., 2017). Aspirin in the context of secondary prevention shows a lower risk of 19 % for major cardiovascular events and a lower risk of 9 % for cardiovascular death than a placebo (Antithrombotic Trialists et al., 2009). After an AMI, patients need an antithrombotic regime, but VKA or VKA plus aspirin results in higher bleeding probability (Anand et al., 2003). Therefore, this type of anticoagulation is not recommended.

The COMPASS trial (**Fig. 6**) was initiated to prove the hypothesis that RIVA alone or in combination with aspirin is more efficient than aspirin alone to prevent repeated cardiovascular events. The group which received RIVA and aspirin together, showed better primary outcome than the aspirin group. Nevertheless, major bleedings occurred in the RIVA + aspirin group, but fewer and with less clinical impact than in the aspirin group. 313 patients died in the RIVA + aspirin group in comparison to the aspirin group with 378 deaths (Eikelboom et al., 2017). No significant differences in the context of primary outcomes were observed between the groups which received RIVA or aspirin alone, but patients under RIVA treatment showed more major bleeding. In this COMPASS trial patients with stable CVD, who received a dose of 2.5 mg RIVA twice a day in combination with aspirin showed better cardiovascular outcome, but also more major bleeding in comparison to patients who received aspirin alone. A dose of 5 mg RIVA twice a day did not show better results in cardiovascular outcomes than aspirin treatment alone and more major bleeding events were recognized (Eikelboom et al., 2017).

The third big trial was the COMMANDER HF trial (**Fig. 7** and **8**). Patients with HF, sinus rhythm and coronary disease received RIVA. In the first few months after diagnosis of HF, patients are often re-hospitalized and the number of deaths are high. HF is associated with thrombin related pathway activation. Therefore, researchers hypothesized that RIVA as FXa-inhibitor reduces the generation of thrombin and the outcome of patients with worsening HF and CAD could be improved (Zannad et al., 2018). In this trial 5022 patients with chronic HF with reduced ejection fraction (EF ≤ 40 %; HFrEF), CAD and increased plasma levels of natriuretic peptides were included. AF was an exclusion criterion. All patients received 2.5 mg RIVA twice a day or placebo. A combination of death from any cause, stroke or myocardial infarction was the primary endpoint, like in the COMPASS trial. From 2507 patients who received RIVA, 626 showed the primary endpoint during a follow-up frame of 21.1 months, in comparison to 658 from 2515 patients in the placebo group (Zannad et al., 2018). In summary, the treatment with 2.5 mg RIVA twice a day did not show significantly lower percentages of death, stroke and AMI in comparison to the placebo treatment in the assigned patients.

In summary, the ATLAS ACS trial, as well as the COMPASS trial, showed that RIVA can reduce the risk of cardiovascular death, stroke or AMI in patients with an ACS (ATLAS ACS) and in patients with CVD (COMPASS). The risk of bleedings in both trials was increased, but neither severe nor clinically relevant. In contrast, the COMMANDER HF trial could not show a successful reduction of all-cause death, stroke or AMI in patients with HF. Three lessons were learned after the big trials about RIVA, Lori-Ann Linkins published in *The Hematologist* in 2019.

1) Thrombotic events were reduced under anticoagulant therapy, but massive bleeding can overshadow this benefit.

2) The target has to be the right one. For example, the COMMANDER HF trial failed, because the thrombin generation was probably not the right mechanism to address, it was probably not the primary mechanism.

3) The anticoagulant therapy is not a “one-size-fits-all”- solution. For secondary prevention, RIVA in low doses is the right decision, but for the prevention of strokes after AF a higher dose is needed. It has to be decided individually for a patient.

However, the role of FXa as a key player in the coagulation cascade, that increases the formation of thrombin in primary hemostasis is investigated extensively. The impact of FXa on platelet activation and the effect in a setting of long-term treatment remains still unclear. Therefore, this thesis focused on the underlying mechanism and the effect of FXa on platelets in context of AMI and stroke. In collaboration with the working group of PD Dr. med Tobias Petzold, our working group found in 2019, that RIVA reduces the arterial thrombosis via inhibition of FXa-driven platelet activation via PAR1 and published these results in *Circulation Research* (Petzold et al., 2020). FXa was identified as direct agonist of the PAR1, which leads to the activation of platelets and also to the formation of a thrombus in mice. The activation of platelets and the thrombus formation could be inhibited by RIVA and also the stability of an induced arterial thrombus in a mouse model was reduced under RIVA treatment. For *in vitro* studies, patients with AF and chronic RIVA treatment for prevention of a stroke, as well as control patients and patients with new-onset AF before and after first treatment with RIVA were assigned. Attenuation of aggregation responses of platelets and the formation of a thrombus in the BioFlux under flow conditions was also observed under RIVA treatment. An antiplatelet effect, was investigated, which seems to be plasma dependent and independent of thrombin and the anticoagulatory capacity of RIVA. The conclusion of this experiments was, that RIVA with its antiplatelet effect and its anticoagulation properties could lead to a reduction of the appearance of atherothrombotic events in patients and improved their outcome (Petzold et al., 2020). With this study, Petzold et al. revealed a direct platelet dependent effect of FXa inhibitors in the context of arterial thrombosis. This effect was identified and confirmed in this thesis. This thesis focused on the effect of the chronic treatment of FXa-inhibitor RIVA on platelets in the context of AMI and stroke. It is important to investigate this in detail to treat patients optimally. Results of this thesis could have a clinical relevance for further administration of FXa-inhibitors like RIVA.

4.3 Effect of FXa inhibition

4.3.1 Effect of FXa inhibition in AMI

Two methods of myocardial infarction in mice are described and both of them have clinical relevance. First method is the permanent ligation of the LAD, which leads to larger infarct sizes and the infarct after ligation results of apoptosis, following hypoxia for a long time. The second setting is the I/R model, which shows more variable sizes of infarction depending on the length of ischemia (De Villiers et al., 2020). In every experiment the method of choice depends on the hypothesis. The setting of ischemia with following reperfusion in mice mimic the scenario of a human suffering from AMI in the clinical context, who is brought to the hospital within minutes and were the occlusion of a vessel is removed via percutaneous coronary intervention (PCI).

Therefore, the I/R method was used in this thesis. To avoid a viable infarct size within the groups of mice, the researcher who performed surgeries in mice was a well-trained and experienced one. In the used setting of starting the FXa inhibitor treatment two days in the acute or 5 weeks in the chronic setting before I/R surgery, mice under chronic FXa-inhibitor treatment showed significant reduced infarct sizes 24 hours after surgery (**Fig. 17**). The results, that short FXa-inhibitor treatment showed no improving effect after 24 hours confirmed to the results of Bode et al. (2018), who treated mice with RIVA directly at the time of surgery and measured similar infarct sizes 24 hours later in treated and in control mice. Bode et al. prolonged the FXa-inhibitor treatment in another group of mice up to 28 days and measured the infarct sizes. After four weeks of RIVA treatment and while the LAD is ligated, mice showed significantly smaller infarct sizes in comparison to the control group. These results showed that RIVA administration also after LAD ligation has an improving effect (Bode et al., 2018). These results of experiments, in different kinds of myocardial infarction surgeries and in an acute and a chronic setting of RIVA treatment, suggest that an unknown mechanism exists, which leads to improvement after MI. Whether the treatment started before or directly with the surgery.

Next to the measurement of the infarct size, echocardiographic parameters were measured as well. The EF and the SV showed an increase in the chronic FXa-inhibitor treated group 24 h after I/R in comparison to the acute treated and the control group of mice (**Fig. 18**). These results are associated with the smaller infarct sizes and show, that RIVA has no poor influence on the heart muscle and its function, because control and acute treated group showed no significant differences.

Different cell types like monocytes, macrophages and neutrophils are known to play essential roles in AMI and atherothrombosis (Bonaventura et al., 2016; Montecucco et al., 2017). To investigate differences in the number of inflammatory cells in murine blood 24 hours after I/R, FACS analyses of the control group and the chronically RIVA treated group of mice were done (**Fig. 19**). Acute treated mice were not investigated, because they did not show significant differences in the previous parameter in comparison to the control mice. The number of $CD4^+$ cells was significantly increased in mice chronically treated with RIVA. It is known, that $CD4^+$ cells, T-helper cells, influence myocardial healing and the formation of a scar after MI (Ramos et al., 2016). FXa-inhibitor treatment leads to an increased recruitment of T-helper cells in mice blood, which supports a better healing of the myocardium and the formation of a scar. In future experiments of the scar formation after 21 days could be investigated to see if the recruitment of T-helper cells leads to a decreased infarct size in comparison to the control group with a lower number of $CD4^+$ cells. Bode et al. (2018) hypothesized that RIVA could reduce inflammation. The infarct size of this work could not be related to murine inflammatory cells

because the infarct size after 21 days was not measured. Nevertheless, an increase of $CD4^+$ cells could be possible in their scenario under RIVA treatment, which could be one advantage for smaller infarct sizes and a better myocardial healing.

Another significant difference was observed in the number of $CD8^+$ cells. Mice under chronic FXa-inhibitor treatment showed lower numbers of $CD8^+$ cell in comparison to control mice. Ilatovskaya et al. showed in 2019, that mice without functional $CD8^+$ cells had an improved cardiac physiology and lower mortality rates post MI in comparison to control mice. These mice showed also a slower removal of necrotic tissue and a poorer formation of a scar in combination with cardiac rupture (Ilatovskaya et al., 2019). Taken together, the differences in the number of murine T-lymphocytes agree with the literature and the result of decreased infarct sizes under chronic RIVA treatment. All other inflammatory cells, like $Ly6G^+$, $Ly6C^+$ and $CD19^+$ were not affected by FXa-inhibitor treatment, though other studies show that RIVA can change inflammation in CVD (J. Liu et al., 2019).

Next to the inflammatory cells in mice whole blood 24 hours after AMI, inflammatory cytokines in mice plasma were investigated with the LEGENDplex assay in all three groups (**Fig. 20**). A significant lower concentration of IL-1α was observed in both FXa-inhibitor treated groups in comparison to the control group. A low level of IL-1α is known to reduce the acute inflammatory response after MI and is accompanied with a reduced expression of IL-6 and MCP-1. Only low systemic levels of IL-1α reduce myocardial inflammation, but not cardiomyocyte-restricted deletion (Dinarello, 2018; Lugrin et al., 2023). IL-1 α is released by necrotic cells which might explain why it is higher in the control group (Frangogiannis, 2015). In this thesis also the levels of IL-6 are reduced in both RIVA treated groups in comparison to the control group. Lower levels of MCP-1 were only observed in the acute FXa-inhibitor treated group. This fits to the context of reduced infarct size and lower levels of specific inflammatory players. RIVA reduces inflammatory responses in this setting. The other cytokines did not show significant differences in their concentrations.

Inflammatory cytokines were measured 5 days post I/R as well and the chronic FXa-inhibitor treated group of mice showed significant higher levels of IL-1β, IL-6, IFN-ɣ and TNF-α in comparison to the control group (**Fig. 21**). A higher IL-1β level is known to trigger the release of IL-6 (Dinarello, 2018) and a big beneficial role in disperse acute inflammation was attributed to IL-1β (Bent et al., 2018). Next to the increased levels of IL-1β and IL-6, the level of IFN-ɣ was increased as well in the group of chronically FXa-inhibitor treated mice. IFN-ɣ seems to have a beneficial effect in the acute phase of MI (Hoyer et al., 2019), but it also has an anti-apoptotic effect in rats after AMI (Zhang et al., 2022). TNF-α as a key inflammatory mediator,

was reported to have a paradoxical effect such as promoting or protecting in myocardial I/R injury. Therefore, the role of TNF-α in this context is not clear (Lecour, 2009). In this experiment TNF-α seems to have a protective effect. Beneficial properties of the significantly higher cytokines correspond to the results of the measured infarct sizes.

After investigation of inflammatory cells in the circulatory system, migrated inflammatory cells in the infarcted myocardium, 5 days post I/R, were analyzed. Referring to the first experiments and the positive effect of chronic FXa-inhibitor treatment, also the number of inflammatory cells, Ly6G and Mac2 positive cells were significantly decreased in comparison to the control and the acute FXa-inhibitor treated group (**Fig. 22** and **23**). However, the number of inflammatory cells, in the acute FXa-inhibitor treated group was significantly higher than in the other groups. An acute FXa-inhibitor treatment is not sufficient to achieve a positive effect; it may worsen it. Next to macrophages and neutrophil granulocytes, NETs in the infarcted tissue were investigated. NETs consist of decondensed chromatin, histones and neutrophil granular proteins (Bonaventura et al., 2020). Higher numbers of NETs are correlated with larger sizes of infarction and they predict major CV events (Bonaventura et al., 2020). The levels of NETs are significantly smaller in the chronically treated group of mice than in the other groups. No significant difference was observed between the control and the acute treated group (**Fig. 24**). Oral FXa-inhibitor treatment reduces the formation of NETs in mice after AMI. Changes in VAMP proteins, because of reduced platelet secretion, were the reason for reduced numbers of NETs after AMI, which resulted in an overall improvement in outcome.

In summary, the chronic treatment with RIVA showed no effect on any vital parameter. Effects did not occur because of changes in blood composition, heartrate, blood pressure or endothelial function in this thesis.

4.3.2 Effect of FXa inhibition in stroke

Chronic FXa inhibition led to smaller infarct sizes after AMI. An infarction, because of ischemia can also happens when a human or a mouse get a stroke. Therefore, mice underwent a tMCAO surgery to investigate if the positive effect of FXa-inhibitor treatment in AMI also occur in the outcome of a stroke. Mice which had a stroke are not really able to eat and drink in a proper way, because of loss of movement control and moving in circles. Therefore, mice in this experiment were euthanized after 24 h. The infarct sizes of mice under chronic RIVA treatment are relatively similar to the infarct sizes of control mice and no significant difference was observed. Mice acutely treated with FXa-inhibitor showed increased infarct sizes in comparison (**Fig. 25**). The outcome after stroke is worsen under acute treatment, but not

affected by long-term treatment with the FXa inhibitor, which inhibits the worsening. Under acute FXa-inhibition mice show larger areas of bleeding in brain tissue, which could be a driver for larger infarct sizes. Dittmeier et al. showed, that rats, pre-treated 8 h with 3 mg/kg RIVA before tMCAO had lower infarct sizes than the control group 24 h after tMCAO (Dittmeier et al., 2016). It is not clear, why these results could not be observed in the tMCAO experiments in this thesis. Differences in the effect of FXa-inhibitor treatment of the organisms of mice and rats could be one possible reason. The RELAXED study showed, that RIVA administered in a time window of ≤ 14 days after stroke, in humans with small or medium infarct sizes, minimizes the risk of recurrence of ischemic stroke and major bleeding events (Yasaka et al., 2019). RIVA does not appear to minimize infarct sizes in case of stroke when it is administered chronically preventively. Furthermore, it can increase infarct sizes when it is administered only short-term before, but it may protect against further strokes and bleeding if taken after a stroke, as in the RELAXED trial.

Inflammatory leukocytes from infarcted brain hemispheres were investigated via FACS analysis, to check if there were differences in the migrated cells - granulocytes, microglia or monocytes. The number of all cell types were slightly decreased in the chronic FXa-inhibitor treated group, but significant differences were only visible in the percentage of microglia (**Fig. 26**). It is reported that RIVA treatment can abolish the generation of prothrombin kringle-2 (pKr-2) and its influx in the brain, which leads to reduced neuroinflammation and improvement in cognitive impairment (Kim et al., 2023). Dittmeier et al. (2016) showed anti-inflammatory properties of pre-treatment of RIVA in rats which underwent tMCAO. Anti-inflammatory properties of RIVA given chronically were visible in numbers of inflammatory cells in the infarcted tissue, even if the infarct size is not reduced.

To investigate if the FXa-inhibitor treatment had an influence on the gene expression in the infarcted hemispheres of mice 24 h after tMCAO, qPCR analyses were performed. Even if the infarct size was significantly higher in the acute FXa-inhibitor treated mice, no significant changes could be observed in gene expression (**Fig. 27**). In comparison to these findings, Dittmeier et al. published significant differences in gene expression of TNF-α and IL-1β in their paper of 2016, where rats underwent a tMCAO. This could be because two different organisms were compared, rats and mice. In contrast to the hypothesis of different organisms, other FXa-inhibitors like apixaban and edoxaban are known to reduce the infarct sizes of treated mice after tMCAO (Bushi et al., 2018; Bieber et al., 2021). In this thesis, RIVA did not have the expected effect in mice after tMCAO with regard to infarct sizes. A higher rate of acute bleeding could lead to those difficulties and was seen in the TTC stained brain tissue of acute treated mice.

After FACS and qPCR analyses, histological analyses were performed. These results are consistent with the infarct size results. The number of counted NETs in the brains was significantly higher in acute FXa-inhibitor treated mice than in the two other groups. The number of $Iba1^+$ cells, which are activated microglia, was also higher in the acute FXa-inhibitor treated group (**Fig. 28**). All surgeries were done by an experienced researcher to avoid problems during surgery. To sum up the tMCAO experiments, mice under acute FXa-inhibitor treatment showed significant higher infarct sizes, due to higher bleeding issues in brain tissue than chronically treated mice and the control group.

4.3.3 Effect of FXa inhibition in depleted mice

Positive effects of the chronic FXa-inhibitor treatment of mice were investigated with the experiments in this thesis. In addition to their central role in primary hemostasis and pathogenesis of acute atherothrombosis, platelets contribute to the maintenance of vascular integrity, defense mechanisms of the innate and adaptive immune system (Menter et al., 2017). They contribute to tissue regeneration in the context of AMI or stroke (Y. Liu et al., 2011; Ziegler et al., 2016). Therefore, mice were depleted with a special antibody to reduce the number of circulating platelets, and underwent AMI induction afterwards. It was shown that the infarct sizes were reduced in comparison to control mice, but bigger in comparison to non-depleted mice under chronic FXa-inhibitor treatment (**Fig. 29**). Mice which were depleted and received a chronic FXa-inhibitor treatment at the same time, showed no difference in comparison to only depleted mice. The infarct size reduction of chronic FXa inhibition 24 h after AMI was blunted by the platelet depletion. These results were also confirmed by echocardiographic assessment of the mice 24 h after AMI. The beneficial effect of chronic FXa inhibition on cardiac function after AMI disappeared in platelet depleted mice. Therefore, the effect of chronic FXa-inhibitor treatment was shown to be platelet-dependent. To discuss limitations of this part of the thesis, it has to be mentioned, that platelet depletion alone also leads to a reduced infarct size (Reusswig et al., 2022). Possibly an additional effect cannot be detected because the infarct size cannot get much smaller in the I/R method.

4.3.4 Effect of FXa inhibition in human platelets

That the positive effect of chronic FXa inhibitor treatment, like reduced infarct sizes in AMI and stroke and reduced thromboinflammation, is a direct platelet dependent one was proofed with platelet depleted mice. Infarct sizes are smaller under FXa-inhibitor treatment and also thromboinflammatory processes are downregulated. It is known, that in most processes, the platelet granule-released secretome plays the crucial role. The platelet secretome consists of

a variety of bioactive substances (Serhan et al., 1990; Yang et al., 1994; Mehta et al., 1999; Frangogiannis et al., 2005; Abdulnour et al., 2014; D. Chen et al., 2015; Basil et al., 2016) and is stored in three intracellular granule types: α-granules, dense granules and lysosomes (Sharda et al., 2018). Direct effects of FXa on platelets in the setting of acute atherothrombosis were elaborated in this thesis. To investigate the role of the FXa-platelet axis and its inhibition in the chronic setting, analyses of the platelet proteome and the platelet transcriptome were performed. A matched platelet proteome analysis by quantitative mass spectrometry and a matched RNA sequencing of the individual patients were performed. This analysis was done for patients with AF or flutter with temporary oral FXa inhibition with apixaban during and four weeks after completion of FXa inhibitor intake (**Fig. 33**). 2128 differentially expressed RNAs and 601 differentially expressed proteins were identified between two time points of blood collection, which underlined a strong FXa-inhibitor promoted effect. In particular, signaling pathways involved in vesicle formation (i.e. membrane trafficking) and vesicle transport were found. VAMP-3 and VAMP-8 are particularly the most important ones (Lemons et al., 1997; Polgár et al., 2002). Both proteins are responsible for secretion of both α- and dense granules (Polgár et al., 2002; Ren et al., 2007; Graham et al., 2009). These granules are of particular importance in the context of cardiovascular events like AMI and stroke. In a murine model of stroke, inhibition of either dense granule or α-granule secretion results in smaller infarct volumes. However, simultaneous inhibition of α- and dense granules increases the risk of hemorrhage in the infarcted tissue (Mezger et al., 2019). Platelet granule secretion requires complex formation between members of different protein families (Lemons et al., 2000; Lai et al., 2003).

The functional relevance of proteomic changes under FXa inhibition were investigated as well. Markedly reduced secretion of the α-granule protein vWF and serotonin stored in dense granules from platelets was revealed after stimulation with different agonists. No evidence was found for differential loading of platelets with vWF or serotonin. Differences with respect to platelet aggregation were not found, suggesting residual vesicle secretion required for platelet aggregation (**Fig. 34**). In addition, compared with platelets from non-anticoagulated patients, an increased number of VAMP-3 positive vesicles with a central distribution pattern within the cell was revealed, demonstrating the functional relevance of chronic FXa inhibition on vesicle formation and transport (**Fig. 35**). Furthermore, human coronary thrombi were investigated on the effect of FXa inhibition on NET formation in humans. High significantly decreased numbers of NETs were found in human coronary thrombi under different FXa-inhibitors in comparison to patients without FXa inhibition (**Fig. 36**). Because platelets play the major role in inducing NET formation, visible in figure 37, FXa-inhibitor treatment had a big impact on formation of NETs and therefore the prediction of major adverse CV events (Bonaventura et al., 2020). It is

known, that FXa substitution to cultured neutrophils does not mediate NETosis (Moschonas, 2020). Therefore, a platelet dependent effect in reduced NETosis is highly conceivable. The investigated platelet-dependent reduction in thromboinflammation could be one reason for reduced NET formation after AMI and stroke and in thrombi in these experiments, which resulted in an overall improvement in outcome.

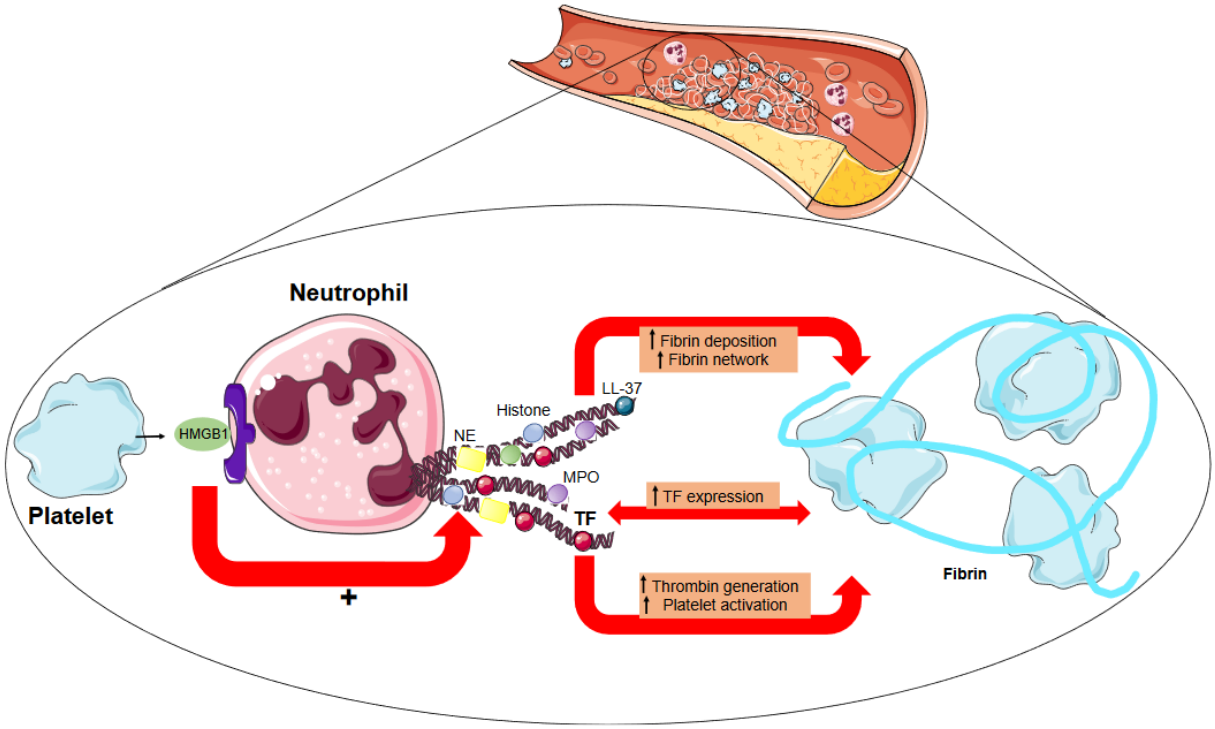

Figure 37: Interplay between NETs and platelets.

The deposition of fibrin by NETs promotes thrombosis. Platelets play a crucial role in the formation of NETs. It is shown, that HMGB1 of activated platelets was presented to neutrophils which lead to their stimulation and results in formation of NETs (Bonaventura et al., 2020).

Other studies also saw an improvement in outcome under chronic FXa inhibition after AMI without referring to the role of platelets in this context (Gadi et al., 2021). The positive effects of FXa inhibition are mostly attributed to a reduction of local or systemic inflammation (Busch et al., 2005; Dittmeier et al., 2016; J. Liu et al., 2019; Ding et al., 2021). A clear effect on systemic inflammation of FXa inhibition was not seen, probably due to the relatively low dosage. A difference between acute and chronic treatment could not be observed in any case. However, in this thesis, the platelet-dependent effect in an isolated and clearer manner was further demonstrated. Overall, a previously completely unknown mechanism of action of FXa inhibition was revealed. FXa inhibition improves outcome after ischemic events by direct platelet-dependent inhibition of thromboinflammation independently of the platelet anticoagulative properties. The inhibition of VAMP proteins was a further aspect of FXa inhibition effects and could be a new drug target in the future.

4.4 Limitations

Different questions remain open after these experiments and should be investigated in the future. It is not known when the effect of FXa inhibitor administration occur and if FXa inhibition mediate changes in the platelet itself or way before in the megakaryocytes. Because platelets do not have a nucleus and contain only less megakaryocyte mRNA, the protein synthesis in platelets is highly reduced. The proteome and transcriptome data suggest, that these massive changes could not be done within the platelets without a nucleus. Therefore, it is conceivable that the impact of FXa inhibition starts in megakaryocytes. Megakaryocytes were tried to cultured, but it turned out to be more difficult, so they are in focus to investigate the underlying mechanism in future. Another question is if the observed effects are group-specific, meaning if they only apply for FXa inhibitors like rivaroxaban, edoxaban and apixaban or also for FIIa inhibitors like dabigatran, and VKA. If these substances show similar effects could be investigated in the future. The next point is that the FXa inhibitory effect is dose- and indication-dependent in which the anticoagulant is used. For example, AF, deep vein thrombosis or pulmonary embolism, as well as atherosclerosis are associated with different patterns of platelet activation. In future experiments, these different patterns could be investigated under FXa inhibition. Another point is if this inhibition has effects on auto- and paracrine platelet activation and platelet-leukocyte interaction, which plays a crucial role in the context of thromboinflammation. And therefore experiments with platelets from patients suffering from storage pool disease could be highly interesting. Platelets of these patients show secretion abnormalities and it would be interesting if inhibition of FXa has additional effects on them as well. More research will be necessary to address these open questions in detail.

5. Abstract

Non-vitamin K oral anticoagulants (NOACs) are first line therapy in prevention of thromboembolic events in atrial fibrillation. In the context of the continued increased clinical use of NOACs, a fundamental understanding of its non-plasmatic effects beyond mere anticoagulation is essential. The aim of this thesis was to investigate if chronic in comparison to acute oral FXa inhibition of platelets influences the infarct size in acute myocardial infarction (AMI) and in stroke and to investigate the underlying mechanism. It was recently shown, that FXa inhibition exerts direct antiplatelet effects. Platelets are crucial not only in thrombosis, but also in inflammatory processes. Hypothetically, this occurs via a reduction in platelet granule secretion and consecutive thromboinflammation based on altered protein synthesis in megakaryocytes and platelets under oral FXa inhibition. The effect of acute and chronic FXa inhibition on mice after AMI and stroke was evaluated. Moreover, granule secretion assays, proteome and RNA expression analysis of platelets of patients treated with oral FXa-inhibitors were conducted. Chronic but not acute FXa inhibition reduced infarct size and improved cardiac function 24 h after AMI in mice. Moreover, chronic FXa inhibition led to smaller infarct size 24 h after acute stroke compared to acute FXa inhibition. Reduced neutrophil extracellular trap (NET) formation was shown to be the underlying reason for this effect. Beneficial effects of chronic FXa inhibition were blunted in platelet-depleted mice. Proteome and RNA expression analysis of FXa-inhibitor treated patients revealed a reduction of vesicle-associated membrane protein (VAMP) synthesis hampering the alpha and dense granule release in platelets. A novel platelet-dependent mechanism by long-term FXa inhibition, improving outcome after AMI and stroke was revealed. The results lead to a better understanding of the effect of FXa on platelets. Based on this, the findings contribute to the development of new treatment approaches for thromboinflammation based on modification of the platelet secretome. Understanding pathophysiological changes and how they can be influenced by pharmacotherapeutic principles is essential for new therapeutic approaches.

6. Zusammenfassung

Nicht-Vitamin-K-abhängige orale Antikoagulanzien (NOAKs) sind die erste Wahl bei der Prävention thromboembolischer Ereignisse bei Vorhofflimmern. Vor dem Hintergrund des weiterhin zunehmenden klinischen Einsatzes von NOAKs ist ein grundlegendes Verständnis ihrer nicht-plasmatischen Wirkungen über die reine Antikoagulation hinaus unerlässlich. Ziel dieser Arbeit war die Untersuchung, ob eine chronische im Vergleich zu einer akuten oralen FXa-Hemmung der Thrombozyten die Infarktgröße bei akutem Myokardinfarkt (AMI) und Schlaganfall beeinflusst und den zugrundeliegenden Mechanismus zu erforschen. Kürzlich wurde gezeigt, dass die FXa-Hemmung eine direkte thrombozytenhemmende Wirkung hat. Thrombozyten spielen nicht nur bei der Thrombose, sondern auch bei Entzündungsprozessen eine wichtige Rolle. Dies geschieht über eine verringerte Sekretion der Thrombozytengranula und eine konsekutive Thromboinflammation, die auf einer veränderten Proteinsynthese in Megakaryozyten und Thrombozyten unter oraler FXa-Hemmung beruht. Die Wirkung der akuten und chronischen FXa-Hemmung wurde bei Mäusen nach AMI und Schlaganfall untersucht. Darüber hinaus wurden Analysen zur Granulasekretion, Proteom- und RNA-Expressionsanalysen von Thrombozyten von Patienten durchgeführt, die mit oralen FXa-Inhibitoren behandelt wurden. Die chronische, aber nicht die akute FXa-Hemmung verringerte die Infarktgröße und verbesserte die Herzfunktion 24 Stunden nach AMI bei Mäusen. Außerdem führte die chronische FXa-Hemmung 24 Stunden nach einem akuten Schlaganfall zu einer geringeren Infarktgröße als die akute FXa-Hemmung. Es wurde gezeigt, dass die reduzierte Bildung von ‚Neutrophil Extracellular Traps' (NET) und damit die verringerte Thromboinflammation der Grund für diesen Effekt ist. Die positive Wirkung der chronischen FXa-Hemmung war bei Mäusen, die keine Thrombozyten mehr hatten, abgeschwächt. Proteom- und RNA-Expressionsanalysen von Patienten, die mit FXa-Inhibitoren behandelt wurden, ergaben eine Verringerung der Synthese von Vesikel-assoziierten Membranproteinen (VAMP), die die Freisetzung von α- und δ-Granula in Thrombozyten behindert. Es wurde ein neuartiger, von den Thrombozyten abhängiger Mechanismus aufgedeckt, der durch eine langfristige FXa-Hemmung das Ergebnis nach einem Herzinfarkt und Schlaganfall verbessert. Die Ergebnisse führen zu einem besseren Verständnis der Wirkung von FXa auf Thrombozyten. Auf dieser Grundlage tragen die Ergebnisse zur Entwicklung neuer Behandlungsansätze für die Thromboinflammation bei, die auf einer Modifizierung des Thrombozytensekretoms basieren. Das Verständnis der pathophysiologischen Veränderungen und deren Beeinflussung durch pharmakotherapeutische Prinzipien ist für neue therapeutische Ansätze unerlässlich.

7. References

Abdulnour, R. E., Dalli, J., Colby, J. K., Krishnamoorthy, N., Timmons, J. Y., Tan, S. H., Colas, R. A., Petasis, N. A., Serhan, C. N., & Levy, B. D. (2014). Maresin 1 biosynthesis during platelet-neutrophil interactions is organ-protective. *Proc Natl Acad Sci U S A, 111*(46), 16526-16531. doi:10.1073/pnas.1407123111

Achilles, A., Mohring, A., Zeus, T., Kelm, M., & Polzin, A. (2017). Dabigatran enhances platelet reactivity and platelet thrombin receptor expression in patients with atrial fibrillation: reply. *J Thromb Haemost, 15*(7), 1524-1525. doi:10.1111/jth.13718

Alexander, J. H., & Singh, K. P. (2005). Inhibition of Factor Xa : a potential target for the development of new anticoagulants. *Am J Cardiovasc Drugs, 5*(5), 279-290. doi:10.2165/00129784-200505050-00001

Alsaid, S., Bode, C., & Duerschmied, D. (2019). Perspektive nach der COMPASS-Studie für KHK- und AVK-Patienten. *Die neue Rolle der oralen Antikoagulationstherapie bei atherosklerotischer Erkrankung, 48*(03), 73-77. doi:10.1055/a-0861-1036

Anand, S. S., & Yusuf, S. (2003). Oral anticoagulants in patients with coronary artery disease. *J Am Coll Cardiol, 41*(4 Suppl S), 62S-69S. doi:10.1016/s0735-1097(02)02776-6

Antithrombotic Trialists, C., Baigent, C., Blackwell, L., Collins, R., Emberson, J., Godwin, J., Peto, R., Buring, J., Hennekens, C., Kearney, P., Meade, T., Patrono, C., Roncaglioni, M. C., & Zanchetti, A. (2009). Aspirin in the primary and secondary prevention of vascular disease: collaborative meta-analysis of individual participant data from randomised trials. *Lancet, 373*(9678), 1849-1860. doi:10.1016/S0140-6736(09)60503-1

Asada, Y., Yamashita, A., Sato, Y., & Hatakeyama, K. (2018). Thrombus Formation and Propagation in the Onset of Cardiovascular Events. *J Atheroscler Thromb, 25*(8), 653-664. doi:10.5551/jat.RV17022

Asada, Y., Yamashita, A., Sato, Y., & Hatakeyama, K. (2020). Pathophysiology of atherothrombosis: Mechanisms of thrombus formation on disrupted atherosclerotic plaques. *Pathol Int, 70*(6), 309-322. doi:10.1111/pin.12921

Aslan, J. E., Itakura, A., Gertz, J. M., & McCarty, O. J. (2012). Platelet shape change and spreading. *Methods Mol Biol, 788*, 91-100. doi:10.1007/978-1-61779-307-3_7

Ay, H., Furie, K. L., Singhal, A., Smith, W. S., Sorensen, A. G., & Koroshetz, W. J. (2005). An evidence-based causative classification system for acute ischemic stroke. *Ann Neurol, 58*(5), 688-697. doi:10.1002/ana.20617

Badimon, L., & Vilahur, G. (2014). Thrombosis formation on atherosclerotic lesions and plaque rupture. *J Intern Med, 276*(6), 618-632. doi:10.1111/joim.12296

Basil, M. C., & Levy, B. D. (2016). Specialized pro-resolving mediators: endogenous regulators of infection and inflammation. *Nat Rev Immunol, 16*(1), 51-67. doi:10.1038/nri.2015.4

Benkhoff, M. (2022). *Lipide und Lipoproteine in der Kardioprotektion.* Heinrich-Heine-University,

Bent, R., Moll, L., Grabbe, S., & Bros, M. (2018). Interleukin-1 Beta-A Friend or Foe in Malignancies? *Int J Mol Sci, 19*(8). doi:10.3390/ijms19082155

Berezin, A. E., & Berezin, A. A. (2020). Adverse Cardiac Remodelling after Acute Myocardial Infarction: Old and New Biomarkers. *Dis Markers, 2020*, 1215802. doi:10.1155/2020/1215802

Bhatt, D. L., Eagle, K. A., Ohman, E. M., Hirsch, A. T., Goto, S., Mahoney, E. M., Wilson, P. W., Alberts, M. J., D'Agostino, R., Liau, C. S., Mas, J. L., Rother, J., Smith, S. C., Jr., Salette, G., Contant, C. F., Massaro, J. M., Steg, P. G., & Investigators, R. R. (2010). Comparative determinants of 4-year cardiovascular event rates in stable outpatients at risk of or with atherothrombosis. *JAMA, 304*(12), 1350-1357. doi:10.1001/jama.2010.1322

Bieber, M., Foerster, K. I., Haefeli, W. E., Pham, M., Schuhmann, M. K., & Kraft, P. (2021). Treatment with Edoxaban Attenuates Acute Stroke Severity in Mice by Reducing Blood-Brain Barrier Damage and Inflammation. *Int J Mol Sci, 22*(18). doi:10.3390/ijms22189893

Bieber, M., Gronewold, J., Scharf, A. C., Schuhmann, M. K., Langhauser, F., Hopp, S., Mencl, S., Geuss, E., Leinweber, J., Guthmann, J., Doeppner, T. R., Kleinschnitz, C., Stoll, G., Kraft, P., & Hermann, D. M. (2019). Validity and Reliability of Neurological Scores in Mice Exposed to Middle Cerebral Artery Occlusion. *Stroke, 50*(10), 2875-2882. doi:10.1161/strokeaha.119.026652

Bode, M. F., Auriemma, A. C., Grover, S. P., Hisada, Y., Rennie, A., Bode, W. D., Vora, R., Subramaniam, S., Cooley, B., Andrade-Gordon, P., Antoniak, S., & Mackman, N. (2018). The factor Xa inhibitor rivaroxaban reduces cardiac dysfunction in a mouse model of myocardial infarction. *Thromb Res, 167*, 128-134. doi:10.1016/j.thromres.2018.05.015

Bonaventura, A., Montecucco, F., & Dallegri, F. (2016). Cellular recruitment in myocardial ischaemia/reperfusion injury. *Eur J Clin Invest, 46*(6), 590-601. doi:10.1111/eci.12633

Bonaventura, A., Vecchie, A., Abbate, A., & Montecucco, F. (2020). Neutrophil Extracellular Traps and Cardiovascular Diseases: An Update. *Cells, 9*(1). doi:10.3390/cells9010231

Bui, Q. T., Prempeh, M., & Wilensky, R. L. (2009). Atherosclerotic plaque development. *Int J Biochem Cell Biol, 41*(11), 2109-2113. doi:10.1016/j.biocel.2009.06.002

Burke, A. P., & Virmani, R. (2007). Pathophysiology of acute myocardial infarction. *Med Clin North Am, 91*(4), 553-572; ix. doi:10.1016/j.mcna.2007.03.005

Busch, G., Seitz, I., Steppich, B., Hess, S., Eckl, R., Schömig, A., & Ott, I. (2005). Coagulation factor Xa stimulates interleukin-8 release in endothelial cells and mononuclear leukocytes: implications in acute myocardial infarction. *Arterioscler Thromb Vasc Biol, 25*(2), 461-466. doi:10.1161/01.ATV.0000151279.35780.2d

Bushi, D., Chapman, J., Wohl, A., Stein, E. S., Feingold, E., & Tanne, D. (2018). Apixaban decreases brain thrombin activity in a male mouse model of acute ischemic stroke. *J Neurosci Res, 96*(8), 1406-1411. doi:10.1002/jnr.24253

Cade, J. F., Buchanan, M. R., Boneu, B., Ockelford, P., Cater, C. J., Cerskus, A. L., & Hirsh, J. (1984). A comparison of the antithrombotic and haemorrhagic effects of low

molecular weight heparin fractions: the influence of the method of preparation. *Thromb Res, 35*(6), 613-625. doi:10.1016/0049-3848(84)90265-2

Cannon, C. P., Bhatt, D. L., Oldgren, J., Lip, G. Y. H., Ellis, S. G., Kimura, T., Maeng, M., Merkely, B., Zeymer, U., Gropper, S., Nordaby, M., Kleine, E., Harper, R., Manassie, J., Januzzi, J. L., Ten Berg, J. M., Steg, P. G., Hohnloser, S. H., Committee, R.-D. P. S., & Investigators. (2017). Dual Antithrombotic Therapy with Dabigatran after PCI in Atrial Fibrillation. *N Engl J Med, 377*(16), 1513-1524. doi:10.1056/NEJMoa1708454

Chaudhry, R., Usama, S. M., & Babiker, H. M. (2023). Physiology, Coagulation Pathways. In *StatPearls*. Treasure Island (FL).

Chen, D., Xia, Y., Zuo, K., Wang, Y., Zhang, S., Kuang, D., Duan, Y., Zhao, X., & Wang, G. (2015). Crosstalk between SDF-1/CXCR4 and SDF-1/CXCR7 in cardiac stem cell migration. *Sci Rep, 5*, 16813. doi:10.1038/srep16813

Chen, Q., Sievers, R. E., Varga, M., Kharait, S., Haddad, D. J., Patton, A. K., Delany, C. S., Mutka, S. C., Blonder, J. P., Dube, G. P., Rosenthal, G. J., & Springer, M. L. (2013). Pharmacological inhibition of S-nitrosoglutathione reductase improves endothelial vasodilatory function in rats in vivo. *J Appl Physiol (1985), 114*(6), 752-760. doi:10.1152/japplphysiol.01302.2012

Cheng, P., Wang, X., Liu, Q., Yang, T., Qu, H., & Zhou, H. (2023). Extracellular vesicles mediate biological information delivery: A double-edged sword in cardiac remodeling after myocardial infarction. *Front Pharmacol, 14*, 1067992. doi:10.3389/fphar.2023.1067992

Chu, H. X., Kim, H. A., Lee, S., Moore, J. P., Chan, C. T., Vinh, A., Gelderblom, M., Arumugam, T. V., Broughton, B. R., Drummond, G. R., & Sobey, C. G. (2014). Immune cell infiltration in malignant middle cerebral artery infarction: comparison with transient cerebral ischemia. *J Cereb Blood Flow Metab, 34*(3), 450-459. doi:10.1038/jcbfm.2013.217

Ciferri, S., Emiliani, C., Guglielmini, G., Orlacchio, A., Nenci, G. G., & Gresele, P. (2000). Platelets release their lysosomal content in vivo in humans upon activation. *Thromb Haemost, 83*(1), 157-164. Retrieved from https://www.ncbi.nlm.nih.gov/pubmed/10669170

Connolly, S. J., Ezekowitz, M. D., Yusuf, S., Eikelboom, J., Oldgren, J., Parekh, A., Pogue, J., Reilly, P. A., Themeles, E., Varrone, J., Wang, S., Alings, M., Xavier, D., Zhu, J., Diaz, R., Lewis, B. S., Darius, H., Diener, H. C., Joyner, C. D., Wallentin, L., Committee, R.-L. S., & Investigators. (2009). Dabigatran versus warfarin in patients with atrial fibrillation. *N Engl J Med, 361*(12), 1139-1151. doi:10.1056/NEJMoa0905561

Cuartero, M. I., Ballesteros, I., Moraga, A., Nombela, F., Vivancos, J., Hamilton, J. A., Corbi, A. L., Lizasoain, I., & Moro, M. A. (2013). N2 neutrophils, novel players in brain inflammation after stroke: modulation by the PPARgamma agonist rosiglitazone. *Stroke, 44*(12), 3498-3508. doi:10.1161/STROKEAHA.113.002470

Dannenberg, L., Trojovsky, K., Ayhan, A., Helten, C., Zako, S., M'Pembele, R., Mourikis, P., Benkhoff, M., Ignatov, D., Sarabhai, T., Petzold, T., Huhn-Wientgen, R., Zeus, T., Kelm, M., Levkau, B., & Polzin, A. (2021). MTX Treatment Does Not Improve Outcome in Mice with AMI. *Pharmacology, 106*(3-4), 225-232. doi:10.1159/000511279

Davie, E. W., & Ratnoff, O. D. (1964). Waterfall Sequence for Intrinsic Blood Clotting. *Science, 145*(3638), 1310-1312. doi:10.1126/science.145.3638.1310

De Villiers, C., & Riley, P. R. (2020). Mouse models of myocardial infarction: comparing permanent ligation and ischaemia-reperfusion. *Dis Model Mech, 13*(11). doi:10.1242/dmm.046565

DeSai, C., & Hays Shapshak, A. (2023). Cerebral Ischemia. In *StatPearls*. Treasure Island (FL).

Dhandapani, K. M., & Brann, D. W. (2003). Transforming growth factor-beta: a neuroprotective factor in cerebral ischemia. *Cell Biochem Biophys, 39*(1), 13-22. doi:10.1385/CBB:39:1:13

Dinarello, C. A. (2018). Overview of the IL-1 family in innate inflammation and acquired immunity. *Immunol Rev, 281*(1), 8-27. doi:10.1111/imr.12621

Ding, Y., Li, X., Zhou, M., Cai, L., Tang, H., Xie, T., Shi, Z., & Fu, W. (2021). Factor Xa inhibitor rivaroxaban suppresses experimental abdominal aortic aneurysm progression via attenuating aortic inflammation. *Vascul Pharmacol, 136*, 106818. doi:10.1016/j.vph.2020.106818

Dirnagl, U., Iadecola, C., & Moskowitz, M. A. (1999). Pathobiology of ischaemic stroke: an integrated view. *Trends Neurosci, 22*(9), 391-397. doi:10.1016/s0166-2236(99)01401-0

Dittmeier, M., Kraft, P., Schuhmann, M. K., Fluri, F., & Kleinschnitz, C. (2016). Pretreatment with rivaroxaban attenuates stroke severity in rats by a dual antithrombotic and anti-inflammatory mechanism. *Thromb Haemost, 115*(4), 835-843. doi:10.1160/th15-08-0631

Dobesh, P. P., & Stacy, Z. A. (2019). Front Matter. In G. Flaker (Ed.), *Stroke Prevention in Atrial Fibrillation* (pp. iii): Elsevier.

Eikelboom, J. W., Connolly, S. J., Bosch, J., Dagenais, G. R., Hart, R. G., Shestakovska, O., Diaz, R., Alings, M., Lonn, E. M., Anand, S. S., Widimsky, P., Hori, M., Avezum, A., Piegas, L. S., Branch, K. R. H., Probstfield, J., Bhatt, D. L., Zhu, J., Liang, Y., Maggioni, A. P., Lopez-Jaramillo, P., O'Donnell, M., Kakkar, A. K., Fox, K. A. A., Parkhomenko, A. N., Ertl, G., Stork, S., Keltai, M., Ryden, L., Pogosova, N., Dans, A. L., Lanas, F., Commerford, P. J., Torp-Pedersen, C., Guzik, T. J., Verhamme, P. B., Vinereanu, D., Kim, J. H., Tonkin, A. M., Lewis, B. S., Felix, C., Yusoff, K., Steg, P. G., Metsarinne, K. P., Cook Bruns, N., Misselwitz, F., Chen, E., Leong, D., Yusuf, S., & Investigators, C. (2017). Rivaroxaban with or without Aspirin in Stable Cardiovascular Disease. *N Engl J Med, 377*(14), 1319-1330. doi:10.1056/NEJMoa1709118

Engelmann, B., & Massberg, S. (2013). Thrombosis as an intravascular effector of innate immunity. *Nat Rev Immunol, 13*(1), 34-45. doi:10.1038/nri3345

Erkens, R., Kramer, C. M., Luckstadt, W., Panknin, C., Krause, L., Weidenbach, M., Dirzka, J., Krenz, T., Mergia, E., Suvorava, T., Kelm, M., & Cortese-Krott, M. M. (2015). Left ventricular diastolic dysfunction in Nrf2 knock out mice is associated with cardiac hypertrophy, decreased expression of SERCA2a, and preserved endothelial function. *Free Radic Biol Med, 89*, 906-917. doi:10.1016/j.freeradbiomed.2015.10.409

Feng, Q., Li, Q., Zhou, H., Sun, L., Lin, C., Jin, Y., Wang, D., & Guo, G. (2022). The role of major immune cells in myocardial infarction. *Front Immunol, 13*, 1084460. doi:10.3389/fimmu.2022.1084460

Frangogiannis, N. G. (2008). The immune system and cardiac repair. *Pharmacol Res, 58*(2), 88-111. doi:10.1016/j.phrs.2008.06.007

Frangogiannis, N. G. (2015). Interleukin-1 in cardiac injury, repair, and remodeling: pathophysiologic and translational concepts. *Discoveries (Craiova), 3*(1). doi:10.15190/d.2015.33

Frangogiannis, N. G., Ren, G., Dewald, O., Zymek, P., Haudek, S., Koerting, A., Winkelmann, K., Michael, L. H., Lawler, J., & Entman, M. L. (2005). Critical role of endogenous thrombospondin-1 in preventing expansion of healing myocardial infarcts. *Circulation, 111*(22), 2935-2942. doi:10.1161/CIRCULATIONAHA.104.510354

Frojmovic, M. M., & Milton, J. G. (1982). Human platelet size, shape, and related functions in health and disease. *Physiol Rev, 62*(1), 185-261. doi:10.1152/physrev.1982.62.1.185

Gadi, I., Fatima, S., Elwakiel, A., Nazir, S., Mohanad Al-Dabet, M., Rana, R., Bock, F., Manoharan, J., Gupta, D., Biemann, R., Nieswandt, B., Braun-Dullaeus, R., Besler, C., Scholz, M., Geffers, R., Griffin, J. H., Esmon, C. T., Kohli, S., Isermann, B., & Shahzad, K. (2021). Different DOACs Control Inflammation in Cardiac Ischemia-Reperfusion Differently. *Circ Res, 128*(4), 513-529. doi:10.1161/circresaha.120.317219

Gage, G. J., Kipke, D. R., & Shain, W. (2012). Whole animal perfusion fixation for rodents. *J Vis Exp*(65). doi:10.3791/3564

Gawaz, M., Langer, H., & May, A. E. (2005). Platelets in inflammation and atherogenesis. *J Clin Invest, 115*(12), 3378-3384. doi:10.1172/JCI27196

Gawaz, M., Neumann, F. J., Ott, I., Schiessler, A., & Schomig, A. (1996). Platelet function in acute myocardial infarction treated with direct angioplasty. *Circulation, 93*(2), 229-237. doi:10.1161/01.cir.93.2.229

Giannakeas, V., Kotsopoulos, J., Cheung, M. C., Rosella, L., Brooks, J. D., Lipscombe, L., Akbari, M. R., Austin, P. C., & Narod, S. A. (2022). Analysis of Platelet Count and New Cancer Diagnosis Over a 10-Year Period. *JAMA Netw Open, 5*(1), e2141633. doi:10.1001/jamanetworkopen.2021.41633

Gibson, C. M., Mehran, R., Bode, C., Halperin, J., Verheugt, F. W., Wildgoose, P., Birmingham, M., Ianus, J., Burton, P., van Eickels, M., Korjian, S., Daaboul, Y., Lip, G. Y., Cohen, M., Husted, S., Peterson, E. D., & Fox, K. A. (2016). Prevention of Bleeding in Patients with Atrial Fibrillation Undergoing PCI. *N Engl J Med, 375*(25), 2423-2434. doi:10.1056/NEJMoa1611594

Gidlof, O., van der Brug, M., Ohman, J., Gilje, P., Olde, B., Wahlestedt, C., & Erlinge, D. (2013). Platelets activated during myocardial infarction release functional miRNA, which can be taken up by endothelial cells and regulate ICAM1 expression. *Blood, 121*(19), 3908-3917, S3901-3926. doi:10.1182/blood-2012-10-461798

Giugliano, R. P., Ruff, C. T., Braunwald, E., Murphy, S. A., Wiviott, S. D., Halperin, J. L., Waldo, A. L., Ezekowitz, M. D., Weitz, J. I., Spinar, J., Ruzyllo, W., Ruda, M., Koretsune, Y., Betcher, J., Shi, M., Grip, L. T., Patel, S. P., Patel, I., Hanyok, J. J.,

Mercuri, M., Antman, E. M., & Investigators, E. A.-T. (2013). Edoxaban versus warfarin in patients with atrial fibrillation. *N Engl J Med, 369*(22), 2093-2104. doi:10.1056/NEJMoa1310907

Gliem, M., Hermsen, D., van Rooijen, N., Hartung, H. P., & Jander, S. (2012). Secondary intracerebral hemorrhage due to early initiation of oral anticoagulation after ischemic stroke: an experimental study in mice. *Stroke, 43*(12), 3352-3357. doi:10.1161/strokeaha.112.666818

Gliem, M., Klotz, L., van Rooijen, N., Hartung, H. P., & Jander, S. (2015). Hyperglycemia and PPARγ Antagonistically Influence Macrophage Polarization and Infarct Healing After Ischemic Stroke. *Stroke, 46*(10), 2935-2942. doi:10.1161/strokeaha.115.010557

Golebiewska, E. M., & Poole, A. W. (2015). Platelet secretion: From haemostasis to wound healing and beyond. *Blood Rev, 29*(3), 153-162. doi:10.1016/j.blre.2014.10.003

Golforoush, P., Yellon, D. M., & Davidson, S. M. (2020). Mouse models of atherosclerosis and their suitability for the study of myocardial infarction. *Basic Res Cardiol, 115*(6), 73. doi:10.1007/s00395-020-00829-5

Gößwald, A., Schienkiewitz, A., Nowossadeck, E., & Busch, M. (2013). Prävalenz von Herzinfarkt und koronarer Herzkrankheit bei Erwachsenen im Alter von 40 bis 79 Jahren in Deutschland. In (Vol. 56): Robert Koch-Institut, Epidemiologie und Gesundheitsberichterstattung.

Graham, G. J., Ren, Q., Dilks, J. R., Blair, P., Whiteheart, S. W., & Flaumenhaft, R. (2009). Endobrevin/VAMP-8-dependent dense granule release mediates thrombus formation in vivo. *Blood, 114*(5), 1083-1090. doi:10.1182/blood-2009-03-210211

Granger, C. B., Alexander, J. H., McMurray, J. J., Lopes, R. D., Hylek, E. M., Hanna, M., Al-Khalidi, H. R., Ansell, J., Atar, D., Avezum, A., Bahit, M. C., Diaz, R., Easton, J. D., Ezekowitz, J. A., Flaker, G., Garcia, D., Geraldes, M., Gersh, B. J., Golitsyn, S., Goto, S., Hermosillo, A. G., Hohnloser, S. H., Horowitz, J., Mohan, P., Jansky, P., Lewis, B. S., Lopez-Sendon, J. L., Pais, P., Parkhomenko, A., Verheugt, F. W., Zhu, J., Wallentin, L., Committees, A., & Investigators. (2011). Apixaban versus warfarin in patients with atrial fibrillation. *N Engl J Med, 365*(11), 981-992. doi:10.1056/NEJMoa1107039

Hamzei Taj, S., Kho, W., Aswendt, M., Collmann, F. M., Green, C., Adamczak, J., Tennstaedt, A., & Hoehn, M. (2016). Dynamic Modulation of Microglia/Macrophage Polarization by miR-124 after Focal Cerebral Ischemia. *J Neuroimmune Pharmacol, 11*(4), 733-748. doi:10.1007/s11481-016-9700-y

Heijnen, H., & van der Sluijs, P. (2015). Platelet secretory behaviour: as diverse as the granules … or not? *J Thromb Haemost, 13*(12), 2141-2151. doi:10.1111/jth.13147

Heiss, C., Sievers, R. E., Amabile, N., Momma, T. Y., Chen, Q., Natarajan, S., Yeghiazarians, Y., & Springer, M. L. (2008). In vivo measurement of flow-mediated vasodilation in living rats using high-resolution ultrasound. *Am J Physiol Heart Circ Physiol, 294*(2), H1086-1093. doi:10.1152/ajpheart.00811.2007

Hewett, S. J., Jackman, N. A., & Claycomb, R. J. (2012). Interleukin-1beta in Central Nervous System Injury and Repair. *Eur J Neurodegener Dis, 1*(2), 195-211. Retrieved from https://www.ncbi.nlm.nih.gov/pubmed/26082912

Hoffman, M., & Monroe, D. M., 3rd. (2001). A cell-based model of hemostasis. *Thromb Haemost, 85*(6), 958-965. Retrieved from https://www.ncbi.nlm.nih.gov/pubmed/11434702

Hoyer, F. F., & Nahrendorf, M. (2019). Interferon-gamma regulates cardiac myeloid cells in myocardial infarction. *Cardiovasc Res, 115*(13), 1815-1816. doi:10.1093/cvr/cvz143

Ibanez, B., James, S., Agewall, S., Antunes, M. J., Bucciarelli-Ducci, C., Bueno, H., Caforio, A. L. P., Crea, F., Goudevenos, J. A., Halvorsen, S., Hindricks, G., Kastrati, A., Lenzen, M. J., Prescott, E., Roffi, M., Valgimigli, M., Varenhorst, C., Vranckx, P., Widimsky, P., & Group, E. S. C. S. D. (2018). 2017 ESC Guidelines for the management of acute myocardial infarction in patients presenting with ST-segment elevation: The Task Force for the management of acute myocardial infarction in patients presenting with ST-segment elevation of the European Society of Cardiology (ESC). *Eur Heart J, 39*(2), 119-177. doi:10.1093/eurheartj/ehx393

Ilatovskaya, D. V., Pitts, C., Clayton, J., Domondon, M., Troncoso, M., Pippin, S., & DeLeon-Pennell, K. Y. (2019). CD8(+) T-cells negatively regulate inflammation post-myocardial infarction. *Am J Physiol Heart Circ Physiol, 317*(3), H581-H596. doi:10.1152/ajpheart.00112.2019

Josefsson, E. C., Vainchenker, W., & James, C. (2020). Regulation of Platelet Production and Life Span: Role of Bcl-xL and Potential Implications for Human Platelet Diseases. *Int J Mol Sci, 21*(20). doi:10.3390/ijms21207591

Joshi, C. J., Ke, W., Drangowska-Way, A., O'Rourke, E. J., & Lewis, N. E. (2022). What are housekeeping genes? *PLoS Comput Biol, 18*(7), e1010295. doi:10.1371/journal.pcbi.1010295

Jung, M., Ma, Y., Iyer, R. P., DeLeon-Pennell, K. Y., Yabluchanskiy, A., Garrett, M. R., & Lindsey, M. L. (2017). IL-10 improves cardiac remodeling after myocardial infarction by stimulating M2 macrophage polarization and fibroblast activation. *Basic Res Cardiol, 112*(3), 33. doi:10.1007/s00395-017-0622-5

Jurk, K., & Kehrel, B. E. (2005). Platelets: physiology and biochemistry. *Semin Thromb Hemost, 31*(4), 381-392. doi:10.1055/s-2005-916671

Kahn, M. L., Nakanishi-Matsui, M., Shapiro, M. J., Ishihara, H., & Coughlin, S. R. (1999). Protease-activated receptors 1 and 4 mediate activation of human platelets by thrombin. *J Clin Invest, 103*(6), 879-887. doi:10.1172/JCI6042

Kalampogias, A., Siasos, G., Oikonomou, E., Tsalamandris, S., Mourouzis, K., Tsigkou, V., Vavuranakis, M., Zografos, T., Deftereos, S., Stefanadis, C., & Tousoulis, D. (2016). Basic Mechanisms in Atherosclerosis: The Role of Calcium. *Med Chem, 12*(2), 103-113. doi:10.2174/1573406411666150928111446

Kamiguti, A. S., Theakston, R. D., Watson, S. P., Bon, C., Laing, G. D., & Zuzel, M. (2000). Distinct contributions of glycoprotein VI and alpha(2)beta(1) integrin to the induction of platelet protein tyrosine phosphorylation and aggregation. *Arch Biochem Biophys, 374*(2), 356-362. doi:10.1006/abbi.1999.1627

Kang, Q., Li, L., Pang, Y., Zhu, W., & Meng, L. (2022). An update on Ym1 and its immunoregulatory role in diseases. *Front Immunol, 13*, 891220. doi:10.3389/fimmu.2022.891220

Kaplan, K., Broekman, M., Chernoff, A., Lesznick, G., & Drillings, M. (1979). Platelet alpha-granule proteins: studies on release and subcellular localization. *Blood, 53*, 604-618.

Kim, S., Sharma, C., Jung, U. J., & Kim, S. R. (2023). Pathophysiological Role of Microglial Activation Induced by Blood-Borne Proteins in Alzheimer's Disease. *Biomedicines, 11*(5). doi:10.3390/biomedicines11051383

Kirchhof, P., Benussi, S., Kotecha, D., Ahlsson, A., Atar, D., Casadei, B., Castella, M., Diener, H. C., Heidbuchel, H., Hendriks, J., Hindricks, G., Manolis, A. S., Oldgren, J., Popescu, B. A., Schotten, U., Van Putte, B., Vardas, P., & Group, E. S. C. S. D. (2016). 2016 ESC Guidelines for the management of atrial fibrillation developed in collaboration with EACTS. *Eur Heart J, 37*(38), 2893-2962. doi:10.1093/eurheartj/ehw210

Kleinschnitz, C., Blecharz, K., Kahles, T., Schwarz, T., Kraft, P., Göbel, K., Meuth, S. G., Burek, M., Thum, T., Stoll, G., & Förster, C. (2011). Glucocorticoid insensitivity at the hypoxic blood-brain barrier can be reversed by inhibition of the proteasome. *Stroke, 42*(4), 1081-1089. doi:10.1161/strokeaha.110.592238

Kumar, A., Stoica, B. A., Sabirzhanov, B., Burns, M. P., Faden, A. I., & Loane, D. J. (2013). Traumatic brain injury in aged animals increases lesion size and chronically alters microglial/macrophage classical and alternative activation states. *Neurobiol Aging, 34*(5), 1397-1411. doi:10.1016/j.neurobiolaging.2012.11.013

Kurihara, T., Warr, G., Loy, J., & Bravo, R. (1997). Defects in macrophage recruitment and host defense in mice lacking the CCR2 chemokine receptor. *J Exp Med, 186*(10), 1757-1762. doi:10.1084/jem.186.10.1757

Kuter, D. J. (1996). The physiology of platelet production. *Stem Cells, 14 Suppl 1*, 88-101. doi:10.1002/stem.5530140711

Lai, K. C., & Flaumenhaft, R. (2003). SNARE protein degradation upon platelet activation: calpain cleaves SNAP-23. *J Cell Physiol, 194*(2), 206-214. doi:10.1002/jcp.10222

LaPelusa, A., & Dave, H. D. (2023). Physiology, Hemostasis. In *StatPearls*. Treasure Island (FL).

Lecour, S. (2009). Multiple protective pathways against reperfusion injury: a SAFE path without Aktion? *J Mol Cell Cardiol, 46*(5), 607-609. doi:10.1016/j.yjmcc.2009.01.003

Lefkovits, J., Plow, E. F., & Topol, E. J. (1995). Platelet glycoprotein IIb/IIIa receptors in cardiovascular medicine. *N Engl J Med, 332*(23), 1553-1559. doi:10.1056/nejm199506083322306

Lemons, P. P., Chen, D., Bernstein, A. M., Bennett, M. K., & Whiteheart, S. W. (1997). Regulated secretion in platelets: identification of elements of the platelet exocytosis machinery. *Blood, 90*(4), 1490-1500.

Lemons, P. P., Chen, D., & Whiteheart, S. W. (2000). Molecular mechanisms of platelet exocytosis: requirements for alpha-granule release. *Biochem Biophys Res Commun, 267*(3), 875-880. doi:10.1006/bbrc.1999.2039

Linkins, L.-A. (2019). Rivaroxaban Clinical Trials in 2018: Successes, Failures, and Lessons Learned. *The Hematologist, 16*(1). Retrieved from https://ashpublications.org/thehematologist/article/doi/10.1182/hem.V16.1.9285/463127/Rivaroxaban-Clinical-Trials-in-2018-Successes

Liu, J., Nishida, M., Inui, H., Chang, J., Zhu, Y., Kanno, K., Matsuda, H., Sairyo, M., Okada, T., Nakaoka, H., Ohama, T., Masuda, D., Koseki, M., Yamashita, S., & Sakata, Y. (2019). Rivaroxaban Suppresses the Progression of Ischemic Cardiomyopathy in a Murine Model of Diet-Induced Myocardial Infarction. *J Atheroscler Thromb, 26*(10), 915-930. doi:10.5551/jat.48405

Liu, Y., Gao, X. M., Fang, L., Jennings, N. L., Su, Y., Q, X., Samson, A. L., Kiriazis, H., Wang, X. F., Shan, L., Sturgeon, S. A., Medcalf, R. L., Jackson, S. P., Dart, A. M., & Du, X. J. (2011). Novel role of platelets in mediating inflammatory responses and ventricular rupture or remodeling following myocardial infarction. *Arterioscler Thromb Vasc Biol, 31*(4), 834-841. doi:10.1161/ATVBAHA.110.220467

Lopes, R. D., Heizer, G., Aronson, R., Vora, A. N., Massaro, T., Mehran, R., Goodman, S. G., Windecker, S., Darius, H., Li, J., Averkov, O., Bahit, M. C., Berwanger, O., Budaj, A., Hijazi, Z., Parkhomenko, A., Sinnaeve, P., Storey, R. F., Thiele, H., Vinereanu, D., Granger, C. B., Alexander, J. H., & Investigators, A. (2019). Antithrombotic Therapy after Acute Coronary Syndrome or PCI in Atrial Fibrillation. *N Engl J Med*. doi:10.1056/NEJMoa1817083

Lowenstein, C. J. (2017). VAMP-3 mediates platelet endocytosis. *Blood, 130*(26), 2816-2818. doi:10.1182/blood-2017-10-808576

Lugrin, J., Parapanov, R., Milano, G., Cavin, S., Debonneville, A., Krueger, T., & Liaudet, L. (2023). The systemic deletion of interleukin-1alpha reduces myocardial inflammation and attenuates ventricular remodeling in murine myocardial infarction. *Sci Rep, 13*(1), 4006. doi:10.1038/s41598-023-30662-4

Maynard, D. M., Heijnen, H. F., Horne, M. K., White, J. G., & Gahl, W. A. (2007). Proteomic analysis of platelet alpha-granules using mass spectrometry. *J Thromb Haemost, 5*(9), 1945-1955. doi:10.1111/j.1538-7836.2007.02690.x

McRae, S. (2011). Physiological Haemostasis. In R. Fitridge & M. Thompson (Eds.), *Mechanisms of Vascular Disease: A Reference Book for Vascular Specialists*. Adelaide (AU).

Mechanic, O. J., Gavin, M., & Grossman, S. A. (2023). Acute Myocardial Infarction. In *StatPearls*. Treasure Island (FL).

Mega, J. L., Braunwald, E., Wiviott, S. D., Bassand, J. P., Bhatt, D. L., Bode, C., Burton, P., Cohen, M., Cook-Bruns, N., Fox, K. A., Goto, S., Murphy, S. A., Plotnikov, A. N., Schneider, D., Sun, X., Verheugt, F. W., Gibson, C. M., & Investigators, A. A. T. (2012). Rivaroxaban in patients with a recent acute coronary syndrome. *N Engl J Med, 366*(1), 9-19. doi:10.1056/NEJMoa1112277

Mehta, J. L., Yang, B. C., Strates, B. S., & Mehta, P. (1999). Role of TGF-beta1 in platelet-mediated cardioprotection during ischemia-reperfusion in isolated rat hearts. *Growth Factors, 16*(3), 179-190. doi:10.3109/08977199909002128

Meinel, T. R., Branca, M., De Marchis, G. M., Nedeltchev, K., Kahles, T., Bonati, L., Arnold, M., Heldner, M. R., Jung, S., Carrera, E., Dirren, E., Michel, P., Strambo, D., Cereda, C. W., Bianco, G., Kagi, G., Vehoff, J., Katan, M., Bolognese, M., Backhaus, R., Salmen, S., Albert, S., Medlin, F., Berger, C., Schelosky, L., Renaud, S., Niederhauser, J., Bonvin, C., Schaerer, M., Mono, M. L., Rodic, B., Tarnutzer, A. A., Mordasini, P., Gralla, J., Kaesmacher, J., Engelter, S., Fischer, U., Seiffge, D. J., & Investigators of the Swiss Stroke, R. (2021). Prior Anticoagulation in Patients with

Ischemic Stroke and Atrial Fibrillation. *Ann Neurol, 89*(1), 42-53. doi:10.1002/ana.25917

Meinel, T. R., Frey, S., Arnold, M., Kendroud, S., Fischer, U., Kaesmacher, J., Heldner, M. R., & Jung, S. (2019). Clinical presentation, diagnostic findings and management of cerebral ischemic events in patients on treatment with non-vitamin K antagonist oral anticoagulants - A systematic review. *PLoS One, 14*(3), e0213379. doi:10.1371/journal.pone.0213379

Meng, R., Wu, J., Harper, D. C., Wang, Y., Kowalska, M. A., Abrams, C. S., Brass, L. F., Poncz, M., Stalker, T. J., & Marks, M. S. (2015). Defective release of alpha granule and lysosome contents from platelets in mouse Hermansky-Pudlak syndrome models. *Blood, 125*(10), 1623-1632. doi:10.1182/blood-2014-07-586727

Menter, D. G., Kopetz, S., Hawk, E., Sood, A. K., Loree, J. M., Gresele, P., & Honn, K. V. (2017). Platelet "first responders" in wound response, cancer, and metastasis. *Cancer Metastasis Rev, 36*(2), 199-213. doi:10.1007/s10555-017-9682-0

Mezger, M., Nording, H., Sauter, R., Graf, T., Heim, C., von Bubnoff, N., Ensminger, S. M., & Langer, H. F. (2019). Platelets and Immune Responses During Thromboinflammation. *Front Immunol, 10*, 1731. doi:10.3389/fimmu.2019.01731

Monnet, E., Sizaret, P., Arbeille, B., & Fauvel-Lafeve, F. (2000). Different role of platelet glycoprotein GP Ia/IIa in platelet contact and activation induced by type I and type III collagens. *Thromb Res, 98*(5), 423-433. doi:10.1016/s0049-3848(00)00199-7

Montecucco, F., Liberale, L., Bonaventura, A., Vecchie, A., Dallegri, F., & Carbone, F. (2017). The Role of Inflammation in Cardiovascular Outcome. *Curr Atheroscler Rep, 19*(3), 11. doi:10.1007/s11883-017-0646-1

Morisch, S. (2017). Antikoagulationstherapie. Retrieved from https://www.journalmed.de/thema/lesen/antikoagulationstherapie#0Was%20ist%20eine%20Antikoagulationstherapie%3F

Moroi, M. (2000). [Platelet receptors for collagen]. *Seikagaku, 72*(7), 543-546. Retrieved from https://www.ncbi.nlm.nih.gov/pubmed/10967686

Moschonas, I. C. P., S.: Sidiropoulou, S.; Tselepis, A. D. (2020). Do platelet mediators and coagulation factors affect the formation of neutrophil extracellular traps? *J Atherosclerosis Prev Treat.* doi:10.53590/japt.02.1013

Mustard, J. F., Packham, M. A., & Kinlough-Rathbone, R. L. (1990). Platelets, blood flow, and the vessel wall. *Circulation, 81*(1 Suppl), I24-27; discussion I40-21.

Nahrendorf, M., Swirski, F. K., Aikawa, E., Stangenberg, L., Wurdinger, T., Figueiredo, J. L., Libby, P., Weissleder, R., & Pittet, M. J. (2007). The healing myocardium sequentially mobilizes two monocyte subsets with divergent and complementary functions. *J Exp Med, 204*(12), 3037-3047. doi:10.1084/jem.20070885

Nikol, S. (2023). Ischämie. *Pschyrembel Online.* Retrieved from https://www.pschyrembel.de/Isch%C3%A4mie/K0B5P

Norrving, B., Barrick, J., Davalos, A., Dichgans, M., Cordonnier, C., Guekht, A., Kutluk, K., Mikulik, R., Wardlaw, J., Richard, E., Nabavi, D., Molina, C., Bath, P. M., Stibrant Sunnerhagen, K., Rudd, A., Drummond, A., Planas, A., & Caso, V. (2018). Action

Plan for Stroke in Europe 2018-2030. *Eur Stroke J, 3*(4), 309-336. doi:10.1177/2396987318808719

NVL chronische KHK. (2022). Nationale VersorgungsLeitlinie (NVL) Chronische KHK, Version 6. Retrieved from https://www.leitlinien.de/themen/khk

Orkin, S. H., Nathan, D. G., Ginsburg, D., & Look, T. (2009). Nathan and Oski's hematology of infancy and childhood. *Elsevier Health Sciences*, 1386.

Papayannopoulos, V. (2018). Neutrophil extracellular traps in immunity and disease. *Nat Rev Immunol, 18*(2), 134-147. doi:10.1038/nri.2017.105

Patel, M. R., Mahaffey, K. W., Garg, J., Pan, G., Singer, D. E., Hacke, W., Breithardt, G., Halperin, J. L., Hankey, G. J., Piccini, J. P., Becker, R. C., Nessel, C. C., Paolini, J. F., Berkowitz, S. D., Fox, K. A., Califf, R. M., & Investigators, R. A. (2011). Rivaroxaban versus warfarin in nonvalvular atrial fibrillation. *N Engl J Med, 365*(10), 883-891. doi:10.1056/NEJMoa1009638

Perzborn, E., Roehrig, S., Straub, A., Kubitza, D., Mueck, W., & Laux, V. (2010). Rivaroxaban: a new oral factor Xa inhibitor. *Arterioscler Thromb Vasc Biol, 30*(3), 376-381. doi:10.1161/ATVBAHA.110.202978

Petzold, T., Thienel, M., Dannenberg, L., Mourikis, P., Helten, C., Ayhan, A., M'Pembele, R., Achilles, A., Trojovky, K., Konsek, D., Zhang, Z., Regenauer, R., Pircher, J., Ehrlich, A., Lusebrink, E., Nicolai, L., Stocker, T. J., Brandl, R., Roschenthaler, F., Strecker, J., Saleh, I., Spannagl, M., Mayr, C. H., Schiller, H. B., Jung, C., Gerdes, N., Hoffmann, T., Levkau, B., Hohlfeld, T., Zeus, T., Schulz, C., Kelm, M., & Polzin, A. (2020). Rivaroxaban Reduces Arterial Thrombosis by Inhibition of FXa-Driven Platelet Activation via Protease Activated Receptor-1. *Circ Res, 126*(4), 486-500. doi:10.1161/CIRCRESAHA.119.315099

Petzold, T., Thienel, M., Dannenberg, L. K., Mourikis, P., Helten, C., Ayhan, A., M'Pembele, R., Achilles, A., Trojovsky, K., Konsek, D., Zang, Z., Regenauer, R., Pircher, J., Ehrlich, A., Lusebrink, E., Nicolai, L., Stocker, T., Brandl, R., Roschentaler, F., Strecker, J., Saleh, I., Spannagl, M., Mayr, C. H., Schiller, H. B., Jung, C., Gerdes, N., Hoffmann, T., Levkau, B., Hohlfeld, T., Zeus, T., Schulz, C., Kelm, M., & Polzin, A. (2019). Rivaroxaban Reduces Arterial Thrombosis by Inhibition of FXa Driven Platelet Activation Via Protease Activated Receptor-1. *Circ Res*. doi:10.1161/CIRCRESAHA.119.315099

Petzold, T., Thienel, M., Konrad, I., Schubert, I., Regenauer, R., Hoppe, B., Lorenz, M., Eckart, A., Chandraratne, S., Lennerz, C., Kolb, C., Braun, D., Jamasbi, J., Brandl, R., Braun, S., Siess, W., Schulz, C., & Massberg, S. (2016). Oral thrombin inhibitor aggravates platelet adhesion and aggregation during arterial thrombosis. *Sci Transl Med, 8*(367), 367ra168. doi:10.1126/scitranslmed.aad6712

Piersma, S. R., Broxterman, H. J., Kapci, M., de Haas, R. R., Hoekman, K., Verheul, H. M., & Jiménez, C. R. (2009). Proteomics of the TRAP-induced platelet releasate. *J Proteomics, 72*(1), 91-109. doi:10.1016/j.jprot.2008.10.009

Polgár, J., Chung, S. H., & Reed, G. L. (2002). Vesicle-associated membrane protein 3 (VAMP-3) and VAMP-8 are present in human platelets and are required for granule secretion. *Blood, 100*(3), 1081-1083. doi:10.1182/blood.v100.3.1081

Polzin, A., Dannenberg, L., Benkhoff, M., Barcik, M., Helten, C., Mourikis, P., Ahlbrecht, S., Wildeis, L., Ziese, J., Zikeli, D., Metzen, D., Hu, H., Baensch, L., Schroder, N. H.,

Keul, P., Weske, S., Wollnitzke, P., Duse, D., Saffak, S., Cramer, M., Bonner, F., Muller, T., Graler, M. H., Zeus, T., Kelm, M., & Levkau, B. (2023). Revealing concealed cardioprotection by platelet Mfsd2b-released S1P in human and murine myocardial infarction. *Nat Commun, 14*(1), 2404. doi:10.1038/s41467-023-38069-5

Polzin, A., Dannenberg, L., Benkhoff, M., Barcik, M., Keul, P., Helten, C., Zeus, T., Kelm, M., & Levkau, B. (2022). S1P Lyase Inhibition Starting After Ischemia/Reperfusion Improves Postischemic Cardiac Remodeling. *JACC Basic Transl Sci, 7*(5), 498-499. doi:10.1016/j.jacbts.2022.03.009

Polzin, A., Dannenberg, L., Thienel, M., Orban, M., Wolff, G., Hohlfeld, T., Zeus, T., Kelm, M., & Petzold, T. (2021). Noncanonical Effects of Oral Thrombin and Factor Xa Inhibitors in Platelet Activation and Arterial Thrombosis. *Thromb Haemost, 121*(2), 122-130. doi:10.1055/s-0040-1716750

Ponomarev, E. D., Maresz, K., Tan, Y., & Dittel, B. N. (2007). CNS-derived interleukin-4 is essential for the regulation of autoimmune inflammation and induces a state of alternative activation in microglial cells. *J Neurosci, 27*(40), 10714-10721. doi:10.1523/JNEUROSCI.1922-07.2007

Ramos, G., Hofmann, U., & Frantz, S. (2016). Myocardial fibrosis seen through the lenses of T-cell biology. *J Mol Cell Cardiol, 92*, 41-45. doi:10.1016/j.yjmcc.2016.01.018

Redfors, B., Shao, Y., & Omerovic, E. (2012). Myocardial infarct size and area at risk assessment in mice. *Exp Clin Cardiol, 17*(4), 268-272.

Ren, Q., Barber, H. K., Crawford, G. L., Karim, Z. A., Zhao, C., Choi, W., Wang, C. C., Hong, W., & Whiteheart, S. W. (2007). Endobrevin/VAMP-8 is the primary v-SNARE for the platelet release reaction. *Mol Biol Cell, 18*(1), 24-33. doi:10.1091/mbc.e06-09-0785

Renne, T., & Gailani, D. (2007). Role of Factor XII in hemostasis and thrombosis: clinical implications. *Expert Rev Cardiovasc Ther, 5*(4), 733-741. doi:10.1586/14779072.5.4.733

Reusswig, F., Polzin, A., Klier, M., Dille, M. A., Ayhan, A., Benkhoff, M., Lersch, C., Prinz, A., Gorressen, S., Fischer, J. W., Kelm, M., & Elvers, M. (2022). Only Acute but Not Chronic Thrombocytopenia Protects Mice against Left Ventricular Dysfunction after Acute Myocardial Infarction. *Cells, 11*(21). doi:10.3390/cells11213500

Ross, E. A., Devitt, A., & Johnson, J. R. (2021). Macrophages: The Good, the Bad, and the Gluttony. *Front Immunol, 12*, 708186. doi:10.3389/fimmu.2021.708186

Ruggeri, Z. (1999). Perspective series: cell adhesion in vascular biology. von Willebrand factor. *J Clin Invest, 99*, 559-564.

Schultz, G. S., Chin, G. A., Moldawer, L., & Diegelmann, R. F. (2011). Principles of Wound Healing. In R. Fitridge & M. Thompson (Eds.), *Mechanisms of Vascular Disease: A Reference Book for Vascular Specialists*. Adelaide (AU).

Scofield, S. L., & Singh, K. (2016). Confirmation of Myocardial Ischemia and Reperfusion Injury in Mice Using Surface Pad Electrocardiography. *J Vis Exp*(117). doi:10.3791/54814

Serhan, C. N., & Sheppard, K. A. (1990). Lipoxin formation during human neutrophil-platelet interactions. Evidence for the transformation of leukotriene A4 by platelet 12-lipoxygenase in vitro. *J Clin Invest, 85*(3), 772-780. doi:10.1172/JCI114503

Sharda, A., & Flaumenhaft, R. (2018). The life cycle of platelet granules. *F1000Res, 7*, 236. doi:10.12688/f1000research.13283.1

Shin, E. K., Park, H., Noh, J. Y., Lim, K. M., & Chung, J. H. (2017). Platelet Shape Changes and Cytoskeleton Dynamics as Novel Therapeutic Targets for Anti-Thrombotic Drugs. *Biomol Ther (Seoul), 25*(3), 223-230. doi:10.4062/biomolther.2016.138

Singh, A., Museedi, A. S., & Grossman, S. A. (2023). Acute Coronary Syndrome. In *StatPearls*. Treasure Island (FL).

Statistisches Bundesamt. (2022). Deaths caused by the 10 most frequent cardiovascular diseases. Retrieved from https://www.destatis.de/EN/Themes/Society-Environment/Health/Causes-Death/Tables/deaths-cardiovascular-disease-total.html

Terry, C. M., He, Y., & Cheung, A. K. (2016). Rivaroxaban improves patency and decreases inflammation in a mouse model of catheter thrombosis. *Thromb Res, 144*, 106-112. doi:10.1016/j.thromres.2016.06.008

Thienel, M., Muller-Reif, J. B., Zhang, Z., Ehreiser, V., Huth, J., Shchurovska, K., Kilani, B., Schweizer, L., Geyer, P. E., Zwiebel, M., Novotny, J., Lusebrink, E., Little, G., Orban, M., Nicolai, L., El Nemr, S., Titova, A., Spannagl, M., Kindberg, J., Evans, A. L., Mach, O., Vogel, M., Tiedt, S., Ormanns, S., Kessler, B., Dueck, A., Friebe, A., Jorgensen, P. G., Majzoub-Altweck, M., Blutke, A., Polzin, A., Stark, K., Kaab, S., Maier, D., Gibbins, J. M., Limper, U., Frobert, O., Mann, M., Massberg, S., & Petzold, T. (2023). Immobility-associated thromboprotection is conserved across mammalian species from bear to human. *Science, 380*(6641), 178-187. doi:10.1126/science.abo5044

Thomas, M. R., & Storey, R. F. (2015). The role of platelets in inflammation. *Thromb Haemost, 114*(3), 449-458. doi:10.1160/TH14-12-1067

Van Herck, H., Baumans, V., Brandt, C. J., Boere, H. A., Hesp, A. P., van Lith, H. A., Schurink, M., & Beynen, A. C. (2001). Blood sampling from the retro-orbital plexus, the saphenous vein and the tail vein in rats: comparative effects on selected behavioural and blood variables. *Lab Anim, 35*(2), 131-139. doi:10.1258/0023677011911499

van Herrewegen, F., Meijers, J. C., Peters, M., & van Ommen, C. H. (2012). Clinical practice: the bleeding child. Part II: disorders of secondary hemostasis and fibrinolysis. *Eur J Pediatr, 171*(2), 207-214. doi:10.1007/s00431-011-1571-x

Vieira, J. M., Norman, S., Villa Del Campo, C., Cahill, T. J., Barnette, D. N., Gunadasa-Rohling, M., Johnson, L. A., Greaves, D. R., Carr, C. A., Jackson, D. G., & Riley, P. R. (2018). The cardiac lymphatic system stimulates resolution of inflammation following myocardial infarction. *J Clin Invest, 128*(8), 3402-3412. doi:10.1172/jci97192

von Bruhl, M. L., Stark, K., Steinhart, A., Chandraratne, S., Konrad, I., Lorenz, M., Khandoga, A., Tirniceriu, A., Coletti, R., Kollnberger, M., Byrne, R. A., Laitinen, I., Walch, A., Brill, A., Pfeiler, S., Manukyan, D., Braun, S., Lange, P., Riegger, J., Ware, J., Eckart, A., Haidari, S., Rudelius, M., Schulz, C., Echtler, K., Brinkmann, V., Schwaiger, M., Preissner, K. T., Wagner, D. D., Mackman, N., Engelmann, B., & Massberg, S. (2012). Monocytes, neutrophils, and platelets cooperate to initiate and propagate venous thrombosis in mice in vivo. *J Exp Med, 209*(4), 819-835. doi:10.1084/jem.20112322

Vornholz, L. C. (2019). *Systemische Wechselbeziehungen zwischen dem ischämischen Schlaganfall
und dem Herzen im Mausmodell.* Freien Universität Berlin,

Wahlgren, N. G., & Ahmed, N. (2004). Neuroprotection in cerebral ischaemia: facts and fancies--the need for new approaches. *Cerebrovasc Dis, 17 Suppl 1*, 153-166. doi:10.1159/000074808

Walsh, T. G., & Poole, A. W. (2018). Do platelets promote cardiac recovery after myocardial infarction: roles beyond occlusive ischemic damage. *Am J Physiol Heart Circ Physiol, 314*(5), H1043-H1048. doi:10.1152/ajpheart.00134.2018

Ware, J. A., & Heistad, D. D. (1993). Seminars in medicine of the Beth Israel Hospital, Boston. Platelet-endothelium interactions. *N Engl J Med, 328*(9), 628-635. doi:10.1056/NEJM199303043280907

White, J. G. (1998). Use of the electron microscope for diagnosis of platelet disorders. *Semin Thromb Hemost, 24*(2), 163-168. doi:10.1055/s-2007-995836

Wright, P. B., McDonald, E., Bravo-Blas, A., Baer, H. M., Heawood, A., Bain, C. C., Mowat, A. M., Clay, S. L., Robertson, E. V., Morton, F., Nijjar, J. S., Ijaz, U. Z., Milling, S. W. F., & Gaya, D. R. (2021). The mannose receptor (CD206) identifies a population of colonic macrophages in health and inflammatory bowel disease. *Sci Rep, 11*(1), 19616. doi:10.1038/s41598-021-98611-7

Wu, J., Cai, Y., Wu, X., Ying, Y., Tai, Y., & He, M. (2021). Transcardiac Perfusion of the Mouse for Brain Tissue Dissection and Fixation. *Bio Protoc, 11*(5), e3988. doi:10.21769/BioProtoc.3988

Yang, B. C., & Mehta, J. L. (1994). Platelet-derived adenosine contributes to the cardioprotective effects of platelets against ischemia-reperfusion injury in isolated rat heart. *J Cardiovasc Pharmacol, 24*(5), 779-785. doi:10.1097/00005344-199424050-00013

Yasaka, M., Minematsu, K., Toyoda, K., Mori, E., Hirano, T., Hamasaki, T., Yamagami, H., Nagao, T., Yoshimura, S., Uchiyama, S., & group, R. s. (2019). Rivaroxaban administration after acute ischemic stroke: The RELAXED study. *PLoS One, 14*(2), e0212354. doi:10.1371/journal.pone.0212354

Yun, S. H., Sim, E. H., Goh, R. Y., Park, J. I., & Han, J. Y. (2016). Platelet Activation: The Mechanisms and Potential Biomarkers. *Biomed Res Int, 2016*, 9060143. doi:10.1155/2016/9060143

Zannad, F., Anker, S. D., Byra, W. M., Cleland, J. G. F., Fu, M., Gheorghiade, M., Lam, C. S. P., Mehra, M. R., Neaton, J. D., Nessel, C. C., Spiro, T. E., van Veldhuisen, D. J., Greenberg, B., & Investigators, C. H. (2018). Rivaroxaban in Patients with Heart Failure, Sinus Rhythm, and Coronary Disease. *N Engl J Med, 379*(14), 1332-1342. doi:10.1056/NEJMoa1808848

Zhang, J., Lu, Y., Mao, Y., Yu, Y., Wu, T., Zhao, W., Zhu, Y., Zhao, P., & Zhang, F. (2022). IFN-gamma enhances the efficacy of mesenchymal stromal cell-derived exosomes via miR-21 in myocardial infarction rats. *Stem Cell Res Ther, 13*(1), 333. doi:10.1186/s13287-022-02984-z

Zhao, X., Ho, D., Gao, S., Hong, C., Vatner, D. E., & Vatner, S. F. (2011). Arterial Pressure Monitoring in Mice. *Curr Protoc Mouse Biol, 1*, 105-122. doi:10.1002/9780470942390.mo100149

Zhou, Y., Xu, Z., & Liu, Z. (2022). Impact of Neutrophil Extracellular Traps on Thrombosis Formation: New Findings and Future Perspective. *Front Cell Infect Microbiol, 12*, 910908. doi:10.3389/fcimb.2022.910908

Ziegler, M., Alt, K., Paterson, B. M., Kanellakis, P., Bobik, A., Donnelly, P. S., Hagemeyer, C. E., & Peter, K. (2016). Highly Sensitive Detection of Minimal Cardiac Ischemia using Positron Emission Tomography Imaging of Activated Platelets. *Sci Rep, 6*, 38161. doi:10.1038/srep38161

8. Supplementary

FIGURE NUMBER	WHICH TEST?	EXACT VALUE n =	DEFINED?	REPORTED?	EXACT VALUE p =	DEGREES OF FREEDOM & F /t/z/R/ETC VALUE
17 A	One-way ANOVA	10,10,10	Control/ acute FXa-inh./ chronic FXa-inh.	Error bars are mean ± SD	p=0.0012	F(2, 27) = 8.751
17 B	One-way ANOVA	10,10,10	Control/ acute FXa-inh./ chronic FXa-inh.	Error bars are mean ± SD	p=0.7849	F(2,26) = 0.2445
18 A	One-way ANOVA	10,10,10	Control/ acute FXa-inh./ chronic FXa-inh.	Error bars are mean ± SD	p=0.4673	F(2, 27) = 0.7826
18 B	One-way ANOVA	10,10,10	Control/ acute FXa-inh./ chronic FXa-inh.	Error bars are mean ± SD	p=0.0007	F(2, 27) = 9.722
18 C	One-way ANOVA	10,10,10	Control/ acute FXa-inh./ chronic FXa-inh.	Error bars are mean ± SD	p=0.0020	F(2, 27) = 7.854
18 A	Unpaired *t*-test	6,6	Control/ chronic FXa-inh	Error bars are mean ± SD	p=0.8533	*t*(10) = 0.1898
19 B	Unpaired *t*-test	6,6	Control/ chronic FXa-inh	Error bars are mean ± SD	p=0.4304	*t*(10) = 0.8217
19 C	Unpaired *t*-test	6,6	Control/ chronic FXa-inh	Error bars are mean ± SD	p=0.0347	*t*(10) = 2.442
19 D	Unpaired *t*-test	6,6	Control/ chronic FXa-inh	Error bars are mean ± SD	p=0.026	*t*(10) = 2.611
19 E	Unpaired *t*-test	6,6	Control/ chronic FXa-inh	Error bars are mean ± SD	p=0.1661	*t*(10) = 1.494
19 F	Unpaired *t*-test	6,6	Control/ chronic FXa-inh	Error bars are mean ± SD	p=0.2498	*t*(10) = 1.222

19 G	Unpaired *t*-test	6,6	Control/ chronic FXa-inh	Error bars are mean ± SD	p=0.4040	$t(10) = 0.8713$
20 A	One-way ANOVA	8,5,9	Control/ acute FXa-inh./ chronic FXa-inh.	Error bars are mean ± SD	p=0.0061	$F(2, 19) = 6.746$
20 B	One-way ANOVA	8,4,9	Control/ acute FXa-inh./ chronic FXa-inh.	Error bars are mean ± SD	p=0.3475	$F(2, 18) = 1.122$
20 C	One-way ANOVA	9,5,9	Control/ acute FXa-inh./ chronic FXa-inh.	Error bars are mean ± SD	p=0.1591	$F(2, 20) = 2.018$
20 D	One-way ANOVA	10,5,8	Control/ acute FXa-inh./ chronic FXa-inh.	Error bars are mean ± SD	p=0.3139	$F(2, 20) = 1.228$
20 E	One-way ANOVA	8,5,7	Control/ acute FXa-inh./ chronic FXa-inh.	Error bars are mean ± SD	p=0.2862	$F(2, 17) = 1.348$
20 F	One-way ANOVA	8,3,9	Control/ acute FXa-inh./ chronic FXa-inh.	Error bars are mean ± SD	p=0.3577	$F(2, 17) = 1.093$
20 G	One-way ANOVA	9,5,8	Control/ acute FXa-inh./ chronic FXa-inh.	Error bars are mean ± SD	p=0.2374	$F(2, 19) = 1.552$
20 H	One-way ANOVA	10,5,10	Control/ acute FXa-inh./ chronic FXa-inh.	Error bars are mean ± SD	p=0.0771	$F(2, 22) = 2.886$
20 I	One-way ANOVA	10,5,10	Control/ acute FXa-inh./ chronic FXa-inh.	Error bars are mean ± SD	p=0.7531	$F(2, 22) = 0.2872$
20 J	One-way ANOVA	9,5,10	Control/ acute FXa-inh./ chronic FXa-inh.	Error bars are mean ± SD	p=0.0663	$F(2, 21) = 3.097$
20 K	One-way ANOVA	10,5,9	Control/ acute FXa-inh./ chronic FXa-inh.	Error bars are mean ± SD	p=0.6890	$F(2, 21) = 0.3792$
20 L	One-way ANOVA	10,5,9	Control/ acute FXa-inh./ chronic FXa-inh.	Error bars are mean ± SD	p=0.6590	$F(2, 21) = 0.4255$

21 A	One-way ANOVA	10,6,6	Control/ acute FXa-inh./ chronic FXa-inh.	Error bars are mean ± SD	p=0.1896	F(2, 19) = 1.817
21 B	One-way ANOVA	10,6,6	Control/ acute FXa-inh./ chronic FXa-inh.	Error bars are mean ± SD	p=0.0327	F(2, 19) = 4.117
21 C	One-way ANOVA	10,6,6	Control/ acute FXa-inh./ chronic FXa-inh.	Error bars are mean ± SD	p=0.0235	F(2, 19) = 4.598
21 D	One-way ANOVA	10,6,6	Control/ acute FXa-inh./ chronic FXa-inh.	Error bars are mean ± SD	p=0.1259	F(2, 18) = 2.331
21 E	One-way ANOVA	10,6,6	Control/ acute FXa-inh./ chronic FXa-inh.	Error bars are mean ± SD	p=0.1604	F(2, 19) = 2.018
21 F	One-way ANOVA	10,4,4	Control/ acute FXa-inh./ chronic FXa-inh.	Error bars are mean ± SD	p=0.3150	F(2, 15) = 1.249
21 G	One-way ANOVA	8,4,5	Control/ acute FXa-inh./ chronic FXa-inh.	Error bars are mean ± SD	p=0.0693	F(2, 14) = 3.250
21 H	One-way ANOVA	11,5,5	Control/ acute FXa-inh./ chronic FXa-inh.	Error bars are mean ± SD	p=0.0567	F(2, 18) = 3.380
21 I	One-way ANOVA	10,6,6	Control/ acute FXa-inh./ chronic FXa-inh.	Error bars are mean ± SD	p=0.6202	F(2, 19) = 0.4899
21 J	One-way ANOVA	10,6,5	Control/ acute FXa-inh./ chronic FXa-inh.	Error bars are mean ± SD	p=0.2156	F(2, 19) = 1.665
21 K	One-way ANOVA	10,6,6	Control/ acute FXa-inh./ chronic FXa-inh.	Error bars are mean ± SD	p=0.0401	F(2, 19) = 3.827
21 L	One-way ANOVA	10,6,6	Control/ acute FXa-inh./ chronic FXa-inh.	Error bars are mean ± SD	p=0.0122	F(2, 19) = 5.601
22	One-way ANOVA	11,6,6	Control/ acute FXa-inh./ chronic FXa-inh.	Error bars are mean ± SD	p<0.0001	F(2,20) = 23.01

23	One-way ANOVA	12,6,6	Control/ acute FXa-inh./ chronic FXa-inh.	Error bars are mean ± SD	p<0.0001	F(2,21) = 30.85
24	One-way ANOVA	10,6,6	Control/ acute FXa-inh./ chronic FXa-inh.	Error bars are mean ± SD	p=0.0027	F(2,19) = 8.21
25	One-way ANOVA	9,9,7	Control/ acute FXa-inh./ chronic FXa-inh.	Error bars are mean ± SD	p=0.0064	F(2, 22) = 6.417
26 A	One-way ANOVA	7,7,7	Control/ acute FXa-inh./ chronic FXa-inh.	Error bars are mean ± SD	p=0.3859	F(2,18) = 1.004
26 B	One-way ANOVA	7,7,7	Control/ acute FXa-inh./ chronic FXa-inh.	Error bars are mean ± SD	p=0.0060	F(2,18) = 6.890
26 C	One-way ANOVA	7,7,7	Control/ acute FXa-inh./ chronic FXa-inh.	Error bars are mean ± SD	p=0.1641	F(2,18) = 2.002
27 A	One-way ANOVA	6,6,6	Control/ acute FXa-inh./ chronic FXa-inh	Error bars are mean ± SD	p=0.1117	F(2,15) = 2.546
27 B	One-way ANOVA	6,6,6	Control/ acute FXa-inh./ chronic FXa-inh	Error bars are mean ± SD	p=0.8637	F(2,15) = 0.148
27 C	One-way ANOVA	6,6,6	Control/ acute FXa-inh./ chronic FXa-inh	Error bars are mean ± SD	p=0.5404	F(2,15) = 0.6414
27 D	One-way ANOVA	6,6,6	Control/ acute FXa-inh./ chronic FXa-inh	Error bars are mean ± SD	p=0.9674	F(2,15) = 0.03325
27 E	One-way ANOVA	6,6,6	Control/ acute FXa-inh./ chronic FXa-inh	Error bars are mean ± SD	p=0.9992	F(2,15) = 0.0008145
27 F	One-way ANOVA	6,6,6	Control/ acute FXa-inh./ chronic FXa-inh	Error bars are mean ± SD	p=0.8185	F(2,15) = 0.203
27 G	One-way ANOVA	6,6,6	Control/ acute FXa-inh./ chronic FXa-inh	Error bars are mean ± SD	p=0.3401	F(2,15) = 1.160

27 H	One-way ANOVA	6,6,6	Control/ acute FXa-inh./ chronic FXa-inh	Error bars are mean ± SD	p=0.6515	F(2,15) = 0.4409
27 I	One-way ANOVA	6,6,6	Control/ acute FXa-inh./ chronic FXa-inh	Error bars are mean ± SD	p=0.2600	F(2,15) = 1.475
28 A	One-way ANOVA	4,4,4	Control/ acute FXa-inh./ chronic FXa-inh.	Error bars are mean ± SD	p=0.0009	F(2,9) = 16.78
28 B	One-way ANOVA	4,4,4	Control/ acute FXa-inh./ chronic FXa-inh.	Error bars are mean ± SD	p<0.0001	F(2,9) = 34.84
29 A	Two-way ANOVA	8,8,8,8	Control/ chronic FXa-inh.	Error bars are mean ± SD	p= 0.0003	F(1,28) = 17.31
29 B	Two-way ANOVA	8,8,8,8	Control/ chronic FXa-inh.	Error bars are mean ± SD	p=0.8403	F(1,28) = 0.04135
29 C	Two-way ANOVA	8,8,8,8	Control/ chronic FXa-inh.	Error bars are mean ± SD	p=0.0851	F(1,28) = 3.186
29 D	Two-way ANOVA	8,8,8,8	Control/ chronic FXa-inh.	Error bars are mean ± SD	p=0.0675	F(1,28) = 3.618
29 E	Two-way ANOVA	8,8,8,8	Control/ chronic FXa-inh.	Error bars are mean ± SD	p=0.0640	F(1,28) = 3.718
30 A	Unpaired *t*-test	5,5	Control/ chronic FXa-inh.	Error bars are mean ± SD	p=0.7607	$t(8) = 0.3152$
30 B	Unpaired *t*-test	5,5	Control/ chronic FXa-inh.	Error bars are mean ± SD	p=0.3175	$t(8) = 1.066$
30 C	Unpaired *t*-test	5,5	Control/ chronic FXa-inh.	Error bars are mean ± SD	p=0.2936	$t(8) = 1.124$
30 D	Unpaired *t*-test	5,5	Control/ chronic FXa-inh.	Error bars are mean ± SD	p=0.2034	$t(8) = 1.385$

30 E	Unpaired *t*-test	5,5	Control/ chronic FXa-inh.	Error bars are mean ± SD	p=0.6938	$t(8) = 0.4082$
30 F	Unpaired *t*-test	5,5	Control/ chronic FXa-inh.	Error bars are mean ± SD	p=0.8337	$t(8) = 0.2169$
31 A	Unpaired *t*-test	5,5	Control/ chronic FXa-inh.	Error bars are mean ± SD	p=0.7920	$t(8) = 0.2727$
31 B	Unpaired *t*-test	5,5	Control/ chronic FXa-inh.	Error bars are mean ± SD	p=0.7956	$t(8) = 0.2679$
31 C	Unpaired *t*-test	5,5	Control/ chronic FXa-inh.	Error bars are mean ± SD	p=0.7893	$t(8) = 0.2763$
32	Mixed-effects analysis	9,5	Control/ chronic FXa-inh.	Error bars are mean ± SD	p=0.172	$F(1.253, 4.594) = 2.642$
36 A	Unpaired *t*-test	5,5	Control/ FXa-inh	Error bars are mean ± SD	$p \leq 0.0001$	$t(8) = 7.748$

Danksagung

An dieser Stelle möchte ich Herrn Prof. Dr. Malte Kelm, für die Möglichkeit meine Forschung im kardiovaskulären Forschungslabor zu betreiben, meinen Dank aussprechen. Ich möchte ebenfalls allen Kooperationspartner*innen danken, die mit ihrer Arbeit und ihren Analysen zum Gesamtbild dieser Dissertation beigetragen haben. Weiter möchte ich mich herzlich bei meinem Doktorvater Herrn PD Dr. Amin Polzin für die Bereitstellung des interessanten Themas und die Betreuung während der gesamten Arbeitszeit bedanken. Ich konnte mich in den letzten 3,5 Jahren in seiner Arbeitsgruppe nicht nur fachlich, sondern auch persönlich weiterentwickeln. Auch möchte ich mich bei Herrn Prof. Dr. Axel Gödecke für die Übernahme des Zweitgutachtens bedanken. Vielen Dank auch an die Mitglieder der AG Polzin und das gesamte Laborteam des CVRL. Ohne euch und eure Unterstützung wäre es manchmal einfach nicht gegangen. Danke für tolle Freundschaften, schöne Erinnerungen und grandiose Kicker-Turniere. Ein großes Dankeschön möchte ich an meine (ehemaligen) Büronachbarn Pia Fiegenbaum, Carolin Helten, Philipp Mourikis und Marcel Benkhoff richten. Ich danke Euch für die gemeinsame Zeit, die konstruktiven aber oft auch witzigen Gespräche, die fachliche und moralische Unterstützung. Einer Person der Gruppe gebührt an dieser Stelle ein ganz besonderer Dank. Danke Marcel für deine Unterstützung von Tag eins an, das du dich mir angenommen hast und bei allen fachlichen und mentalen Höhen und Tiefen an meiner Seite warst. Ohne dich wäre die Zeit mit Sicherheit deutlich schwerer geworden!

Ganz herzlich möchte ich mich auch bei meinen Freunden bedanken, die immer hinter mir stehen, für alles Verständnis haben und eine große Stütze sind. Der größte Dank gebührt meiner Familie, vor allem meinem Mann Dennis, für die bedingungslose Liebe und Unterstützung bei allem was ich mir vorgenommen habe, auch wenn ihr in den letzten Jahren oft auf mich verzichten musstet. Danke für euer Verständnis, denn ohne euch wäre das alles überhaupt nicht möglich gewesen. Danke das ihr immer an mich glaubt! Danke Dennis, dass du dich so aufopfernd kümmerst und das Ding mit der Verantwortung füreinander so ernst nimmst. Ich kann mir keinen besseren Teampartner vorstellen!

Eigenständigkeitserklärung

Ich versichere an Eides Statt, dass die Dissertation von mir selbständig und ohne unzulässige fremde Hilfe unter Beachtung der „Grundsätze zur Sicherung guter wissenschaftlicher Praxis an der Heinrich-Heine-Universität Düsseldorf“ erstellt worden ist.

Düsseldorf, den 18.09.2023

_____

Unterschrift